



Politecnico di Torino

Master's degree in Mechatronic Engineering

A.y. 2021/2022  
Degree session: 7/2022

Master thesis

**Motion simulator of an underwater drone  
for the study of maneuverability**

Supervisor:  
Prof. Alessandro Rizzo

Candidate:  
Lorenzo Augusto Core

Co-supervisor:  
Eng. Andrea Marchese



## Acknowledgements

Prima di procedere con la trattazione, vorrei dedicare qualche riga a tutti coloro che mi sono stati vicini in questo percorso di crescita personale e professionale.

Un sentito grazie al mio relatore Rizzo per la sua infinita disponibilità e tempestività ad ogni mia richiesta, grazie per avermi fornito ogni materiale utile alla stesura dell'elaborato.

Un ringraziamento all'ingegnere Marchese per avermi seguito durante il progetto e avermi aiutato a superare le difficoltà incontrare, ringrazio anche tutto l'ufficio di CETENA per avermi accolto e fatto trascorrere i mesi del progetto in compagnia.

Ringrazio mia madre Ester e mio padre Angelo, senza i loro insegnamenti e senza il loro supporto, questo lavoro di tesi non esisterebbe nemmeno. I loro sacrifici mi hanno permesso di portare avanti i miei studi fino a questo giorno.

Ringrazio mia sorella Bianca, ragazza di cuore di una sensibilità unica.

Ringrazio Mario per essermi stato di supporto in questi anni di università e avermi reso la vita più serena anche in momenti di difficoltà.

Ringrazio anche mia nonna Teresa, fonte di saggezza e sincerità, e mio nonno Angiolino, che ricorderò per sempre per la sua oggettività e praticità.

Infine, ringrazio tutti i miei amici, coloro che mi sono stati vicini in ogni momento, ci tengo molto a tutti voi e vorrei che fosse limpido quanto siete importanti per me.

Grazie a tutti, senza di voi non ce l'avrei mai fatta.

# Abstract

Man's first attempts to build a submarine can be placed in 440 BC, however the first true marine vehicle with engine propulsion and capable of diving was created in Spain in 1867 and could dive up to 30 meters. Currently modern models reach much higher depths (about 400 meters). However, to overcome limitations as the space to be dedicated to the crew and the oxygen production plants, they are opting to produce drone submarines. Drones would allow the achievement of greater depth and autonomy, moreover, maintaining smaller dimensions that would allow better maneuverability.

My thesis aims to develop a motion simulator and a control system able to drive a submarine drone in several maneuvers meeting specific requirements. The hypothesized vehicle uses a single electric propeller maneuvered from a rudders system composed by a X configuration at the stern and two horizontal rudders in the bow.

This work starts from the mathematical formulation describing the 6-degree dynamics of a drone in water, and in the final phase the topic becomes the develop of an automatic control system and its tuning based on a genetic algorithm.

Several maneuvers have been analyzed to validate the capability of the genetic algorithm to identify the control system parameters that maximize the maneuver's performance indicators.

The thesis work was supervised and done with Cetena, a naval engineering company that is developing this software for the control and design of experimental drone submarines.

# Table of contents

Acknowledgements.....	i
Abstract.....	ii
List of Figure.....	5
List of Tables .....	7
Thesis outline .....	1
1 Introduction.....	1
1.1 Brief introduction on Cetena and the Fincantieri group.....	2
1.2 Introduction to submarine .....	4
1.2.1 Working principle for submersion .....	4
1.2.2 Archimede’s principle.....	5
1.2.3 Uses of submarines .....	6
1.3 History of submarine evolution.....	7
1.3.1 Submarines in first and second World war .....	8
1.3.2 Submarine in Cold War and modern characteristic .....	10
1.4 Emersion system and leaks .....	12
1.5 Example of modern Italian submarine .....	12
1.6 Unmanned drone submarine .....	13
1.7 Objectives .....	14
1.8 Drone model.....	15
2 Dynamic model applied to the simulator .....	17
2.1 Inertial Forces .....	19
2.2 A recall force.....	20
2.3 Hydrodynamic Forces.....	21
2.3.1 Feltman .....	22
2.3.2 Gertler .....	25
2.4 Force of rudders (X configuration).....	28
2.4.1 Feltman .....	30
2.4.2 Gertler .....	31
2.5 Force of the propeller.....	32
2.6 Mass variation in leak condition emergency.....	33
2.6.1 Determination of the flow rate of water expelled from the ballast tanks .....	35
2.6.2 Calculation of mass, center of gravity and moments of inertia.....	37
3 Automatic control system .....	39
3.1 Analysis of submarine model.....	39
3.2 PID control.....	41
3.2.1 PID introduction.....	41
3.2.2 PID tuning.....	44

3.2.3	PID distribution.....	45
3.3	Maneuver configuration.....	46
3.4	Gain scheduling .....	49
4	Simulator.....	50
4.1	Software structure .....	50
4.2	Interface .....	51
5	Genetic Algorithm .....	57
5.1	Introduction to genetic algorithms .....	57
5.1.1	Selection.....	59
5.1.2	Crossover .....	60
5.1.3	Mutation.....	62
5.2	Setting the algorithm for the problem .....	63
6	Analysis and results .....	66
6.1	Simulation in case of a leak .....	66
6.2	Behavior in case of leak.....	70
6.3	Simulation at 120 depth and 0 rpm .....	71
6.3.1	Open-loop analysis.....	71
6.3.2	Closed loop analysis.....	74
6.3.3	Optimization with Genetic Algorithm .....	77
6.4	Simulation at 250 depth and 60 rpm .....	79
6.4.1	Open-loop analysis.....	79
6.4.2	Closed loop analysis.....	82
6.4.3	Optimization with Genetic Algorithm .....	85
6.5	Simulation at 350 depth and 148 rpm .....	87
6.5.1	Open-loop analysis.....	87
6.5.2	Closed loop analysis.....	90
6.5.3	Optimization with Genetic Algorithm .....	93
6.6	Speed depth graph.....	95
6.7	Considerations.....	98
7	Conclusions.....	99
	Bibliography .....	100

## List of Figure

Figure 1 Fincantieri's informative graphic.....	3
Figure 2 Example of working principle of ballast tanks.....	4
Figure 3 Archimede principle.....	5
Figure 4 Density of water in rapport to depth.....	5
Figure 5 NR-1 scientific purpose submarine .....	6
Figure 6 Wooden replica of Ictineo II .....	7
Figure 7 Picture of Aigrette submarine .....	8
Figure 8 Refiguration of U-boat .....	9
Figure 9 Refiguration of I402, submarine aircraft carrier .....	9
Figure 10 Seawolf ss197 American submarine .....	10
Figure 11 Scheme of nuclear reactor.....	11
Figure 12 Italian u212 .....	12
Figure 13 Example of unmanned underwater drone of big dimension.....	13
Figure 14 3D model of the underwater drone.....	15
Figure 15 Nomenclature of the drone.....	15
Figure 16 Dimensions and centre of mass and bouyancy.....	15
Figure 17 Top view of the drone .....	16
Figure 18 Front view of the drone .....	16
Figure 19 Back view of the drone .....	16
Figure 20 Representation of software sections.....	17
Figure 21 Coordinate system.....	23
Figure 22 Nomenclature of rudders.....	28
Figure 23 Open Loop DC gain vs drone speed .....	40
Figure 24 Natural frequency vs speed .....	40
Figure 25 Variation of damping vs speed.....	41
Figure 26 PID scheme .....	43
Figure 27 Angles and principal direction of the drone, roll and pitch are controlled.....	44
Figure 28 Basic block system.....	45
Figure 29 PID for each rudder.....	45
Figure 30 PID for front rudders and back rudders.....	45
Figure 31 Pitch control configuration.....	46
Figure 32 Change of depth with discord configuration.....	46
Figure 33 Change of depth with concord rudders .....	47
Figure 34 Roll control configuration.....	47
Figure 35 Overlapping rudder effects.....	48
Figure 36 Force distribution of total configuration .....	48
Figure 37 Example of PID variable adjustments.....	49
Figure 38 Software structure .....	50
Figure 39 Main interface .....	51
Figure 40 File loading .....	51
Figure 41 Basic parameters choice.....	52
Figure 42 Parameters of Hydrodynamic coefficients .....	52
Figure 43 Vortex effect .....	53
Figure 44 Rudders configuration.....	53
Figure 45 PID interface .....	54
Figure 46 General maneuver settings.....	55
Figure 47 Specific manouver settings .....	56
Figure 48 Genetic algorithm flow chart .....	58
Figure 49 One point crossover working principle .....	61
Figure 50 Two point crossover.....	61
Figure 51 Uniform crossover.....	61
Figure 52 Mutation.....	62

Figure 53 Constant of PID and their ranges .....	63
Figure 54 Scheme of used genetic algorithm .....	64
Figure 55 Progressive crossover and mutation for diversification .....	65
Figure 56 General settings for leak simulation.....	68
Figure 57 Interface with standard data for manoeuvrer.....	69
Figure 58 Example of Forces During the Leak Situation .....	69
Figure 59 Behavior in case of leak with 0 speed.....	70
Figure 60 Behavior in case of leak with 40 rpm.....	70
Figure 61 Pitch angle.....	71
Figure 62 Roll angle .....	71
Figure 63 Mass of the vessel with respect to the leak and filling of the crates .....	72
Figure 64 System speed.....	72
Figure 65 X-Z plane .....	73
Figure 66 X-Y plane.....	73
Figure 67 Pitch with PID.....	74
Figure 68 Roll with PID .....	74
Figure 69 Rudder angles respect pitch and roll .....	75
Figure 70 Speed of the drone.....	75
Figure 71 X-Z plane .....	76
Figure 72 X-Y plane.....	76
Figure 73 Genetic Algorithm results .....	77
Figure 74 Results with tuned PID on pitch.....	78
Figure 75 Pitch angle.....	79
Figure 76 Roll angle .....	79
Figure 77 Mass of the drone respect the filling by compressed air .....	80
Figure 78 Drone speed.....	80
Figure 79 X-Z plane .....	81
Figure 80 X-Y plane.....	81
Figure 81 Pitch with PID .....	82
Figure 82 Roll with PID .....	82
Figure 83 Rudders angles .....	83
Figure 84 Speed of the drone.....	83
Figure 85 X-Z plane .....	84
Figure 86 X-Y plane.....	84
Figure 87 Genetic Algoritm results .....	85
Figure 88 Results with tuned PID on pitch.....	86
Figure 89 Pitch angle during the test.....	87
Figure 90 Roll angle during the test .....	87
Figure 91 Mass of the vessel with respect to the leak and filling of the crates .....	88
Figure 92 Drone speed.....	88
Figure 93 X-Z plane .....	89
Figure 94 X-Y plane.....	89
Figure 95 Pitch with PID.....	90
Figure 96 Roll with PID .....	90
Figure 97 Rudders angles .....	91
Figure 98 Speed of the drone.....	91
Figure 99 X-Z plane .....	92
Figure 100 X-Y plane.....	92
Figure 101 Genetic Algoritm results .....	93
Figure 102 Results with tuned PID on pitch.....	94
Figure 103 Region of emergence.....	96
Figure 104 Constant behaviour.....	98

# List of Tables

Table 1 Configuration of rudder angles for movements.....29

Table 2 PID tuning effect .....44

Table 3 Simulation results of 120 depth and 0 rpm.....78

Table 4 Simulation results 250 depth and 60 rpm .....86

Table 5 Results of simulation at 350 depth at 148 rpm .....94

Table 6 Table containing pitch angle of emersion in different depth with different speed.....95

Table 7 Table containing pitch angle of emersion in different depth with different speed with PID .....96

Table 8 Difference between closed loop and closed loop with tuned PID .....97

.....

# Thesis outline

This document is divided in the following sections:

## **Chapter 1: introduction**

The first chapter contains a general introduction of the project and the company that is developing it and an introduction on submarines up to the most modern examples as like submarine drones.

## **Chapter 2: Dynamic model of the simulator**

The second chapter focuses on the mathematical model of the simulator, containing the main formulas used for the study of the motion of the vessel. Two main models are highlighted with which the simulator calculates the different forces acting on the hull and the center of thrust.

## **Chapter 3: Automatic control system**

Chapter on the control system implemented in the simulator and model analysis in the complex frequency domain. This chapter wants to specify what type of control has been considered and what are the possible improvements.

## **Chapter 4: Structure of the simulator**

Chapter concerning the general operation of the simulator, the flow charts of the main parts of the program are reported but due to the sensitivity of the data the code parts are not shown.

## **Chapter 5: Algorithm for tuning parameters**

The chapter talks about the development of the genetic algorithm for the optimization of PID parameters according to certain requests and objectives for the tests.

## **Chapter 6: Analysis and Results**

In this part are reported the graphs of the simulations with all the variables necessary for the analysis of the drone's behaviour, are also shown the effects of the genetic algorithm.

## **Chapter 7: Conclusions**

The last chapter is intended to be a summary of what will be the evolving situation of the project.

# 1 Introduction

This master thesis aims to analyze the dynamics in the marine environment of an underwater drone obtained with a simulator able to generate specific situations, understand the behavior of the submarine based on different speed and depth conditions, trying to create a control system necessary for the maneuvers. In particular, the development of a control and optimization algorithms for the worst situation for the vessel, which is the simulation in case of a leak, where the drone increase its mass in a short time causing a deterioration in handling.

This thesis was made under the supervision of Cetena and Fincantieri, some sensitive data and reserved topics have been purposely hidden or modified to maintain confidentiality. The working principle of the simulator and the optimization algorithms will be described but all the sensitive material related to them will be hidden, for example the code parts.

The work behind this project began with the studies of the physical models already implemented in a previous version of the simulator developed by Cetena for Fincantieri. It was necessary to modify the code by inserting a control system for the pitch and roll, new type of emergence tests and the crate filling system used to assist the drone during the leak test. Another important addition was the X rudders configuration choice for the drone, in fact this allows greater maneuverability and efficiency of the submarine. The previous version provided only the cross-type configuration.

After making the new software work, with the data of an experimental drone in current development, it was possible to evaluate the behavior of the vessel in various situations. Subsequently, thanks to the tests carried out at different depths, a depth graph was created in relation to the rpms of the submarine indicating when was able to emerge and at what pitch angle value. The final goal was to consider the profundity where the submarine, in case of unmanaged flaw for a time of 20 seconds (time considered from the first embarkation of water and first intervention), could still emerge at an angle of less than 45 degrees and the necessary speed of the engine for this result. Thanks to the implementation of a genetic algorithm for the values of the constants of the control system, it was possible to improve the performance previously obtained and found the physical limits of the emersion of the drone.

## *1.1 Brief introduction on Cetena and the Fincantieri group*

### **Cetena Spa**



CETENA S.p.A. – a study center in the maritime field – which was established in 1962 and is a Fincantieri company with headquarters in Genova. CETENA provides support for its customers with a wide range of consultancy, on-board activities, specific products, laboratory tests and training programmes in the maritime field in both civil and naval sectors.

To maintain a direct link with shipyard activities (engineering and production), CETENA has different offices and test laboratories in strategic positions all over Italy (Trieste - Riva Trigoso - Castellammare - Palermo) and also collaborates with different research centers in Italy and Europe and it is involved in many research projects with universities, various Ministries and industrial companies.

The company includes various operation units in which engineers with different competences and skills work together to find tailored solutions and to solve critical technical issues.

The dual principal aspects of CETENA are research and customer support, which distinguish the company in the market giving tangible advantages to its customers: on one hand, customer support is innovative because it is provided by technicians who are also involved in research activities and on the other hand, research support is effective due to the expertise of CETENA to properly address research activities related to the input received from industrial companies.

Within the European frame, CETENA recently participated as coordinator and as a partner to projects focusing on:

- Advanced materials (polymeric composites and special steel)
- Structural monitoring, fuel consumption monitoring, maintenance systems and decision support systems for ship management and operation
- Innovative structures and advanced structural design methodologies
- Noise emissions, both in air and water
- “Green” technologies and reduction systems of emissions
- Life Cycle Analysis and Multi Criteria Analysis tools and methodologies
- Hydrodynamic analysis methodologies, propulsion and propeller design.

**Fincantieri group**

Fincantieri is one of the world’s largest shipbuilding groups, global Italian leader in cruise ship design, reference player in all high-tech shipbuilding industry sectors, from naval to offshore vessels, from high-complexity ferries to mega yachts, as well as production of systems and component equipment for mechanical and electrical segments, from cruise ship interiors solutions, electronic and software systems, to infrastructures and maritime constructions, as well as after-sales services.

With over 230 years of history and more than 7,000 ships built, Fincantieri maintains its know-how, expertise and management centres in Italy, here employing 10,000 workers and creating around 90,000 jobs, which double worldwide thanks to a production network of 18 shipyards operating in four continents and with over 20,000 employees.



Figure 1 Fincantieri's informative graphic

## 1.2 Introduction to submarine

Submarines are self-propelled submarine ships designed and built to perform underwater operations for a certain period of time. The submarine design consists of a single or double hull system that houses all the systems and manpower needed to complete their mission. Submarines are used for a wide range of purposes such as underwater search, underwater rescue and submarine warfare; the last one is the most used. The underwater vehicle is often referred to as a boat or vessel.

### 1.2.1 Working principle for submersion

A submarine floats when the mass of water it pushes away is equal to the mass of the vessel. This displaced water causes an upward force called buoyancy that acts in the opposite direction to gravity, which instead pushes the ship down. A normal boat cannot control or change its buoyancy, but a submarine can, and this allows it to dive underwater or rise to the surface. To control its buoyancy, the submarine has ballast tanks that can be filled with water or filled with air. When the submarine is on the surface, the ballast tanks are filled with air which makes the density of the submarine lower than the density of the water instead when the submarine dives, the water is pumped into the ballast tanks to replace the air which makes the density of the submarine greater than the density of the water. Compressed air tanks are generally used to emerge, and when the crew needs to return to the surface, they pump air into the ballast tanks to push the water out (figure 2).

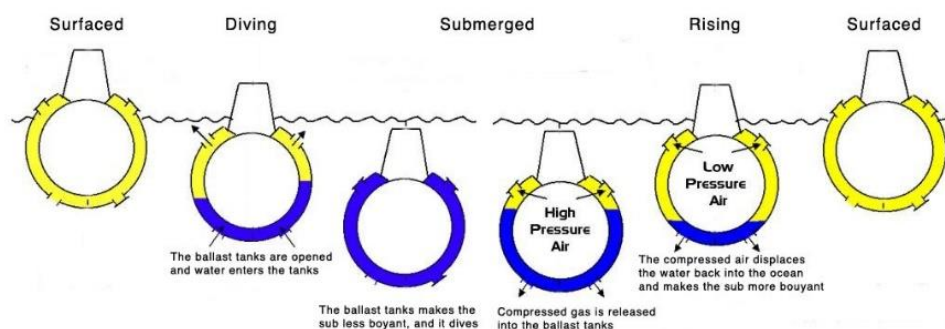


Figure 2 Example of working principle of ballast tanks

### 1.2.2 Archimede's principle

The floating principle is governed by the Archimede's formula, which states that the buoyant force on a fluid is equal to the weight of the displaced fluid (figure 3). To calculate the buoyant force, we use the equation:

$$F_a = \rho g V$$

$F_a$  = buoyant force

$\rho$  = density of fluid

$gV$  = volume of displaced fluid x acceleration due to gravity

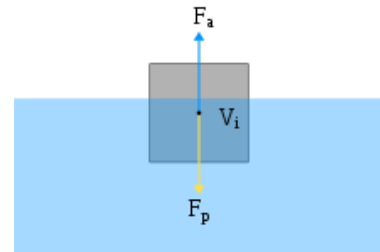


Figure 3 Archimede principle

By indicating with  $F_p$  as the gravitational force on the object is

possible to analyze the three conditions of the problem: when  $F_p$  is greater the body will tend to float, when is smaller the body will sink and in the case in which the two forces are equal is possible to maintain a balance in the submarine.

This condition implies that  $F_a = F_p$  so  $\rho_{fluid} g V_{fluid} = \rho_{submarine} g V_{submarine}$  and since the 2 volumes are the same, we can state that a submarine, for maintain the same depth, must be in a state where it has the same density as the surrounding water.

$$\rho_{fluid} = \rho_{submarine}$$

The density of ocean water at the sea surface is generally about 1027 kg/m<sup>3</sup> and the two main factors that affect density of ocean water are the temperature of the water and the salinity of the water. So, it will change depending on the position in the globe. Temperature has a greater effect on the density of water than salinity. So, a parcel of water with higher salinity can float on top of water with lower salinity if the parcel with higher salinity is quite a bit warmer than the lower salinity parcel. This behavior creates a zone called Pycnocline where the density increases rapidly and then begins to increase slowly (figure 4).

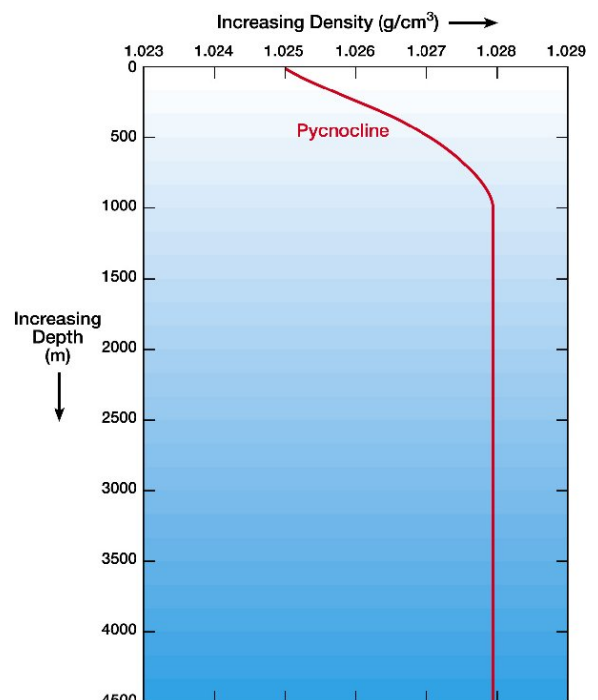


Figure 4 Density of water in rapport to depth

### *1.2.3 Uses of submarines*

The curiosity of man regarding the depths of the sea is certainly the first stimulus that led to the development of this type of vehicle. The first uses, dating in the early 1800s, consisted essentially in exploratory purposes, made by the first prototypes without even an engine apparatus. But it was during the two World Wars that increased the progress of them, in fact the tactical advantage of an underwater vehicle was enormous, until the early 1900s some working models had already been created but with just enough performance. After the development during the two World Wars, the foundations were established to make the submarine a useful tool also for the study of the seabed and for rescue operations.

The three main uses of this vehicle can in fact be listed as:

- Scientific

The importance of the submarine as a tool for the exploration of the abyss reached its peak only in the mid-fifties of the last century when technological progress and the use of advanced materials allowed the construction of submarines capable of reaching very high depths. Bathyscaphs and submarines are widely used in the scientific field for the exploration of the seabed and the analysis of the marine environment, in figure 5 is shown an example of a scientific submarine.



*Figure 5 NR-1 scientific purpose submarine*

- Rescue

Special types of submarines are used for rescue under certain marine conditions either for crews of other submarines or ships, generally they are smaller and carried by other ships.

- Military

The development of submarines in the military field is the main reason why the technology is in continuous evolution, in fact most of the submarines were built for war purposes and their production has allowed the continuous improvement of the performance and technologies used on board.

### *1.3 History of submarine evolution*

The idea of being able to travel underwater has always stimulated man, in fact the first stories about diving methods date back to 300 BC. Although theories were developed during the Middle Ages to accomplish this feat, the first human-powered prototypes were made around 1600, an example being the Submarine of Cornelius Jacobszoon Drebbel, used to cross the Thames.

The first major developments were made in 1800s and already in 1860 was created the first examples of mechanically propelled submarines, an example is the Ictineo 2 designed by the Spanish inventor Narcís Monturiol and built in 1867. Ictineo 2 (figure 6) is one of the very first examples of a man-made submarine with dual propulsion, the ability to go underwater was limited to 27 meters and operated with an engine based on the reaction to peroxide for diving and a coal one for the surface.



*Figure 6 Wooden replica of Ictineo II*

In the following years many advances were made especially from the point of view of propulsion, starting to use electric motors thanks to the discovery of batteries in 1880. The first electrically powered submarines were built by the Polish engineer Stefan Drzewiecki in Russia, James Franklin Waddington and the team of James Ash and Andrew Campbell in England, Dupuy de Lôme and Gustave Zédé in France and Isaac Peral in Spain. Following this period of experimentation, with the beginning of 1900, there was a standardization of the models always using two propulsion systems, one electric for submarine movement and a diesel one for surface motion, also began to become standard submarine's equipment such as the periscope.

The depths reached in these years were around 50 meters, but the French submarine Aigrette (figure 7) launched in February 1904 was able to reach the goal of going underwater up to 100 meters. It had a single shaft powered by one diesel engine for surface and an electric motor for submerged propulsion. The maximum speed was 11.2 Km/H submerged. It was mainly an experimental submarine but also saw its use during the first World War.

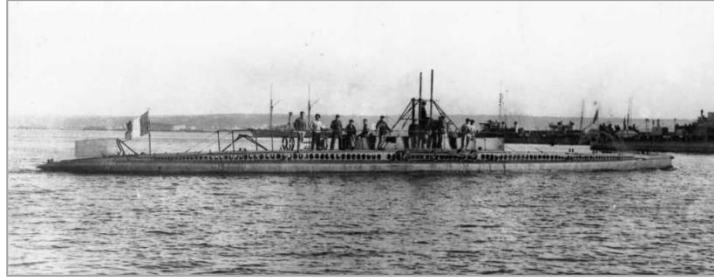


*Figure 7 Picture of Aigrette submarine*

### ***1.3.1 Submarines in first and second World war***

#### **First world war**

The development of submarines over the last decade had pushed many navies to equip themselves with them, so much so that in the First World War this weapon had a fundamental use. Submarines played an important role in the attempt by Germany, and more limitedly also by Austria, to remedy the Allied naval blockade imposed by the naval supremacy of Great Britain and the United States and were a determining cause for the entry of the United States into the war.

Emblem of the technical evolution were the German U-boats (figure 8), for example the introduction of the double hull on these models will then be applied to all submarines introduced since the Second World War. Their fame is also such for the sinking of the British ocean liner Lusitania loaded with American civilians that conditioned American public opinion in favor of the entry into the war of the United States against Germany, two years later.

The ability of U-boats to function as practical war machines was based on new tactics, their numbers and submarine technologies such as the diesel-electric combined fuel system developed in previous years. More submersible than real submarines, U-boats operated mainly on the surface occasionally diving to attack under battery power.

In 1914 U-boats were considered quite advanced, these ships could reach maximum depths of 50 meters, reach speed of 16 knots on the surface and 8 knots underwater, and had a range of up to 25,000 miles.

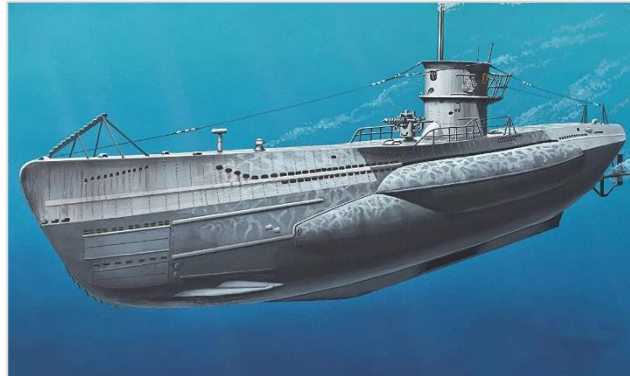


*Figure 8 Refiguration of U-boat*

### **Second world war**

By the outbreak of World War II, the number of navies with submarines had increased considerably. Nevertheless, most of the units had remained substantially the same as those that operated at the end of the Great War. The Germans upgraded their U-boat with a better communication system and opted to organize mass attacks to create embargoes on British supply lines.

The Imperial Japanese Navy was the one to experiment the most on submarines, coming to have the most varied fleet during the war. They had the submarines with the highest submerged speeds during World War II (I-201 class submarines) and developed submarines that could carry more aircraft (I-400 class submarines, figure 9).

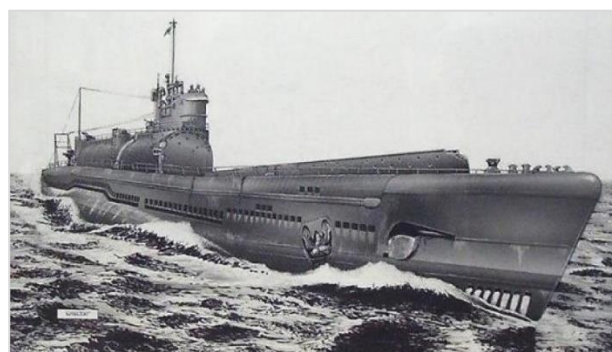


*Figure 9 Refiguration of I402, submarine aircraft carrier*

The United States also made extensive use of submarines (figure 10), which although only about 2% of the U.S. Navy, destroyed more than 30% of the Japanese Navy, including 8 aircraft carriers, 1 battleship, and 11 cruisers. U.S. submarines have also destroyed more than 60% of Japan's merchant fleet, crippling Japan's ability to supply its military forces and industrial warfare effort. To get an idea of their military strength, Allied submarines in the Pacific War destroyed more Japanese ships than all the other weapons combined. This feat was greatly aided by the inability of the Imperial Japanese Navy to provide adequate escort forces for the nation's merchant fleet.



*Figure 10 Seawolf ss197 American submarine*

The submarines of this era could reach depths of 270 m, the advantage of reaching greater depths was that they could resist the attack of other submarines and above all survive the depth charges that were one of the main ways to damage the submerged submarines.

### ***1.3.2 Submarine in Cold War and modern characteristic***

During the Cold War the biggest innovations were the replacement of electric propulsion with nuclear one and the creation of equipment to extract oxygen from seawater, which gave submarines the opportunity to remain submerged for weeks or months. From the Cold War to nowadays the changes have remained more or less the same, they have managed to reach greater depths and speeds, but modern submarines are built based on stealth. Advanced propeller designs, extensive sound insulation and special machinery help a submarine to stay as quiet as the ambient noise of the ocean, making them difficult to detect. Modern nuclear attack submarines such as the American Seawolf class are estimated to have a test depth of 490 m (1,600 ft), which would imply a collapse depth of 730 m (2,400 ft). That is, the submerged depth at which it is assumed that the structure of the hull of a submarine suffer a catastrophic failure up to the point of total collapse due to pressure.

## Nuclear power

A nuclear submarine is a submarine powered by a nuclear reactor, but not necessarily nuclear-armed. Nuclear submarines have considerable performance advantages over "conventional" (typically diesel-electric) submarines. Nuclear propulsion (figure 11), being completely independent from air, lets free the submarine from the need to surface frequently, as is necessary for conventional submarines. The large amount of power generated by a nuclear reactor allows nuclear submarines to operate at high speed for long periods, and the long interval between refueling grants a range virtually unlimited, making the only limits on voyage times being imposed by such factors as the need to restock food or other consumables.

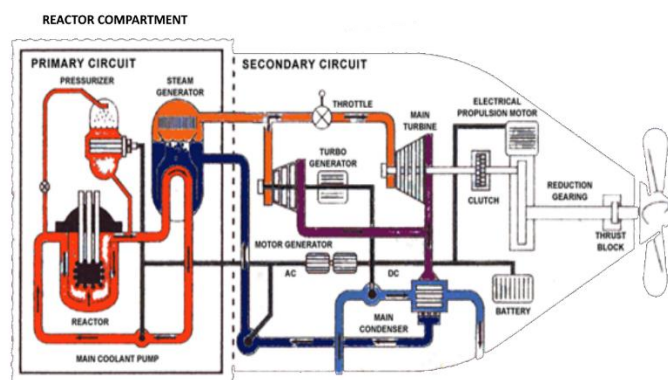


Figure 11 Scheme of nuclear reactor

## Oxygen generators

There are several sources of oxygen aboard a submarine, the main systems are oxygen generators operating by electrolysis or canisters that release massive amounts of oxygen. Electrolytic oxygen generator (EOG) is one of the most reliable technologies and works with several inlet and outlet that extract water that will be distilled with a process of evaporation. After is applied a current that passes through the distilled water in the EOG and causes a physical process called electrolysis, separating the water molecules into hydrogen gas molecules ( $H_2$ ) and oxygen ( $O_2$ ) gas molecules. The process occurs under very high pressure. The  $O_2$  molecules are passed to high pressure flasks then re-distributed to within the boat's pressure hull. The  $H_2$  molecules are immediately passed from the EOG to a diffuser that is located outside the pressure hull. This diffuser breaks up larger  $H_2$  bubbles into tinier  $H_2$  bubbles, reducing the chance of detection either visually or by waterborne  $H_2$  gas sensors.

### *1.4 Emersion system and leaks*

Given the high depth reached by modern submarines, it is necessary to talk about emergence systems for vehicle rescue. One of the situations in which the submarine is considered lost is the case of a leak. There are no technologies capable of saving a vessel of this size at depths where pressure makes it impossible to use air to fill the crates.

Common methods for saving the crew are to use external vehicle capable of reach bigger depths and special suit are used by the crew for escape and float to the surface. In case of military submarine, a direct hit by a torpedo is always considered to be a fatal cause for the integrity and a certain cause for a sinking. Another of the biggest problems that can lead to sinking is the embarkation of water from one of the seacocks that can be damaged by shock waves or other factors such as external pressure, from these leaks several tons of water can enter and fill the premises floodable making the submarine much heavier and difficult to steer.

### *1.5 Example of modern Italian submarine*

An example of a modern Italian submarine is the 212 class (figure 12). The program, which began in 1994 as a part of the German Submarine Consortium, led to the construction of six units for the German Navy and, in Italy, of the two boats *Todaro* and *Scirè*, delivered by Fincantieri in 2006 and 2007 respectively. The submarines were initially designed as a class 212 according to the requests of the German Navy, which provided for their prevalent use in the North Sea and the Baltic. When the Italian navy joined in 1996, the program was modified according to some Italian needs, which concern the largest depths of the Mediterranean Sea; hence the change of the designation from 212 to 212A, which is also common for all submarines in the class, German and Italian, built until 2020.



*Figure 12 Italian u212*

## 1.6 Unmanned drone submarine

Unmanned underwater vehicles (UUV), sometimes known as underwater drones, are submersible vehicles that can operate underwater without a human occupant. These vehicles may be divided into two categories: remotely operated underwater vehicles (ROUVs) and autonomous underwater vehicles (AUVs). ROUVs are remotely controlled by a human operator. AUVs are automated and operate independently of direct human input.

Marine drones can be of different sizes ranging from 10 centimeters up to 50 meters, the design of these vehicles varies depending on the use. In the case of this thesis, the use of a large submarine drone (figure 13) with a torpedo shape and dual-fuel propulsion, both from an electric and diesel motor, will be hypothesized. The stern rudders are X-shaped while horizontal sail rudders are maintained at the bow.

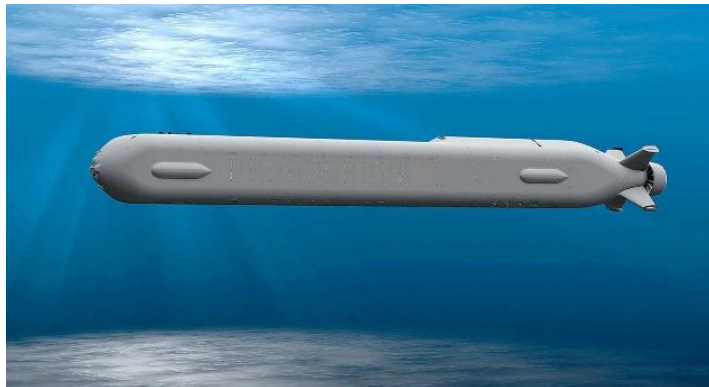


*Figure 13 Example of unmanned underwater drone of big dimension*

The advantages of using a drone are innumerable, starting from the design where it is possible to dedicate much more space to the crates for diving, maintaining a general structure similar to those of a torpedo, thanks to the fact that isn't needed an internal space to devote to the crew and the oxygen transformation systems, the hull can be much more resistant and needs fewer inlets allowing the achievement of greater sea depths, moreover, given the smaller empty internal space, the drone in case of a leak will embark a limited amount of water.

## *1.7 Objectives*

The objective of this project was to create a simulator to analyze the underwater motion of a large drone. The simulator must allow to modify the input data and provide an accurate behavior of the submarine through the three angles of roll pitch and yaw and the 3 speeds surge, heave and sway.

Subsequently, certain maneuvering behaviors would have to be verified and a control system would be implemented that could guarantee certain performances.

The steps for the development of the simulator were:

1. Verification and implementation of the physical equation of the model
2. Analysis of rudders and their configuration for permit maneuvers
3. Transition from cross rudder configuration to X rudder configuration
4. Make an interface to manage drone data entry
5. Development of the maneuver to be performed
6. Insertion of the Control System
7. Creation of the genetic algorithm for tuning the control system

After completing the update of the simulator, the tests were carried to check:

1. Correct behaviour of the software
2. Validity of the dynamic model
3. Reliability of the applied control system

## 1.8 Drone model

For reasons of confidentiality, the model (figure 14,15) approximates a possible example of a large submarine drone. The dimensions below (Figure 16,17,18,19) are indicative and serve the reader to get a general idea about the performance and capabilities of such vehicle.



Figure 14 3D model of the underwater drone

The underwater drone used in the simulator can be represented in the following way. It has the classic torpedo shape and a very low sail containing the communication systems. It is 5 meters high and is 30 meters long, weight 1000 tons and have a top speed of 20 Kn. It has 2 ballast tanks one in the back and one in front.

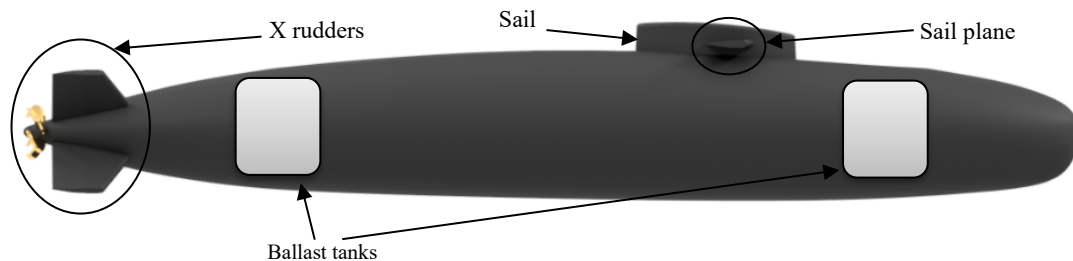


Figure 15 Nomenclature of the drone

The buoyancy remains below the center of gravity, which is located at 18 meters from the back.

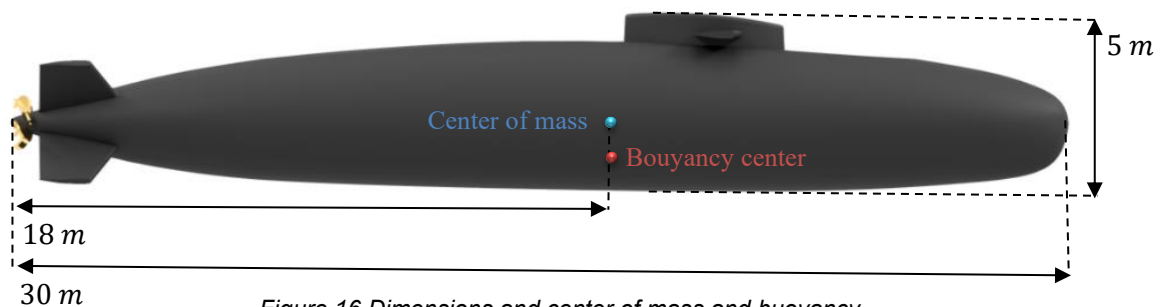
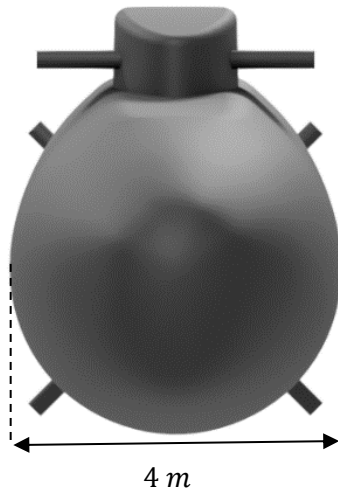


Figure 16 Dimensions and center of mass and buoyancy



*Figure 17 Top view of the drone*



*Figure 18 Front view of the drone*



*Figure 19 Back view of the drone*

## 2 Dynamic model applied to the simulator

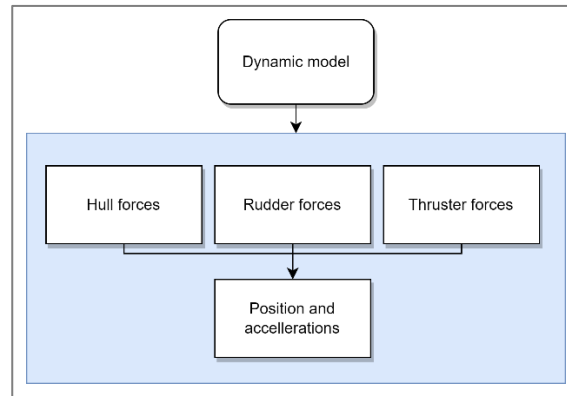


Figure 20 Representation of software sections

The general equations of motion underlying the theoretical model are based on the second law of dynamics:

$$M \cdot \vec{a} = \vec{F}$$

Where:

- $M$  = Submarine mass
- $a$  = Accelerations
- $F$  = Total force applied to the submarine

The total force  $F$  can be divided into three major forces:

$$\vec{F} = \vec{F}_{\text{HULLTOT}} + \vec{F}_{\text{RUDD}} + \vec{F}_{\text{PROP}}$$

Where:

- $\vec{F}$  = Total force on the submarine
- $\vec{F}_{\text{HULLTOT}}$  = Total forces acting on the hull
- $\vec{F}_{\text{RUDD}}$  = Rudder forces
- $\vec{F}_{\text{PROP}}$  = Thruster forces

to simplify the dynamic model, the following forces have been omitted

- 1) forces of the appendages (experience has shown that the hull hydrodynamic coefficients implicitly contain the content of appendages)
- 2) environmental forces (wind, sea, current);

By virtue of the fact that forces are calculated in the subsea reference system (which is not inertial), the equations reported by Feltman and Gertler of the 6 degrees of freedom considered (forward, drift, jump, roll, pitch and yaw) are modified as follows:

$$\left\{ \begin{array}{l} M[\dot{u} - vr + wq - x_G(q^2 + r^2) + y_G(pq - \dot{r}) + z_G(pr + \dot{q})] = X_{\text{HULLTOT}} + X_{\text{RUDD}} + X_{\text{PROP}} \\ M[\dot{v} - wp + ur - y_G(r^2 + p^2) + z_G(qr - \dot{p}) + x_G(qp + \dot{r})] = Y_{\text{HULLTOT}} + Y_{\text{RUDD}} + Y_{\text{PROP}} \\ M[\dot{w} - uq + vp - z_G(p^2 + q^2) + x_G(rp - \dot{q}) + y_G(rq + \dot{p})] = Z_{\text{HULLTOT}} + Z_{\text{RUDD}} + Z_{\text{PROP}} \\ I_x \dot{p} + (I_z - I_y)qr - (\dot{r} + pq)I_{zx} + (r^2 - q^2)I_{yz} + (pr - \dot{q})I_{xy} + \\ + M[y_G(\dot{w} - uq + vp) - z_G(\dot{v} - wp + ur)] = K_{\text{HULLTOT}} + K_{\text{RUDD}} + K_{\text{PROP}} \\ I_y \dot{q} + (I_x - I_z)rp - (\dot{p} + qr)I_{xy} + (p^2 - r^2)I_{zx} + (qp - \dot{r})I_{yz} + \\ + M[z_G(\dot{u} - vr + wq) - x_G(\dot{w} - uq + vp)] = M_{\text{HULLTOT}} + M_{\text{RUDD}} + M_{\text{PROP}} \\ I_z \dot{r} + (I_y - I_x)pq - (\dot{q} + rp)I_{yz} + (q^2 - p^2)I_{xy} + (rq - \dot{p})I_{zx} + \\ + M[x_G(\dot{v} - wp + ur) - y_G(\dot{u} - vr + wq)] = N_{\text{HULLTOT}} + N_{\text{RUDD}} + N_{\text{PROP}} \end{array} \right.$$

Known that in the forces  $\vec{F}_{\text{HULLTOT}}$  there are components dependent on accelerations (added mass) and components dependent on velocities, the equations can be rewritten by bringing to the left of the equal all the terms proportional to the accelerations and to the right of the equal the remaining ones. In this way the problem can be traced back to the following linear system of differential equations:

$$\underline{\underline{A}} \cdot \vec{\ddot{X}} = \vec{b}$$

Where:

- $\underline{\underline{A}}$  = Matrix (6 x 6) of mass (takes count of added mass);
- $\vec{\ddot{X}}$  = Vector (6 x 1) of accelerations.
- $\vec{b}$  = Vector (6 x 1) of forces and moments acting on the submarine (not dependent on accelerations; known terms).

Those matrices are developed in this way:

$$\underline{A} = \begin{bmatrix} M - \frac{\rho}{2}L^3X_{\dot{u}} & 0 & 0 & 0 & M z_G & -M y_G \\ 0 & M - \frac{\rho}{2}L^3Y_{\dot{v}} & 0 & -M z_G - \frac{\rho}{2}L^4Y_{\dot{p}} & 0 & M x_G - \frac{\rho}{2}L^4Y_{\dot{r}} \\ 0 & 0 & M - \frac{\rho}{2}L^3Z_{\dot{w}} & M y_G & -M x_G - \frac{\rho}{2}L^4Z_{\dot{q}} & 0 \\ 0 & -M z_G - \frac{\rho}{2}L^4K_{\dot{v}} & M y_G & I_x - \frac{\rho}{2}L^5K_{\dot{p}} & -I_{xy} & -I_{zx} - \frac{\rho}{2}L^5K_{\dot{r}} \\ M z_G & 0 & -M x_G - \frac{\rho}{2}L^4M_{\dot{w}} & -I_{xy} & I_y - \frac{\rho}{2}L^5M_{\dot{q}} & -I_{yz} \\ -M y_G & M x_G - \frac{\rho}{2}L^4N_{\dot{v}} & 0 & -I_{zx} - \frac{\rho}{2}L^5N_{\dot{p}} & -I_{yz} & I_z \end{bmatrix}$$

$$\vec{\ddot{X}} = \begin{bmatrix} \ddot{X} \\ \ddot{Y} \\ \ddot{Z} \\ \ddot{\phi} \\ \ddot{\theta} \\ \ddot{\psi} \end{bmatrix} = \begin{bmatrix} \dot{u} \\ \dot{v} \\ \dot{w} \\ \dot{p} \\ \dot{q} \\ \dot{r} \end{bmatrix}$$

$$\vec{b} = \vec{F}_{INER} + \vec{F}_{RICH} + \vec{F}_{HULL} + \vec{F}_{RUDD} + \vec{F}_{PROP} = \begin{bmatrix} X_{INER} + X_{RICH} + X_{HULL} + X_{RUDD} + X_{PROP} \\ Y_{INER} + Y_{RICH} + Y_{HULL} + Y_{RUDD} + Y_{PROP} \\ Z_{INER} + Z_{RICH} + Z_{HULL} + Z_{RUDD} + Z_{PROP} \\ K_{INER} + K_{RICH} + K_{HULL} + K_{RUDD} + K_{PROP} \\ M_{INER} + M_{RICH} + M_{HULL} + M_{RUDD} + M_{PROP} \\ N_{INER} + N_{RICH} + N_{HULL} + N_{RUDD} + N_{PROP} \end{bmatrix}$$

$\vec{F}_{INER}$ ,  $\vec{F}_{RICH}$ ,  $\vec{F}_{HULL}$ ,  $\vec{F}_{RUDD}$  e  $\vec{F}_{PROP}$  they are calculated according to the formulations reported in the following paragraphs, differentiating the theories developed by Feltman and Gertler.

## 2.1 Inertial Forces

This paragraph describes the equations relating to the calculation of inertial forces, common to both models implemented within the software. The presence of these forces is linked to the fact that the forces are calculated with respect to a non-inertial reference system (that of the submarine).

$$\vec{F}_{INER} = \begin{bmatrix} X_{INER} \\ Y_{INER} \\ Z_{INER} \\ K_{INER} \\ M_{INER} \\ N_{INER} \end{bmatrix}$$

The inertial forces are calculated according to the following expressions:

$$X_{INER} = M[vr - wq + x_G(q^2 + r^2) - y_Gpq - z_Gpr]$$

$$Y_{INER} = M[wp - ur + y_G(r^2 + p^2) - z_Gqr - x_Gqp]$$

$$Z_{INER} = M[uq - vp + z_G(p^2 + q^2) - x_Grp - y_Grq]$$

$$K_{INER} = -(I_z - I_y)qr + I_{zx}pq - (r^2 - q^2)I_{yz} - I_{xy}pr + M[y_G(uq - vp) + z_G(ur - wp)]$$

$$M_{INER} = -(I_x - I_z)rp + I_{xy}qr - (p^2 - r^2)I_{zx} - I_{yz}qp + M[z_G(vr - wq) + x_G(vp - uq)]$$

$$N_{INER} = -(I_y - I_x)pq + I_{yz}rp - (q^2 - p^2)I_{xy} - I_{zx}rq + M[x_G(wp - ur) + y_G(wq - vr)]$$

## 2.2 A recall force

This paragraph describes the equations relating to the calculation of the recall forces, common to both models implemented within the software. These forces include the terms due to the gravitational effect and the terms due to the hydrostatic action

$$\vec{F}_{INER} = \begin{bmatrix} X_{RICH} \\ Y_{RICH} \\ Z_{RICH} \\ K_{RICH} \\ M_{RICH} \\ N_{RICH} \end{bmatrix}$$

The forces and moments of gravitational origin are dependent on the weight of the body  $W$ , on the hydrostatic thrust  $B$  on the pitch and roll angles according to the following expressions:

$$X_{RICH} = -(W - B)\sin\theta$$

$$Y_{RICH} = +(W - B)\cos\theta\sin\phi$$

$$Z_{RICH} = +(W - B)\cos\theta\cos\phi$$

$$K_{RICH} = +(y_GW - y_BB)\cos\theta\cos\phi - (z_GW - z_BB)\cos\theta\sin\phi$$

$$M_{RICH} = -(x_GW - x_BB)\cos\theta\cos\phi - (z_GW - z_BB)\sin\theta$$

$$N_{RICH} = +(x_GW - x_BB)\cos\theta\sin\phi + (y_GW - y_BB)\sin\theta$$

### 2.3 Hydrodynamic Forces

The hydrodynamic terms are calculated as a function of coefficients depending on the characteristics of the hull and appendages.

The hydrodynamic components of the two models differ mainly in the different approaches used to derive the Cross flow Drag forces and the contribution due to the lift forces of the sail. In particular, as regards the cross flow drag, in the Gertler model these forces are considered through global hydrodynamic coefficients, such as for example  $Yv|v|$ ,  $Yr|r|$ ,  $Zw|w|$ ,  $Zq|q|$ ,  $Mw|w|$ ,  $Nv|v|$  and  $Nr|r|$ , while in the model developed by Feltman the sum of the contributions of each section is considered, calculated through a sectional cross flow drag coefficient, whose contribution is integrated along the entire length of the submarine.

Once the value of the cross-flow sectional coefficients  $c_d$  has been defined, the contribution of these forces and moments is obtained by integrating the values of the coefficients  $c_d$  multiplied by the local values along the length of the half square of the transverse velocity and of the effective projected area. In the simulation program, a single cross flow drag coefficient  $c_d$  was considered for each equation as the differences between the individual sections can be incorporated in the distribution of the widths and heights of the areas projected horizontally and longitudinally. It is appropriate to underline that the terms of the type  $Yv/v/R$ , for example, represent the difference between the experimental value of  $Yv/v/$ , and the contribution due to the "cross-flow" force. sail and the resulting vortex effect, in the Gertler model this contribution is considered globally within the hydrodynamic coefficients  $Yvw$ ,  $Zvv$ ,  $Kvw$ ,  $Mvv$  and  $Nvw$ , while in the model developed by Feltman, the sail effect is considered by taking into account both the effective distribution of speed in the single sections aft of the sail, and the value of the transverse speed calculated at the point of departure of the vortex of the sail at time  $t - \tau(x)$ , where  $\tau(x)$  is the interval of time required by the vorticity to transfer from the sail to the generic section  $x$  along the hull.

This time interval is obtained implicitly by integrating the longitudinal component  $u$  of the speeds over the same interval of time  $\tau(x)$ : The values of the starting coefficients  $CL$  instead are obtained from the total coefficients in the hypothesis that the transverse velocity is uniformly distributed.

In addition, there are some differences regarding the calculation of the rolling moment. In the expression of the roll moment, Feltman considers the moment due to the stern appendages during the combined roll and yaw motion, induced on the stern appendages by the vorticity generated by the sail, represented by the term  $Ki$ . Furthermore, Feltman considers the moment

generated by the aft appendages caused by the difference in lift caused by the hull covering the leeward appendage, represented by the terms  $K4s$  and  $K8s$ .

### 2.3.1 Feltman

This paragraph describes the equations relating to the Feltman model for the calculation of hydrodynamic forces

$$\vec{F}_{HULL} = \begin{bmatrix} X_{HULL} \\ Y_{HULL} \\ Z_{HULL} \\ K_{HULL} \\ M_{HULL} \\ N_{HULL} \end{bmatrix}$$

The hydrodynamic terms are calculated as a function of coefficients depending on the characteristics of the hull and appendages. Before describing the equations, the symbols used in them are listed except for the hydrodynamic coefficients.

$\rho$	the density of the water,
$m$	the mass of the submarine,
$u$	the surge speed,
$v$	the sway speed,
$w$	the heave speed,
$u_c$	command speed: full speed corresponding to the number of revolutions considered, in the event that the drift and rudder angle is zero,
$r$	the speed of rotation around the vertical axis,
$p$	the roll speed,
$q$	the pitch speed,
$\theta$	pitch angle,
$\Phi$	roll angle,
$\Psi$	yaw angle,
$x_G$	x coordinate of the center of gravity,
$y_G$	y coordinate of the center of gravity
$z_G$	z coordinate of the center of gravity,
$x_B$	x coordinate of the hull center,,
$y_B$	y-coordinate of the hull center,
$z_B$	z coordinate of the hull center,
$L$	the length between the perpendiculars,
$h(x)$	local hull height,
$b(x)$	local hull width,
$v_{FW}$	speed along the y axis on the sail at the point $(x_{FW}, z_{FW})$
$\tilde{v}_{FW}$	speed along the y axis on the sail at the point $(x_1, z_{FW})$
$x_{FW}$	x coordinate of the point at a quarter of the sail string
$z_{FW}$	z coordinate of the point at $0.42 * \text{span of the sail}$
$x_1$	coordinate of the starting position of the vortex generated by the sail
$x_2$	x coordinate of the furthest position reached by the vortex generated by the sail
$\tau(x)$	$\tau(x) = x_1 - x$

The hydrodynamic forces are calculated as follows.

### Surge

$$\begin{aligned}
 X_{HULL} &= \frac{\rho}{2} L^4 [X_{qq} q^2 + X_{rr} r^2 + X_{rp} rp] \\
 &+ \frac{\rho}{2} L^3 [X_{vr} vr + X_{wq} wq] \\
 &+ \frac{\rho}{2} L^2 [X_{vv} v^2 + X_{ww} w^2] \\
 &- \text{Resistenza}
 \end{aligned}$$

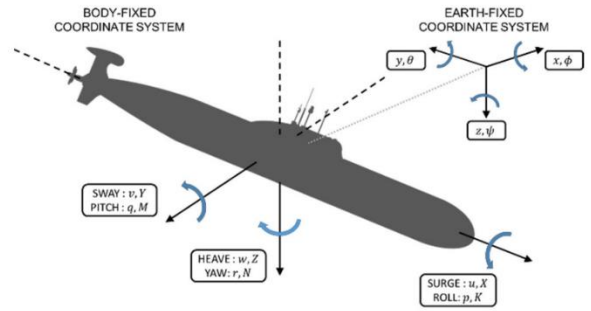


Figure 21 Coordinate system

### Sway

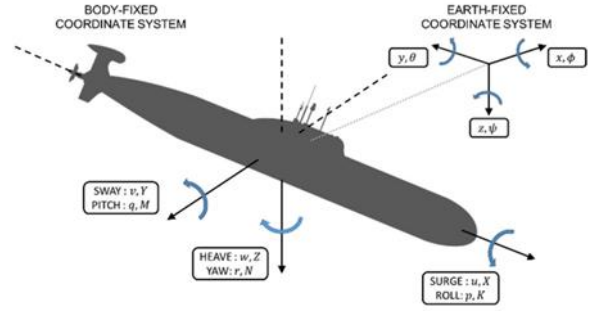
$$\begin{aligned}
 Y_{HULL} &= \frac{\rho}{2} L^4 [Y_{p|p|} p|p| + Y_{pq} pq] \\
 &+ \frac{\rho}{2} L^3 [Y_{rur} + Y_{pup} + Y_{wpp}] \\
 &+ \frac{\rho}{2} L^2 [Y_* u^2 + Y_v uv + Y_{v|R} v |(v^2 + w^2)^{0.5}] \\
 &- \frac{\rho}{2} C_D \int_L h(x) v(x) [w^2(x) + v^2(x)]^{0.5} dx \\
 &- \frac{\rho}{2} LC_L \int_{x_2}^{x_1} w(x) \tilde{v}_{FW}(t - \tau(x)) dx
 \end{aligned}$$

### Heave

$$\begin{aligned}
 Z_{HULL} &= \frac{\rho}{2} L^3 [Z_q uq + Z_{vp} vp] \\
 &+ \frac{\rho}{2} L^2 [Z_* u^2 + Z_w uw] \\
 &- \frac{\rho}{2} C_D \int_L b(x) w(x) [w^2(x) + v^2(x)]^{0.5} dx \\
 &+ \frac{\rho}{2} LC_L \int_{x_2}^{x_1} w(x) \tilde{v}_{FW}(t - \tau(x)) dx
 \end{aligned}$$

### Roll

$$\begin{aligned}
K_{HULL} &= \frac{\rho}{2} L^5 [K_{qr}qr + K_{p|p|p|p|}] \\
&+ \frac{\rho}{2} L^4 [K_p up + K_r ur + K_{wp}wp] \\
&+ \frac{\rho}{2} L^3 [K_* u^2 + K_{vR}uv + K_i uv_{FW}(t - \tau_T)] \\
&+ \frac{\rho}{2} L^3 (u^2 + v_S^2 + w_S^2) \beta_S^2 [K_{4S} \sin 4\Phi_S - K_{8S} \sin 8\Phi_S] \\
&+ \frac{\rho}{2} L^2 x_1 C_L \int_{x_2}^{x_1} w(x) \tilde{v}_{FW}(t - \tau(x)) dx
\end{aligned}$$



### Pitch

$$\begin{aligned}
M_{HULL} &= \frac{\rho}{2} L^5 M_{rp}rp \\
&+ \frac{\rho}{2} L^4 M_q uq \\
&+ \frac{\rho}{2} L^3 [M_* u^2 + M_w uw + M_{w|w|R} w |(v^2 + w^2)^{0.5}] \\
&+ \frac{\rho}{2} L^3 [M_{|w|u|w|} + M_{ww} |w|(v^2 + w^2)^{0.5}] \\
&+ \frac{\rho}{2} C_D \int_L x b(x) w(x) [w^2(x) + v^2(x)]^{0.5} dx \\
&+ \frac{\rho}{2} L C_L \int_{x_2}^{x_1} x v(x) \tilde{v}_{FW}(t - \tau(x)) dx
\end{aligned}$$

### Yaw

$$\begin{aligned}
N_{HULL} &= \frac{\rho}{2} L^5 N_{pq}pq \\
&+ \frac{\rho}{2} L^4 [N_p up + N_r ur] \\
&+ \frac{\rho}{2} L^3 [N_* u^2 + N_v uv + N_{v|v|R} v |(v^2 + w^2)^{0.5}] \\
&- \frac{\rho}{2} C_D \int_L x h(x) v(x) [w^2(x) + v^2(x)]^{0.5} dx \\
&- \frac{\rho}{2} L C_L \int_{x_2}^{x_1} x w(x) \tilde{v}_{FW}(t - \tau(x)) dx
\end{aligned}$$

### 2.3.2 Gertler

This paragraph describes the equations relating to the Gertler model for the calculation of hydrodynamic forces:

$$\vec{F}_{HULL} = \begin{bmatrix} X_{HULL} \\ Y_{HULL} \\ Z_{HULL} \\ K_{HULL} \\ M_{HULL} \\ N_{HULL} \end{bmatrix}$$

Hydrodynamic terms are calculated as a function of coefficients dependent on the characteristics of the hull and appendages. Before writing the equations, the symbols used in them are listed, except for the hydrodynamic coefficients.

$\rho$	the density of the water,
$m$	the mass of the submarine,
$u$	the surge speed,
$v$	the sway speed,
$w$	the heave speed,
$u_c$	command speed: full speed corresponding to the number of revolutions considered, in the event that the drift and rudder angle is zero,
$r$	the speed of rotation around the vertical axis,
$p$	the roll speed,
$q$	the pitch speed,
$\theta$	pitch angle,
$\Phi$	roll angle,
$\Psi$	yaw angle,
$x_G$	x coordinate of the center of gravity,
$y_G$	y coordinate of the center of gravity
$z_G$	z coordinate of the center of gravity,
$x_B$	x coordinate of the hull center,,
$y_B$	y-coordinate of the hull center,
$z_B$	z coordinate of the hull center,
$L$	the length between the perpendiculars,
$\eta$	$u_c / u$

This other part of hydrodynamics forces are calculated as:

### Surge

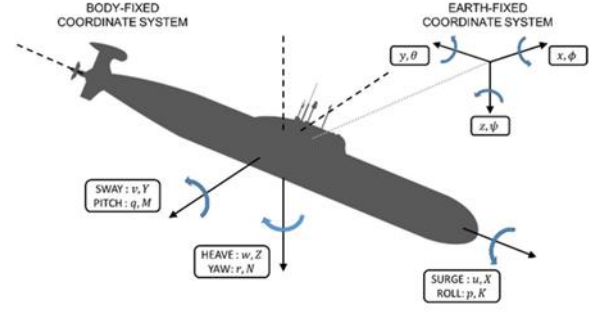
$$\begin{aligned}
 X_{HULL} = & + \frac{\rho}{2} L^3 [X_{vr} vr + X_{wq} wq] \\
 & + \frac{\rho}{2} L^2 [X_{uu} u^2 + X_{vv} v^2 + X_{ww} w^2] \\
 & + \frac{\rho}{2} L^2 [X_{vv\eta} v^2 + X_{ww\eta} w^2] (\eta - 1)
 \end{aligned}$$

### Sway

$$\begin{aligned}
 Y_{HULL} = & + \frac{\rho}{2} L^4 [Y_{p|p|} p|p| + Y_{pq} pq + Y_{qr} qr] \\
 & + \frac{\rho}{2} L^3 [Y_{vq} vq + Y_{wp} wp + Y_{wr} wr] \\
 & + \frac{\rho}{2} L^3 \left[ Y_{r*} ur + Y_p up + Y_{v|r|} \frac{v}{|v|} |(v^2 + w^2)^{0.5}| |r| \right] \\
 & + \frac{\rho}{2} L^2 [Y_{*} u^2 + Y_v uv + Y_{v|v|} v |(v^2 + w^2)^{0.5}|] \\
 & + \frac{\rho}{2} L^2 [Y_{vw} vw] \\
 & + \frac{\rho}{2} L^3 [Y_{r\eta} ur] (\eta - 1) \\
 & + \frac{\rho}{2} L^2 [Y_{v\eta} uv + Y_{v|v|\eta} v |(v^2 + w^2)^{0.5}|] (\eta - 1)
 \end{aligned}$$

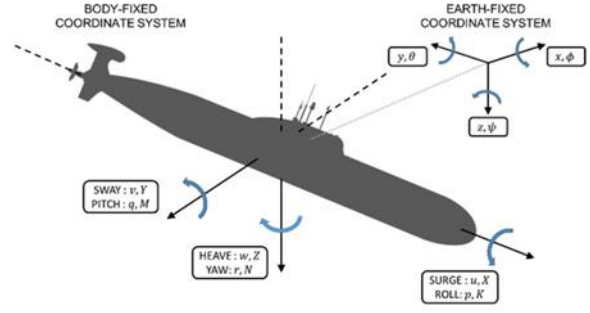
### Heave

$$\begin{aligned}
 Z_{HULL} = & \frac{\rho}{2} L^4 [Z_{pp} p^2 + Z_{rr} r^2 + Z_{rp} rp] \\
 & + \frac{\rho}{2} L^3 [Z_{vr} vr + Z_{vp} vp] \\
 & + \frac{\rho}{2} L^3 \left[ Z_q uq + Z_{w|q|} \frac{w}{|w|} |(v^2 + w^2)^{0.5}| |q| \right] \\
 & + \frac{\rho}{2} L^2 [Z_{*} u^2 + Z_w uw + Z_{w|w|} w |(v^2 + w^2)^{0.5}|] \\
 & + \frac{\rho}{2} L^2 [Z_{|w|} u|w| + Z_{ww} |w|(v^2 + w^2)^{0.5}] \\
 & + \frac{\rho}{2} L^2 [Z_{vv} v^2] \\
 & + \frac{\rho}{2} L^3 [Z_{q\eta} uq] (\eta - 1) \\
 & + \frac{\rho}{2} L^2 [Z_{w\eta} uw + Z_{w|w|\eta} w |(v^2 + w^2)^{0.5}|] (\eta - 1)
 \end{aligned}$$



### Roll

$$\begin{aligned} K_{HULL} &= \frac{\rho}{2} L^5 [K_{qr}qr + K_{pq}pq + K_{p|p|p|p|}] \\ &+ \frac{\rho}{2} L^4 [K_p up + K_r ur] \\ &+ \frac{\rho}{2} L^4 [K_{vq}vq + K_{wp}wp + K_{wr}wr] \\ &+ \frac{\rho}{2} L^3 [K_* u^2 + K_v uv + K_{v|v|v|} (v^2 + w^2)^{0.5}] \\ &+ \frac{\rho}{2} L^3 [K_{vw}vw] \\ &+ \frac{\rho}{2} L^3 [K_{*\eta} u^2] (\eta - 1) \end{aligned}$$



### Pitch

$$\begin{aligned} M_{HULL} &= \frac{\rho}{2} L^5 [M_{pp}p^2 + M_{rr}r^2 + M_{rp}rp + M_{q|q|q|q|}] \\ &+ \frac{\rho}{2} L^4 [M_{vr}vr + M_{vp}vp] \\ &+ \frac{\rho}{2} L^4 [M_q uq + M_{|w|q|} (v^2 + w^2)^{0.5} |q|] \\ &+ \frac{\rho}{2} L^3 [M_* u^2 + M_w uw + M_{w|w|w|} (v^2 + w^2)^{0.5}] \\ &+ \frac{\rho}{2} L^3 [M_{|w|u|w|} + M_{ww} |w| (v^2 + w^2)^{0.5}] \\ &+ \frac{\rho}{2} L^3 [M_{vv}v^2] \\ &+ \frac{\rho}{2} L^4 [M_{q\eta} uq] (\eta - 1) \\ &+ \frac{\rho}{2} L^3 [M_{w\eta} uw + M_{w|w|\eta} |w| (v^2 + w^2)^{0.5}] (\eta - 1) \end{aligned}$$

### Yaw

$$\begin{aligned} N_{HULL} &= \frac{\rho}{2} L^5 [N_{pq}pq + N_{qr}qr + N_{r|r|r|r|}] \\ &+ \frac{\rho}{2} L^4 [N_{wr}wr + N_{wp}wp + N_{vq}vq] \\ &+ \frac{\rho}{2} L^4 [N_p up + N_r ur + N_{|v|r|} (v^2 + w^2)^{0.5} |r|] \\ &+ \frac{\rho}{2} L^3 [N_* u^2 + N_v uv + N_{v|v|v|} (v^2 + w^2)^{0.5}] \\ &+ \frac{\rho}{2} L^3 [N_{vw}vw] \\ &+ \frac{\rho}{2} L^4 [N_{r\eta} ur] (\eta - 1) \\ &+ \frac{\rho}{2} L^3 [N_{v\eta} uv + N_{v|v|\eta} |v| (v^2 + w^2)^{0.5}] (\eta - 1) \end{aligned}$$

## 2.4 Force of rudders (X configuration)

X-form rudder has the higher rudder efficiency and its manipulate surface area is smaller about 10% than cross rudder, so that submarine can avoid collision problems when are mooring. Secondly, X-form rudder reduces the serious consequences by rudder-blocked and improves the security and the underwater dynamic unsinkability. Besides, X-form rudder reduces the heeling moment, weight, and stern heaviness when cross-rudder submarine turning and having an advantage to sail steadily when it is attacked. Finally, X-form rudder lower interaction between propeller and rudder and the noise.

Cross-form rudder control surface has two blades, which appears orthogonal with the horizontal and vertical, and X-form rudder control surface consists of four rudder blades, which are distributed with the X-form. Cross-form rudder blades has two sets of control system, which consist of the horizontal control system and the elevator control system instead the X-form rudder blades need 4 sets of control system respectively. Submarine cross-form rudder blades are named as the rudder and the elevator, which corresponding rudder Angle are  $\delta_r$  and  $\delta_s$ , and comparing with cross-form rudder, X-form rudder blades are named as Num.1 rudder, Num.2 rudder, Num.3 rudder and Num.4 rudder (figure 22), which corresponding rudder Angle are  $\delta_1$ ,  $\delta_2$ ,  $\delta_3$  and  $\delta_4$ .

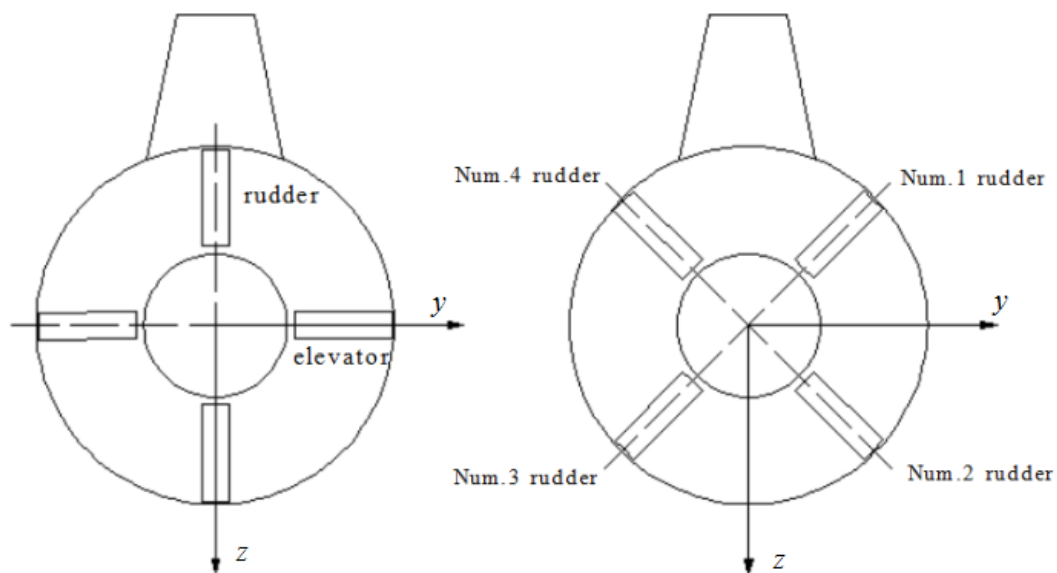


Figure 22 Nomenclature of rudders

Firstly, is necessary to establish submarine coordinate system in cross-form rudder control surface, among that, the y axis points to the starboard side of the submarine, the z axis points to the center of the earth. In order to analyze expediently, we might have cross-form rudder force is proportional to the corresponding rudder Angle, namely the rudder steering force (torque) is proportional to the rudder Angle, and the elevator force (torque) is proportional to the elevator Angle. Setting the coefficient of cross-form rudder effect as  $Y\delta_r$  and  $Z\delta_s$ , get the force (torque) formula expressions of cross-form rudder

$$\begin{aligned}\vec{F}_y &= (Y\delta, \delta_r, 0) \\ \vec{F}_z &= (0, Z_r, \delta_s)\end{aligned}$$

In the same way, establishing submarine coordinate system in X-form rudder control surfaces, each rudder blade of X-form rudder control is at an angle of  $45^\circ$  with longitudinal or vertical surface. Therefore, a blade could produce a space force and a torque, unlike the cross-form rudder which makes a single force. For the rudder force (torque) effect of X-form rudder

Rudder Angle $\delta_i$	Plus Or Minus	Movements
$\delta_1$	$>0$	Turn right, Diving, Heel left
	$<0$	Turn left, Floating, Heel right
$\delta_2$	$>0$	Turn right, Floating, Heel right
	$<0$	Turn left, Diving, Heel left
$\delta_3$	$>0$	Turn right, Diving, Heel right
	$<0$	Turn left, Floating, Heel left
$\delta_4$	$>0$	Turn right, Floating, Heel left
	$<0$	Turn left, Diving, Heel right

Table 1. Configuration of rudder angles for movements

The formula expression for the single rudder can be get as:

$$\begin{aligned}F_1 &= (Y_1\delta_1 \cos \pi/4, Y_1\delta_1 \sin \pi/4) \\ F_3 &= (Y_3\delta_3 \cos \pi/4, Y_3\delta_3 \sin \pi/4) \\ F_2 &= (-Z_2\delta_2 \cos \pi/4, Z_2\delta_2 \sin \pi/4) \\ F_4 &= (-Z_4\delta_4 \cos \pi/4, Z_4\delta_4 \sin \pi/4)\end{aligned}$$

Among that,  $Y_1=Y_3=0.5Y_r$ ,  $Z_2=Z_4=0.5Z_s$ . as the  $\delta_1=\delta_3=(-\delta_2)=(-\delta_4)$  and  $\delta_1=\delta_3=\delta_2=\delta_4$ ,

X-form rudder effect in y-axis and z-axis:

$$\begin{aligned}F_y &= Y_1\delta_1\cos 45^\circ + Y_3\delta_3\cos 45^\circ + Z_2\delta_2\sin 45^\circ + Z_4\delta_4\sin 45^\circ = 1.414Y_r\delta_r \\ F_z &= Y_1\delta_1\sin 45^\circ + Y_3\delta_3\sin 45^\circ + Z_2\delta_2\cos 45^\circ + Z_4\delta_4\cos 45^\circ = 1.414Z_s\delta_s\end{aligned}$$

It is not difficult to find that rudder effect improves obvious when the cross-form rudder equivalently transforms X-form rudder.

### 2.4.1 Feltman

The symbols used in the equations except for the hydrodynamic coefficients are listed below.

$u$	surge speed
$\delta$	rudder angle,
$\eta$	$u/u_s$
$u_s$	speed which corresponds to a hull resistance value equal to the propeller thrust $T$
$C$	coefficient used to scale the lift and drag values from model to full scale

$C$  parameter is calculated as above

:

$$\Delta X = \Delta X_1 + \frac{\Delta X_2}{(\Delta X_3 + \log_{10} u)^2}$$

$$C = C_6 + (C_7 + C_8 \Delta X)^{0.5}$$

Where:

$C_6, C_7, C_8, \Delta X_1, \Delta X_2, \Delta X_3$  are constant

The components due to the contributions of the different rudders are indicated by different subscripts relating to the case of cross rudders. In particular, the subscript  $r$  indicates the vertical aft rudders, the subscript  $s$  indicates the horizontal aft rudders, while the subscript  $b$  indicates the horizontal forward rudders.

#### Surge

$$X_{RUDD} = \frac{\rho}{2} L^2 [X_{\delta r \delta r} u^2 \delta_r^2 + X_{\delta s \delta s} u^2 \delta_s^2 + X_{\delta b \delta b} u^2 \delta_b^2]_{-}$$

#### Sway

$$Y_{RUDD} = \frac{\rho}{2} L^2 \left[ Y_{\delta r} u^2 \delta_r + Y_{\delta r \eta} u^2 \delta_r \left( \eta - \frac{1}{C} \right) C \right]$$

#### Heave

$$Z_{RUDD} = \frac{\rho}{2} L^2 \left[ Z_{\delta s} u^2 \delta_s + Z_{\delta b} u^2 \delta_b + Z_{\delta s \eta} u^2 \delta_s \left( \eta - \frac{1}{C} \right) C \right]$$

#### Roll

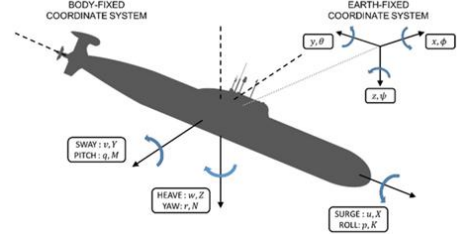
$$K_{RUDD} = \frac{\rho}{2} L^3 \left[ K_{\delta r} u^2 \delta_r + K_{\delta r \eta} u^2 \delta_r \left( \eta - \frac{1}{C} \right) C \right]$$

#### Pitch

$$M_{RUDD} = \frac{\rho}{2} L^3 \left[ M_{\delta s} u^2 \delta_s + M_{\delta b} u^2 \delta_b + M_{\delta s \eta} u^2 \delta_s \left( \eta - \frac{1}{C} \right) C \right]$$

#### Yaw

$$N_{RUDD} = \frac{\rho}{2} L^3 \left[ N_{\delta r} u^2 \delta_r + N_{\delta r \eta} u^2 \delta_r \left( \eta - \frac{1}{C} \right) C \right]$$



### 2.4.2 Gertler

The symbols used in the equations with the exception of the hydrodynamic coefficients are listed below.

- u surge speed,
- $\delta$  rudder angle,
- u<sub>c</sub> command speed: full speed corresponding to the number of revolutions considered, in the event that the drift and rudder angle is zero,
- $\eta$  u<sub>c</sub> / u

The components due to the contributions of the different rudders are indicated by different subscripts relating to the case of cross rudders. In particular, the subscript **r** indicates the vertical aft rudders, the subscript **s** indicates the horizontal aft rudders, while the subscript **b** indicates the horizontal forward rudders.

#### Surge

$$X_{RUDD} = \frac{\rho}{2} L^2 [X_{\delta r \delta r} u^2 \delta_r^2 + X_{\delta s \delta s} u^2 \delta_s^2 + X_{\delta b \delta b} u^2 \delta_b^2] \\ + \frac{\rho}{2} L^2 [X_{\delta r \delta r \eta} u^2 \delta_r^2 + X_{\delta s \delta s \eta} u^2 \delta_s^2] (\eta - 1)$$

#### Sway

$$Y_{RUDD} = \frac{\rho}{2} L^3 [Y_{|r| \delta r} u |r| \delta_r] \\ + \frac{\rho}{2} L^2 [Y_{\delta r} u^2 \delta_r] \\ + \frac{\rho}{2} L^2 [Y_{\delta r \eta} u^2 \delta_r] (\eta - 1)$$

#### Heave

$$Z_{RUDD} = \frac{\rho}{2} L^3 [Z_{|q| \delta s} u |q| \delta_s] \\ + \frac{\rho}{2} L^2 [Z_{\delta s} u^2 \delta_s + Z_{\delta b} u^2 \delta_b] \\ + \frac{\rho}{2} L^2 [Z_{\delta s \eta} u^2 \delta_s] (\eta - 1)$$

#### Roll

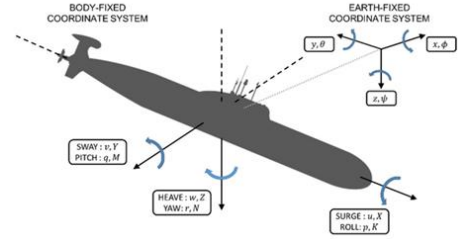
$$K_{RUDD} = \frac{\rho}{2} L^3 [K_{\delta r} u^2 \delta_r]$$

#### Pitch

$$M_{RUDD} = \frac{\rho}{2} L^4 [M_{|q| \delta s} u |q| \delta_s] \\ + \frac{\rho}{2} L^3 [M_{\delta s} u^2 \delta_s + M_{\delta b} u^2 \delta_b] \\ + \frac{\rho}{2} L^3 [M_{\delta s \eta} u^2 \delta_s] (\eta - 1)$$

#### Yaw

$$N_{RUDD} = \frac{\rho}{2} L^4 [N_{|r| \delta r} u |r| \delta_r] \\ + \frac{\rho}{2} L^3 [N_{\delta r} u^2 \delta_r] \\ + \frac{\rho}{2} L^3 [N_{\delta r \eta} u^2 \delta_r] (\eta - 1)$$



## 2.5 Force of the propeller

An accurate schematization of the forces developed by the propeller is of considerable importance in the context of a correct simulation of maneuvers and of those that involve the inversion of the thrust and the consequent inversion of the speed, such as the case of the forced arrest.

The thrust supplied by the propeller to the underwater vehicle is introduced in the mathematical model equal to the thrust developed by the propeller, less the suction coefficient which in the simulation model is assumed to be constant despite varying the speed. Both the thrust (T) supplied by the propeller and the torque (Qp) absorbed by it are functions of the number of revolutions and the advance speed of the propeller. It should be noted that in this context the traditional isolated helix diagram can lead to situations of ambiguity as the same value of the surplus coefficient characterizes two different operating conditions of the helix, together with the fact that this representation is not valid for number of revolutions close to zero. Furthermore, when the submarine is in maneuver, the propeller will find itself operating at values of the surplus coefficient different from those reported in the usual isolated propeller diagrams.

To overcome these drawbacks, use was made of the representation of the Wageningen propellers in the four Error quadrants. The reference origin has not been found. In this work the operating coefficients of the helix  $C_T$  and  $C_Q$ , dimensionless in terms of the axial and circumferential speed, are reported, relative to many helices, as a function of the pitch angle hydrodynamic with values between 0 and  $2\pi$ .

$$\beta = \arctg \frac{u(1-w)}{0.7 \pi n D}$$
$$C_T = \frac{T}{0.5 \rho \pi D^2 [u^2(1-w)^2 + (0.7 \pi n D)^2]}$$
$$C_Q = \frac{Q}{0.5 \rho \pi D^3 [u^2(1-w)^2 + (0.7 \pi n D)^2]}$$

The simulation program makes it possible to modify the characteristic of the isolated propeller in the first quadrant by entering the experimental values obtained from any tests obtained on the actual propeller of the underwater vehicle.

The mathematical simulation model does not provide for the study of the dynamic behavior of the motor apparatus. Except for the free stop maneuver, the variations of the propeller revolutions over time are schematized as linear delays with the angular coefficient supplied as input.

The differential equation that regulates the dynamics of the engine during the free stop maneuver is the following:

$$2\pi(I_m + I_p) \frac{dn}{dt} = -Q_P - Q_F$$

Where:

$I_m$	polar moment of inertia of the motor
$I_p$	polar moment of inertia of the propeller
$Q_p$	propeller torque
$Q_f$	friction torque

## 2.6 Mass variation in leak condition emergency

The solution of the equations of motion requires the temporal variations of mass, center of gravity and moments of inertia to be known.

In the case of a submersible vehicle, note the geometry of the ballast tanks and of the rooms subject to possible leaks due to the breakage of a sea cock, (considering this to be the most serious condition), the laws of variation over time will be a function of the flow rate of water entering through the leak and of water coming out of the ballast tanks. This flow rate depends on the geometry of the leak opening, on the discharge points of the ballast tanks and on the characteristics of the apparatus that favors its expulsion.

The laws of mass variation, center of gravity and moments of inertia during the ascent of the underwater vehicle in the event of a leak are analyzed in detail below.

The ascent in the event of a leak has been studied considering the following phases:

- determination of the flow of water that flows through the hole over time.
- from the determination of the flow of water that is disembarked over time by the ballast tanks.
- calculation of the mass of the center of gravity and of the moments of inertia of the underwater vehicle over time following the embarkation and disembarkation of the water.

The mass flow rate of water  $q$  that enters the room subject to flooding can be defined as:

$$Q = \rho \mu A_F \sqrt{2gH(t)}$$

Being:

- $\rho$  = sea water density considered constant.
- $\mu$  = inflow coefficient of the section.
- $A_F$  = area of the leak light.
- $g$  = gravity.
- $H$  = piezometric height at the phallus light.
- 

The value of  $H(t)$  is thus defined

$$H(t) = z(t) + X_F \sin\theta + Y_F \cos\theta \sin\varphi + Z_F \cos\theta \cos\varphi + \frac{V_F^2}{2g} + \frac{p_a - p_i}{\rho g}$$

Being:

- $z(t)$  the z-coordinate of the hull center of the vehicle in the absolute reference system.
- $X_F, Y_F, Z_F$  the coordinates of the fault light in the solid reference system originating in the center of the hull.
- $\theta$  the pitch angle.
- $\varphi$  the roll angle.
- $V_F$  the rate of outflow of water at the leakage light.
- $P_a$  atmospheric pressure.
- $P_i$  the internal pressure of the flooded room.
- 

The coefficient of efflux  $\mu$ , that is, the ratio between the real and the ideal flow rate, which can be determined experimentally, can also be written as a product between the speed coefficient and the contraction coefficient

$$\mu = C_C C_V$$

Being:

- $C_C$  = coefficient of contraction equal to the ratio (Contracted section area / Fault light area).
- $C_V$  = speed coefficient equal to the ratio (Speed in the contracted section / Ideal average speed  $(\sqrt{2gh})$ ).

Numerical values of  $\mu$  (0.5 - 0.7) are given in engineering manuals.

### 2.6.1 Determination of the flow rate of water expelled from the ballast tanks

The true technology used for the ascent, for reasons of confidentiality, will not be mentioned and the formulas regarding its operation will be omitted, the explanation of the generic crate filling system with compressed air is used below.

The flow rate of water expelled from each individual ballast box can be considered as the sum of the following three contributions:

- Air flow rate fed into the case through the high-pressure compressed air system.
- Flow rate due to the expansion of the air following the change in altitude of the underwater vehicle.
- Flow rate due to the heat exchange between the sea water and the air contained in the case.

Thus, the expression of the mass of water expelled from the single case at the generic instant  $t$  is given by the expression:

$$m_c = \rho \int_{t_0}^t \left[ q_a(t) + m_a(t) - \frac{dh(t)}{h(t)} + m_a(t) d \left( \frac{T_{as}}{T_a} \right) \right] dt$$

where:

- $\rho$  is the density of seawater, considered constant.
  - $q_a$  volumetric air flow rate fed into the ballast box.
  - $m_a$  mass flow rate of the air introduced into the ballast box.
  - $h(t)$  absolute piezometric height of the air in the case.
  - $T_a$  air temperature in the ballast box without taking into account the heat exchange.
  - $T_{as}$  air temperature in the ballast box taking into account the heat exchange.
- $t_0$  start time emptying case.

$$h(t) = z(t) + X_c \sin \theta + Y_c \cos \theta \sin \varphi + Z_c \cos \theta \cos \varphi + \frac{V_D^2}{2g} - hac + \frac{p_a}{\rho g}$$

where:

- $z$  is the share of the hull center of the vehicle in the absolute reference system.  
 $X_c, Y_c, Z_c$  are the coordinates of the light of the ballast boxes in the solidarity reference system originating in the center of the hull.
- $\theta$  is the pitch angle.
- $\varphi$  is the roll angle.
- $V_D$  speed of water outflow at the light of the case.
- $hac$  water height in the ballast crate.
- $p_a$  atmospheric pressure.

The values of the air temperature with and without heat exchange are given by the expression:

$$T_{as} = \frac{\int_{t_0}^t m_a T_u dt}{\int_{t_0}^t m_a dt} + \frac{\int_{t_0}^t Q_c dt}{C_p \int_{t_0}^t m_a dt}$$

$$T_a = \frac{\int_{t_0}^t m_a T_u dt}{\int_{t_0}^t m_a dt}$$

where:

- $T_u$  air temperature at the outlet of the compressed air system.
- $Q_c$  heat flow rate function of the exchange surface of the case, the total heat transfer coefficient, the seawater temperature and the  $T_{as}$  temperature of the air in the case.
- $C_p$  specific heat at constant pressure.

The mass of water landed from the ballast box is obtained by integrating the expression of the  $m_c$  once the values of the volumetric flow rate of the  $q_a$  output air, the mass flow rate but and the output temperature  $tu$  of the air in the box are known as a function of time.

Given the complexity of the compressed air circuits, in order to calculate the above quantities, it is necessary to reduce the entire network and a simple hydraulically equivalent line.

The calculation of the flow rate and temperature at the outlet was carried out based on what is reported in. Analytical development is omitted because it is beyond the limits of the present work.

Note the characteristics of the supply network and those of the air in the cylinders (pressure, temperature, volume) for each case it is possible to calculate for different values, of the discharge pressure the values of the weight flow rate, of the volumetric flow rate and of the temperature at the outlet in the case as a function of the pressure in the cylinders.

To derive the expression as a function of time it has been assumed that the pressure of the cylinders varies with the characteristic law of perfect gases:

$$PB(t + dt) = \frac{m_B(t) - m_a}{V_B} R \cdot TB(t)$$

where:

- $m_B(t)$  = mass of the air contained in the cylinders instantly  $t$ .
- $V_B$  = total volume of cylinders.
- $R$  = constant characteristic of perfect gases.
- $T_B$  = air temperature in the cylinders instantly  $t$ .
- $PB(t+dt)$  = air pressure in the cylinders instantly  $t + dt$ .
- $m_a$  = mass flow rate function of pressure in cylinders and at the outlet

Assuming that the expansion is adiabatic with exponent  $K$  we have:

$$PB(t + dt) = \frac{m_B(t) - m_a}{V_B} R \cdot TBo \left( \frac{PB(t)}{PBo} \right)^{\frac{k-1}{k}}$$

where:

- TBo initial temperature in the cylinders.
- PBo initial pressure in cylinders.

Note the expression of PB as a function of time it is possible at any time to calculate the values of ma, qa and Tu and by means of the expression of mc derive the mass of water landed from each individual box.

### 2.6.2 Calculation of mass, center of gravity and moments of inertia

Note the initial values of the following quantities:

- $X_{Go}, Y_{Go}, Z_{Go}$  coordinates of the center of gravity with respect to the CB hull center.
- $m_o$  initial mass of the submarine.
- $I_{xGo}, I_{yGo}, I_{zGo}$  barycentric moments of inertia.
- $I_{xyGo}, I_{yzGo}, I_{zxGo}$  barycentric inertia products;

the expression of the mass of the coordinates of the center of the hull and of the inertias in the treatment of ascent in case of leak vary with the following temporal laws:

$$m(t) = m_o + \sum_i m_i(t)$$

$$X_G(t) = X_{Go} + \frac{\sum_i m_i(X_{ci} - X_{Go})}{m(t)}$$

$$Y_G(t) = Y_{Go} + \frac{\sum_i m_i(Y_{ci} - Y_{Go})}{m(t)}$$

$$Z_G(t) = Z_{Go} + \frac{\sum_i m_i(Z_{ci} - Z_{Go})}{m(t)}$$

$$I_{X_B}(t) = I_{X_G}(t) + m(t)[Y_G^2(t) + Z_G^2(t)]$$

$$I_{Y_B}(t) = I_{Y_G}(t) + m(t)[X_G^2(t) + Z_G^2(t)]$$

$$I_{Z_B}(t) = I_{Z_G}(t) + m(t)[X_G^2(t) + Y_G^2(t)]$$

$$I_{XY_B}(t) = I_{XY_G}(t) + m(t) \cdot X_G(t) \cdot Y_G(t)$$

$$I_{YZ_B}(t) = I_{YZ_G}(t) + m(t) \cdot Y_G(t) \cdot Z_G(t)$$

$$I_{XZ_B}(t) = I_{XZ_G}(t) + m(t) \cdot X_G(t) \cdot Z_G(t)$$

$$\begin{aligned}
I_{X_G}(t) &= I_{X_{Go}} + \sum_i m_i [(Y_{Ci} - Y_{Go})^2 + (Z_{Ci} - Z_{Go})^2] + \sum_i I_{X_{pi}} \\
I_{Y_G}(t) &= I_{Y_{Go}} + \sum_i m_i [(X_{Ci} - X_{Go})^2 + (Z_{Ci} - Z_{Go})^2] + \sum_i I_{Y_{pi}} \\
I_{Z_G}(t) &= I_{Z_{Go}} + \sum_i m_i [(X_{Ci} - X_{Go})^2 + (Y_{Ci} - Y_{Go})^2] + \sum_i I_{Z_{pi}} \\
I_{XY_G}(t) &= I_{XY_{Go}} + \sum_i m_i (X_{Ci} - X_{Go})(Y_{Ci} - Y_{Go}) + \sum_i I_{XY_{pi}} \\
I_{YZ_G}(t) &= I_{YZ_{Go}} + \sum_i m_i (Y_{Ci} - Y_{Go})(Z_{Ci} - Z_{Go}) + \sum_i I_{YZ_{pi}} \\
I_{ZX_G}(t) &= I_{ZX_{Go}} + \sum_i m_i (X_{Ci} - X_{Go})(Z_{Ci} - Z_{Go}) + \sum_i I_{ZX_{pi}}
\end{aligned}$$

where:

- $X_G(t)$ ,  $Y_G(t)$ ,  $Z_G(t)$  position of the center of gravity with respect to the CB at instant t.
- $m_i$  generic mass embarked (positive)/landed (negative).
- $X_{ci}$ ,  $Y_{ci}$ ,  $Z_{ci}$  position of the center of the mass  $m_i$  with respect to the CB of the medium.
- $I_{X_B}(t)$ ,  $I_{Y_B}(t)$ ,  $I_{Z_B}(t)$  moments of inertia of the medium with respect to a backhoe through the CB: these are the moments that enter the equation of motion.
- $I_{XY_B}(t)$ ,  $I_{YZ_B}(t)$ ,  $I_{ZX_B}(t)$  products of inertia of the medium with respect to a backhoe through the CB: these are the inertia products that enter the equation of motion.
- $I_{X_G}(t)$ ,  $I_{Y_G}(t)$ ,  $I_{Z_G}(t)$ ,  $I_{XY_G}(t)$ ,  $I_{YZ_G}(t)$ ,  $I_{ZX_G}(t)$  moments and products of inertia with respect to a barycentric backhoe at the instant t.
- $m(t)$  massa all'istante t del mezzo;
- $I_{X_{pi}}$ ,  $I_{Y_{pi}}$ ,  $I_{Z_{pi}}$ ,  $I_{XY_{pi}}$ ,  $I_{YZ_{pi}}$ ,  $I_{ZX_{pi}}$  moments and products of inertia proper to the mass m.

## 3 Automatic control system

### 3.1 Analysis of submarine model

The analysis of the transfer functions of a torpedo-shaped submarine drone can be traced back to the experimental studies of Peter Corke and Peter Ridley, who developed linearized equations able to indicate the behavior of the drone and verify the stability of the system to apply automatic controls.

The transfer functions of the 3 angles are simplified in the shape:

$$\frac{\theta(s)}{\delta_s(s)} = \frac{K}{\frac{s^2}{w_n^2} + \frac{2\varepsilon}{w_n} s + 1}$$

Especially:

#### Pitch

$$\frac{\psi(s)}{\delta_r(s)} = \frac{\left(\frac{2N_{uu}\delta_r}{N_{uv}}\right)}{\left(\frac{I_{zz}-N_{\dot{r}}}{N_{uv}V^2}\right) s^2 + \left(\frac{-mX_g-N_{ur}}{N_{uv}V^2}\right) V s + 1}$$

#### Yaw

$$\frac{\theta(s)}{\delta_s(s)} = \frac{\left(\frac{2M_{uu}\delta_s V^2}{Z_g W - M_{uw} V^2}\right)}{\left(\frac{I_{yy}-M_{\dot{q}}}{Z_g W - M_{uw} V^2}\right) s^2 + \left(\frac{mX_g - M_{uq}}{Z_g W - M_{uw} V^2}\right) V s + 1}$$

#### Roll

$$\frac{\phi(s)}{\delta_a(s)} = \frac{\left(\frac{4K_{uu}\delta_a}{Z_g W}\right)}{\left(\frac{I_{xx}-K_{\dot{p}}}{Z_g W}\right) s^2 + 1}$$

- $(\delta_r, \delta_s, \delta_a)$ = rudder, stern plane and aileron angles
- $N_{uu}\delta_r, N_{uu}\delta_s, N_{uu}\delta_a$  = rudder, stern plane and aileron effectiveness
- $N_{ur}, M_{uw}$ = body moment
- $N_{\dot{r}}, M_{\dot{q}}, K_{\dot{p}}$ = added mass
- $N_{ur}, M_{uw}$ = added mass cross terms
- $X_g, Z_g$ =coordinate relative to the CG respect to the center of gravity
- $s$ =variable  $s$  of transfer functions

From the transfer functions it is possible to understand how the system reacts according to the variables and it can be observed how speed influence the pitch and yaw transfer function while the roll remains unchanged. As a result, any change in speed will lead to a different response curve. In addition, open loop pitch and yaw analyses are stable.

The analysis of the Dc gain (figure 23) of these transfer functions shows how it is modified with respect to the pitch while for yaw and roll remains unchanged.

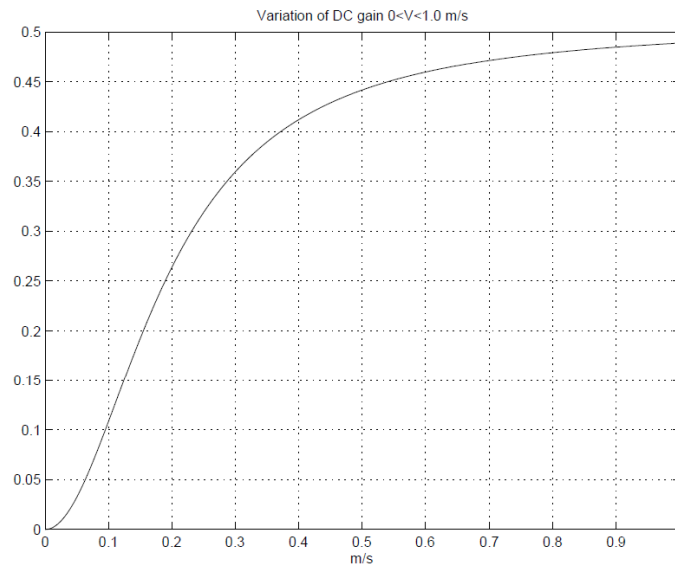


Figure 23 Open Loop DC gain vs drone speed

While the natural frequency and damping ratio of the pitch poles (figure 24,25) maintain a proportional behavior like the Dc gain.

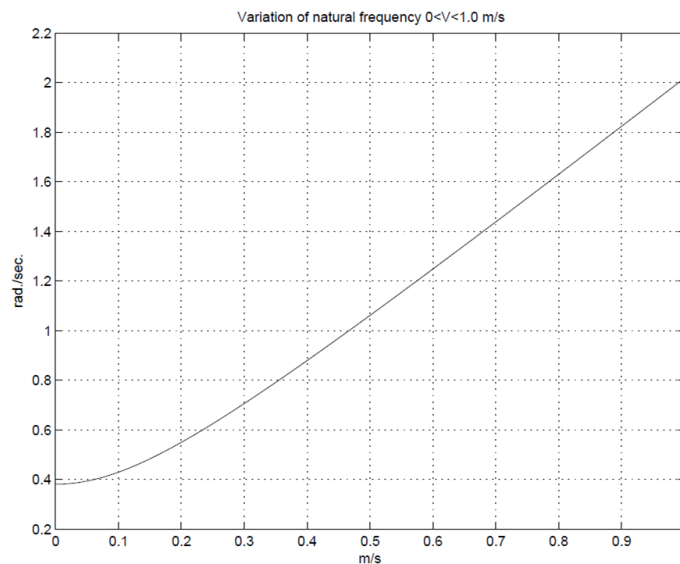


Figure 24 Natural frequency vs speed

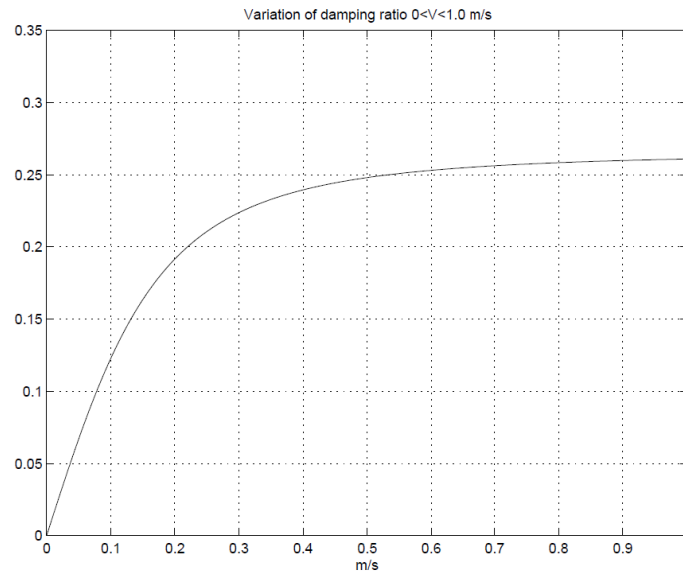


Figure 25 Variation of damping vs speed

From the following analysis of the closed loops based on the speed it is possible to choose which control system utilize, in our case it was necessary to apply a control on the pitch angle and one on the roll that acted simultaneously to stabilize the movements during the tests.

### 3.2 PID control

Various options for the Control System were evaluated but it was chosen a PID system to start dealing with the problem in a standard way trying to operate in a simple ambient with a control system that can be easily implemented on visual studio. However, this is to be considered as a first approach to insert a control system. Is assumed, once drone will be completed, to use other types of control systems.

#### 3.2.1 PID introduction

The PID controller was born in 1922, from a theoretical study by the Russian American engineer Nicolas Minorsky. Minorsky who was researching and designing the ship's automatic steering for the US Navy. He had his analysis of the observations of a helmsman. As the helmsman adjusted the course not only according to the present error, but also to the past one and the current increase in change, this allowed him to understand how these 3 parameters are able to manage the control of a system.

As the name suggests, PID algorithm consists of three basic coefficients which are varied to get optimal response (figure 26):

- proportional,
- integral
- derivative

### **proportional**

The proportional term produces an output value proportional to the current error value. The proportional response can be adjusted by multiplying the error by a constant  $K_p$ , called the proportional gain constant.

The proportional term is given by  $P = K_p e(t)$

If the proportional gain is too high, the system can become unstable. On the contrary, a small gain results in a small output response to a large input error and a less responsive or less sensitive controller. If the proportional gain is too low, the control action may be too small when responding to system disturbances. The importance of  $K_p$  is high and often must be compared to the response of the closed loop system

### **Integral**

The contribution from the integral term is proportional to both the magnitude of the error and the duration of the error. The integral in a PID controller is the sum of the instantaneous error over time and gives the accumulated offset that should have been corrected previously. The accumulated error is then multiplied by the integral gain ( $K_i$ ) and added to the controller output.

The integral term is given by  $I_{out} = K_i \int_0^t e(\tau) dt$

The integral term accelerates the movement of the process towards setpoint and eliminates the residual steady-state error that occurs with a pure proportional controller. However, since the integral term responds to accumulated errors from the past, it can cause the present value to overshoot the setpoint value (see the section on loop tuning).

## Derivative

The derivative of the process error is calculated by determining the slope of the error over time and multiplying this rate of change by the derivative gain  $K_d$ . The magnitude of the contribution of the derivative term to the overall control action is termed the derivative gain,  $K_d$ .

The derivative term is given by 
$$D_{out} = K_d \frac{de(t)}{dt}$$

Derivative action predicts system behavior and improves settling time and stability of the system. An ideal derivative is not causal, so that implementations of PID controllers include an additional low-pass filtering for the derivative term to limit the high-frequency gain and noise. Derivative action is seldom used in practice though by one estimate in only 25% of deployed controllers, because of its variable impact on system stability in real-world applications.

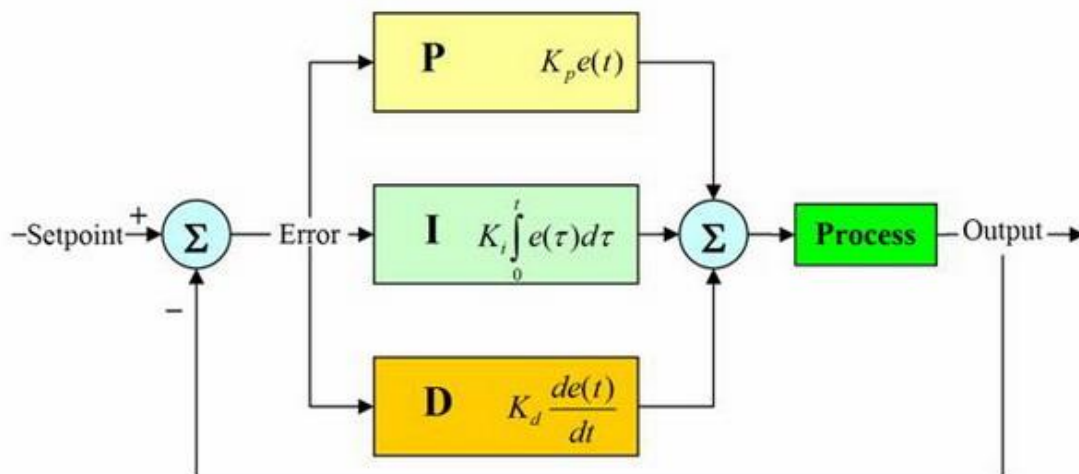


Figure 26 PID scheme

### 3.2.2 PID tuning

The tuning of the PID depends mainly on the type of objective that the System must achieve, in our case a target angle was required to be maintained during certain tests, for example in the emergence the drone should keep a pitch of  $30^\circ$  with maximum at  $35^\circ$ .

In table 2 is shown the effects of changing PID parameters:

Table 2. PID tuning effect

	Rise time	Overshoot	Settling Time	Steady-state error	stability
<b>Kp</b>	decrease	increase	Small change	decrease	decrease
<b>Ki</b>	decrease	increase	increase	eliminate	degrade
<b>Kd</b>	Minor change	decrease	decrease	No effect in theory	Improve if $Kd$ small

For the tuning of the PID parameters of the pitch it was chosen to use a genetic algorithm in order to obtain more accurate values for each test performed, however this does not apply to the PID of the roll as it was done manually since speed doesn't affect roll response.

The two PID controllers therefore work balancing, as previously mentioned, but it was chosen to compensate the roll angle only with the rear rudders, as those in the bow work better for changes in altitude. The main angles compensated are shown in figures 27.

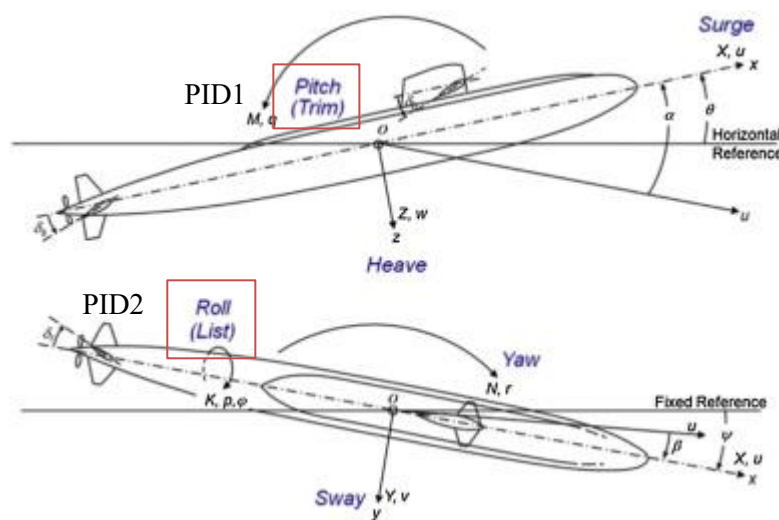


Figure 27 Angles and principal direction of the drone, roll and pitch are controlled

### 3.2.3 PID distribution

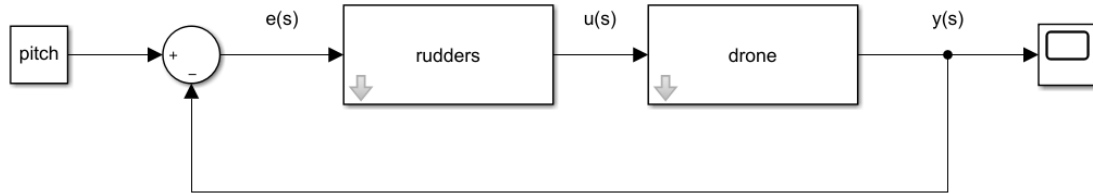


Figure 28 Basic block system

An important fact for the analysis of the system is the limit of the rudders; in fact, it is assumed that the rear rudders can individually reach a maximum of  $35^\circ$ , while the front ones  $20^\circ$ . Initially the drone used only one PID for both rudders (figure 29), so those in front went in saturation earlier compared to the rear ones.

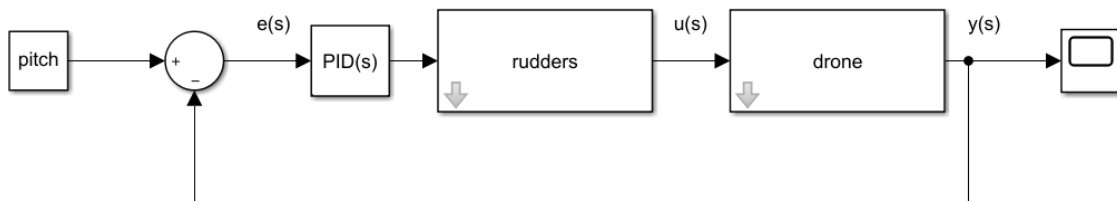


Figure 29 PID for each rudder

To avoid this behavior, it was created a second PID for the sail rudders, proportionate to make sure that they reach saturation together with the rear ones (figure 30).

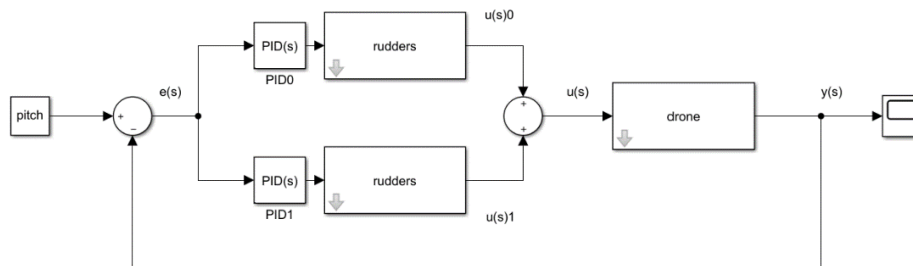
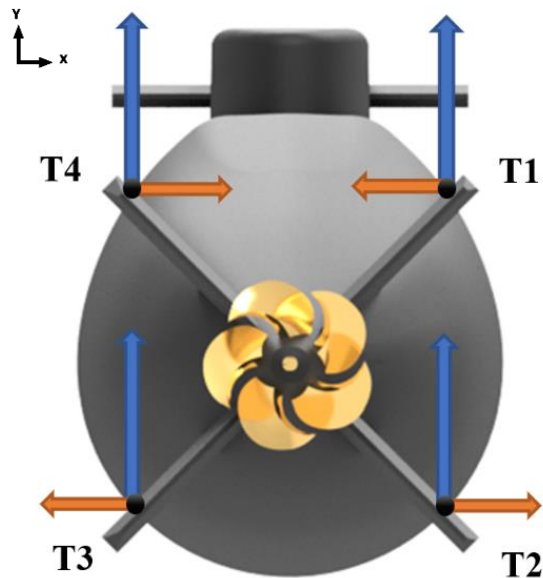
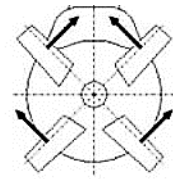


Figure 30 PID for front rudders and back rudders

### 3.3 Maneuver configuration

#### Pitch Control

The control of the pitch is carried out by the 4 stern rudders together with the bow ones, to create an upward thrust the configuration below is applied (figure 31):



The four forces applied on the 4 rudders (Named T) create a sum on Y of the vertical components while on X are canceled. In this way create a thrust from the stern that with respect to the center of mass generates a moment to counteract the pitch angle.

Figure 31 Pitch control configuration

It is possible to carry out the maneuver keeping the stern rudders in concord or discord configuration with respect to the bow, so two different maneuvers are obtained:

- Discord rudders:

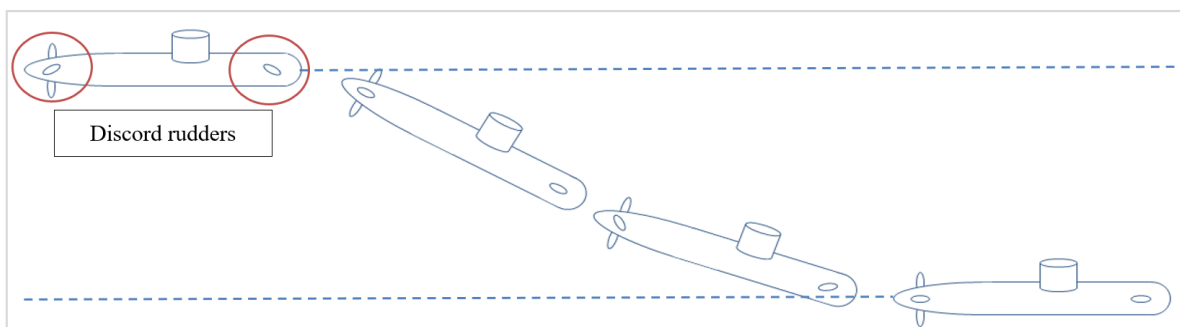


Figure 32 Change of depth with discord configuration

The drone execute the maneuver using the front rudders in a discordant way with respect to the frontal ones to better control the change of angle (figure 32).

- Concord rudders:

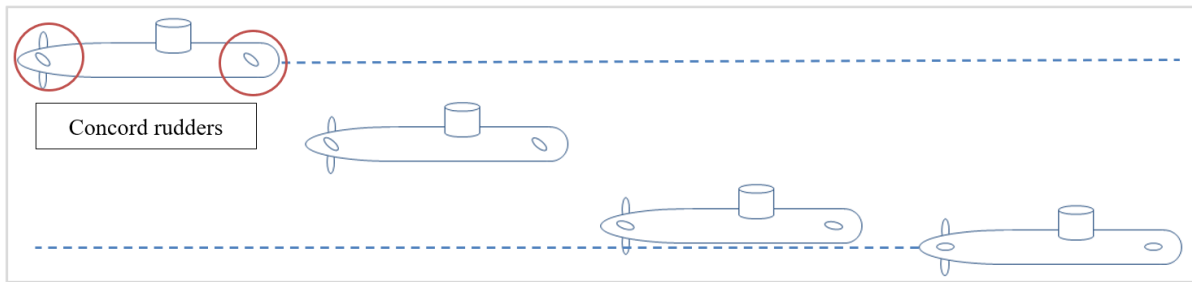


Figure 33 Change of depth with concord rudders

For this type of maneuver, the two rudders are kept in concord. The advantage that is obtained is that the pitch angle of the drone remains at 0 for the entire duration of the altitude change (figure 33).

### Roll control

The control applied to the roll angle takes place with stern rudders and the configuration to counteract a possible roll is done by adding to all 4 rudders a positive or a negative value, the same for everyone. It is possible to avoid the roll using the front rudders, but for request they were used just for the pitch control (figure 34).

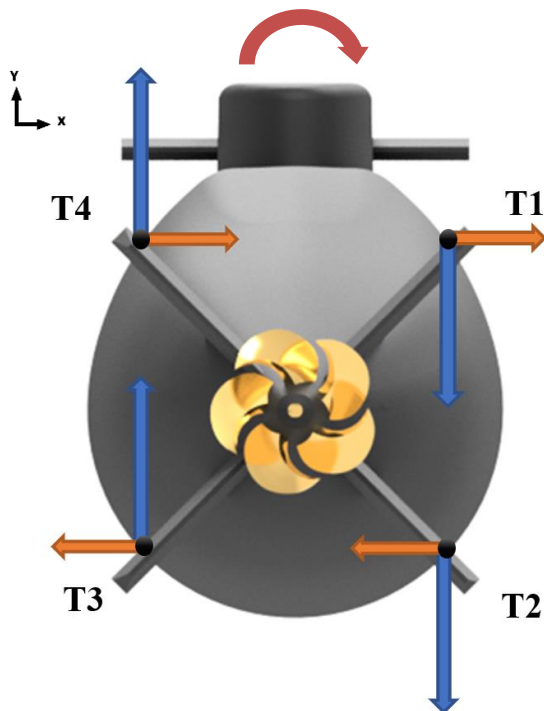
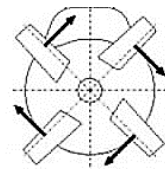


Figure 34 Roll control configuration

For the roll control, all four rudders act simultaneously going to cancel the components on X and Y however remains the moment generated on the Z-axis by both forces.

## Total angle configuration

The final angle of the rudders is an overlap of the two controls of the pitch and the roll, at the code level it was important to distribute the angles to avoid saturation on the rudders, for example, if all the four back rudders are at  $35^\circ$  and the roll increase positively, is possible only to operate with rudder T1 (upper right) and T2 (lower right) because the other 2 cannot go further  $35^\circ$  (figure 35).

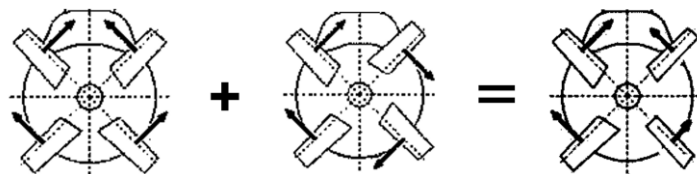


Figure 35 Overlapping rudder effects

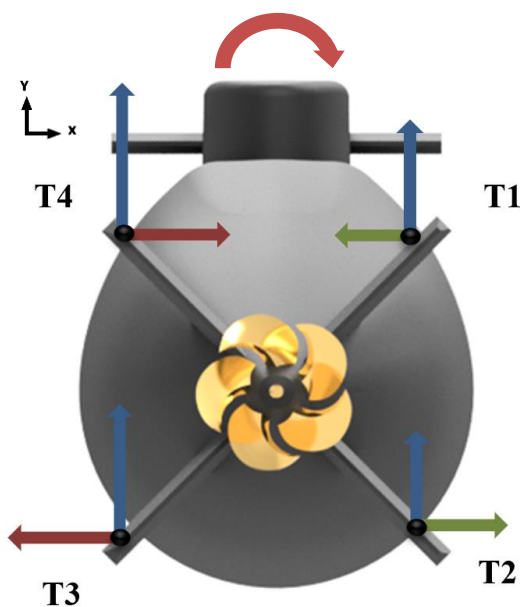


Figure 36 Force distribution of total configuration

The total force generated by the double configuration is due to the sum of the forces towards Y while the components along X cancel each other out (figure 36).

The difference of the two upward forces of left and right create an opposite moment useful to counteract the roll, while still control the pitch.

### 3.4 Gain scheduling

Gain scheduling is an empirical solution to make an adaptive controller, used in aeronautical applications and later in automotive applications. Thanks to tools such as Lyapunov's definition of stability and hyperstability theory, it is possible to synthesize adaptive control algorithms that guarantee greater robustness and better performance (figure 37).

Gain scheduling applies to nonlinear systems, for which a classic linear control does not meet the specifications in terms of stability and performance. The first step is to identify a so-called scheduling variable, which is a parameter that characterizes system variations, for example, for an internal combustion engine the rotation speed is chosen. The choice of the scheduling variable determines in an important way the performance of the controller and is carried out through considerations on the nature of the system to be controlled.

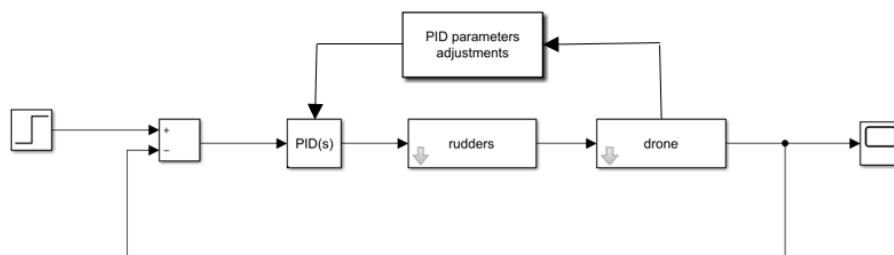


Figure 37 Example of PID variable adjustments

The drone during the simulations undergoes a change of mass and speed, these two variables change its response to any corrections with rudders, it was therefore chosen to implement a gain scheduling to the variables of the PID in order to better control the submarine according to its speed condition. To obtain precise constants, a genetic algorithm was used that for each test at constant speed found the best configuration of  $K_p$ ,  $K_i$  and  $K_d$ . For the emergence test, the starting depth was also taken into account, this is because to minimize the ascent times for greater depths it is necessary to set a gain scheduling to vary the response of the system.

## 4 Simulator

### 4.1 Software structure

The simulator developed by Cetena is designed to work in c sharp language and was developed in a visual basic (C#) environment while the test optimization tool for PID values, containing the genetic algorithm, is written in python.

The current simulator, called Simos, is an updated version of a block system developed by CETENA capable of calculating all the forces and acceleration acting on the submarine, the flow chart of the software is shown in figure 38.

The block system works thanks to a file that considers all the inputs, outputs and values of the individual blocks and makes them communicate with each other.

After starting the software, the first step is to load the data of the drone from an external file or manually, then the second step is to choose the type of simulation to be performed. The main code has the task of communicating with block system and provide the results that are saved in a separate file and are also shown in a customizable graph able to print all the variable of the block system.

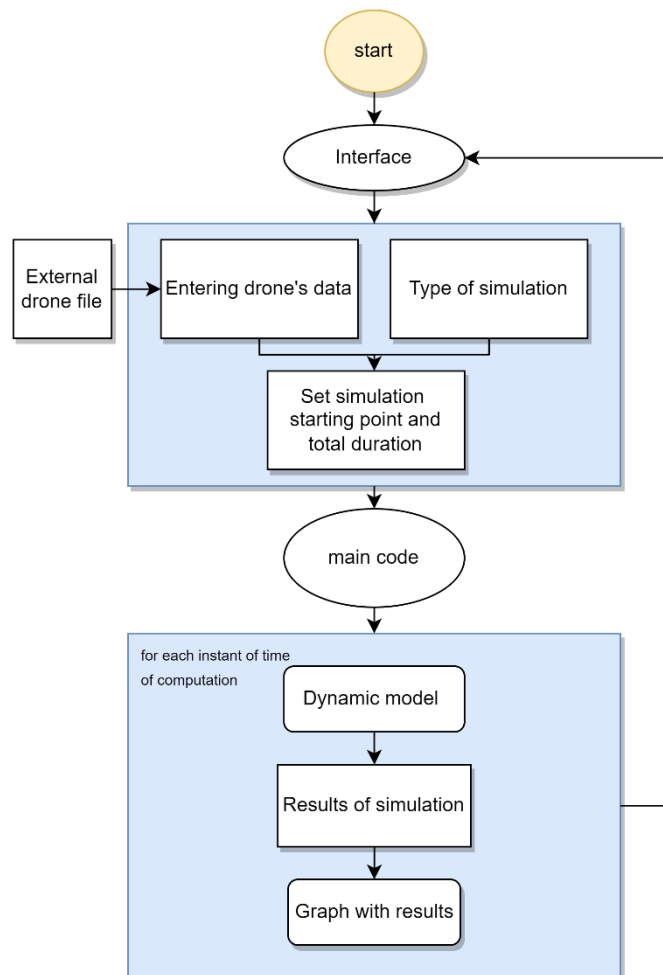


Figure 38 Software structure

## 4.2 Interface

The interface of the program is set by a menu with 3 main options (figure 39), the figures showing the interface are in Italian:

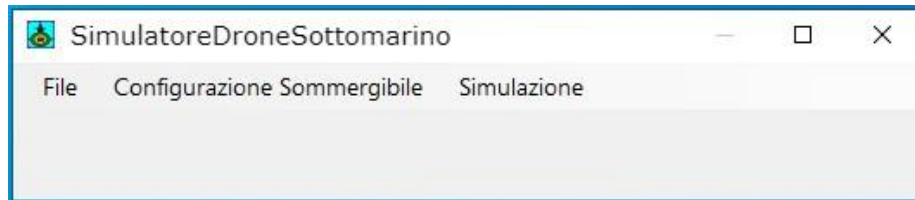


Figure 39 Main interface

1. File: section to upload the file containing the entire sizing of an underwater drone
2. Drone Configuration: Section to be able to access the values loaded from files and make changes
3. Simulation: Part containing the choice of the maneuver and the variables for the simulation

### 1) File

"File" section allows to create a new file containing all the specifications to be initialized, to load it is necessary to indicate the path where the drone folder is saved (figure 40).

This folder contains the basic information and all the specifications on hydrodynamic coefficients.

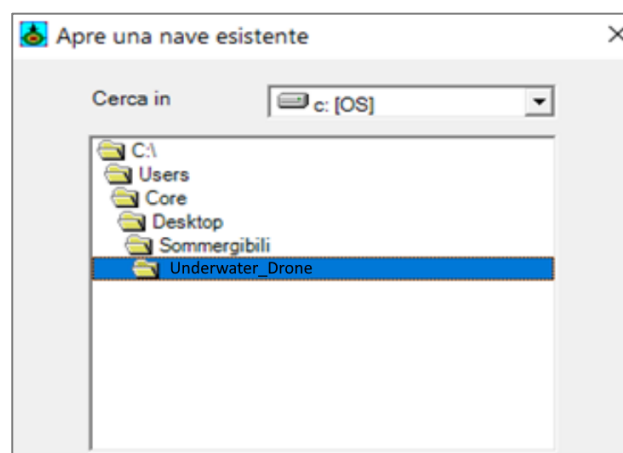


Figure 40 File loading

For the rudder specifics is load a second file in the program, since rudders values needs a very specific theory for calculation and all the hydrodynamics coefficients about them are obtained separately with experimental methods, so changing the size of the rudders means changing all their coefficients as well. To simplify the testing of the maneuvers with various rudders, are used already complete files of existing ones already tested.

## 2) Drone configuration

This option allows you to access all the individual parameters previously loaded and be able to make changes to evaluate actual changes on the design of the drone (figure 41).

The section is divided into:

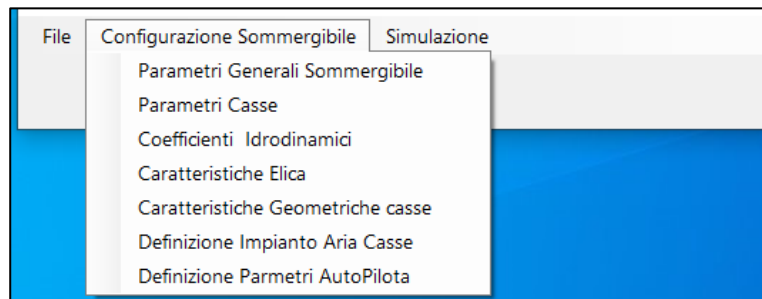


Figure 41 Basic parameters choice

- General drone parameters

Here are contained all the values of the hull geometry, the inherent inertias, and the resistance curves due to the sizing

- Ballast tanks parameters

In this section are contained all coordinates of the ballast tanks, internal temperature, maximum capacity, initial value of air contained and the size of the loading and unloading valves.

It is also possible to set the temperature of external water, in our simulation will be 20°

- Hydrodynamic coefficients

The section allows the calculation of hydrodynamic coefficients through standard formulations. which are all the values used to calculate the added mass (figure 42).

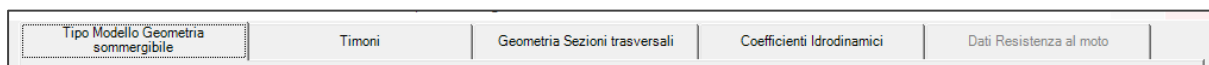


Figure 42 Parameters of Hydrodynamic coefficients

- a. Sail: submarine sails generate a vortex effect that cause added mass to the simulation (figure 43).

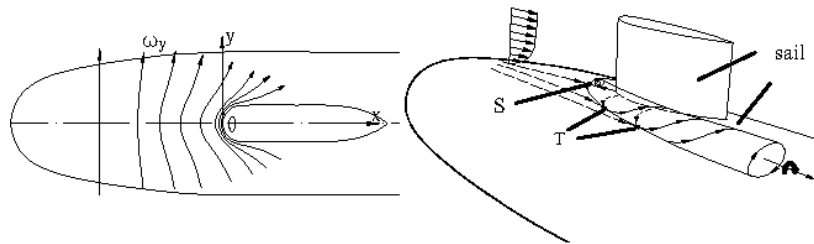


Figure 43 Vortex effect

- b. Rudders: containing the information of the rudder file, from this section is also possible to change the maximum angle of response and the speed response (figure 44).

Tipo Modello Geometria sommergibile Timoni Geometria Sezioni trasversali Coefficienti Idrodinamici Dati Resistenza al moto

T1, T2, T3, T4: Max.ang [°] 35.0 Angolo neutro [°] 0.000 Vel.Ang. [°/sec] 58.0

TTOAV: Max.ang [°] 20.0 Angolo neutro [°] 0.000 Vel.Ang. [°/sec] 55.0

PRODIERI POPPIERI

Distanza LCB - Asse timone [m] 6.30 27.15 Semiangolo del cono poppiere [°] 20.10

Distanza Asse sommergibile - Radice [m] 1.50 1.40  $\theta_1$  [°] 45.00  $\theta_2$  [°] 45.00

Tipologia Timoni:  Timoni a croce "+-"/>  Timoni a X

Modalità di calcolo:  Formulazione timoni isolati

	Area Proiettata [m <sup>2</sup> ]	Altezza Media [m]	Corda Media [m]	Spessore massimo [m]	% Span
TTOAV	3.170	1.850	1.720	0.310	1.000
T2	6.380	3.100	2.060	0.370	0.820
T3	6.380	3.100	2.060	0.370	0.820
T1	6.380	3.100	2.060	0.370	0.820
T4	6.380	3.100	2.060	0.370	0.820

.01 < x < 100 04/02/02 12:11 INS ,,:  
 Salva File Idrodinamico Salva dati Esci Annulla modifiche File Idrodinamico

Figure 44 Rudders configuration

- c. Transversal section geometry: Contains the sections of the drone along its entire length.

With the inserted data, with the “Hydrodynamic coefficient” option, is possible to recalculate eventual changes made to the geometry of the drone.

- Propeller characteristics: part containing all the coefficients of the epics, it is possible to change the number of blades together with the pitch and diameter.
- Characteristics of the geometry of the crates: Containing the geometric description of the ballast crates and the floodable room.
- Definition of the air system for crates: part dedicated to technology for the emergence and filling of crates.
- Definition of autopilot parameters: PID controller parameters and typology, which can be chosen static or dynamic, dynamic change its values according to the depth of the drone and its speed (figure 45).

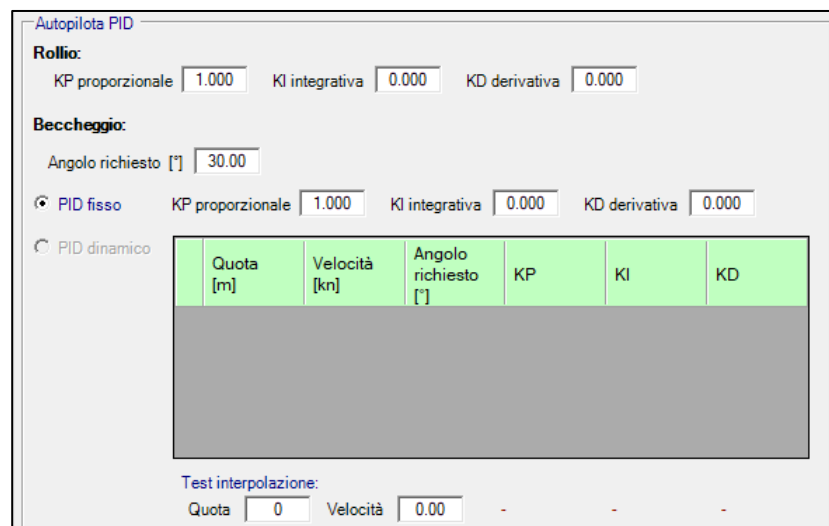


Figure 45 PID interface

From the PID interface can be changed the three parameters of the roll controller that is always static, but the pitch controller can be set as static or dynamic. For the dynamic PID were used the values found by the genetic algorithm that will be described in the next chapter.

### 3) Simulation

In this section it is possible to create a simulation test by choosing all the starting parameters and the type of maneuver (figure 46).

In "general settings" is chosen the integration step of the simulator and all the starting conditions of the simulation start.

For example:

Impostazioni Generali		Impostazioni Manovra	
Scelta Manovra: 01 - Simulazione in caso di falla			
Descrizione: [ ]		Data: 4-3-2022	
Spostamento longitudinale [m]	0	Spostamento trasversale [m]	0
Quota [m]	-165	Angolo di rollio [°]	0
Angolo beccheggio [°]	0	Angolo di rotta [°]	0
Velocità avanzo [nodi]	2.70	Velocità trasversale [nodi]	0
Velocità verticale [nodi]	0	Numero giri elica [rpm]	19.98
Tempo totale simulazione [s]	3600	Modello coeff. idrodinamici	
Intervallo memorizzazione [s]	1	<input type="radio"/> Sperimentale	
Passo integrazione [s]	0.1	<input checked="" type="radio"/> Teorico 1	
Condizioni di Terminazione		<input type="radio"/> Teorico 2	
Rollio Limite	89	Variabili da stampare	
Beccheggio Limite	89	Angolo beccheggio [°]	
Velocità Limite	40	Angolo rollio [°]	
		Quota z [m]	
		Angolo T1 Attuato [°]	
		Angolo T2 Attuato [°]	
		edita lista <	

Figure 46 General maneuver settings

1. Initial positioning relative to the starting center
2. Initial speeds
3. Total simulation time and storage and integration step
4. Initial number of revolutions
5. Choice of theoretical model (Feltman or Gerteld)
6. Variables to print on graph
7. Condition for ending simulation

The printable variables are all the individual calculated within the dynamic model; in this way it is possible to fully analyze the results of any test.

In "**maneuver settings**" is chosen the actual maneuver and at software level is created the conditions for each simulation. For example, the altitude change maneuver sets a target depth and the drone, through the error with respect to the goal, changes its depth by acting on the rudders (figure 47).

In the interface is possible to see how scheduled activation solutions of the crates have been implemented, but in my simulations, was chose to activate all of them simultaneously with the control system, we wanted to analyze the effect of the total thrust of the 9 crates together with the control system in order to evaluate the results of both active conditions.

However, the use of scheduling or auto-scheduling allow to manage the thrust of the crates filled by the air generators with controlled activations that make a further improvement of the ascent.

These analyzes will be evaluated during the realization of the drone and will not be part of this thesis.

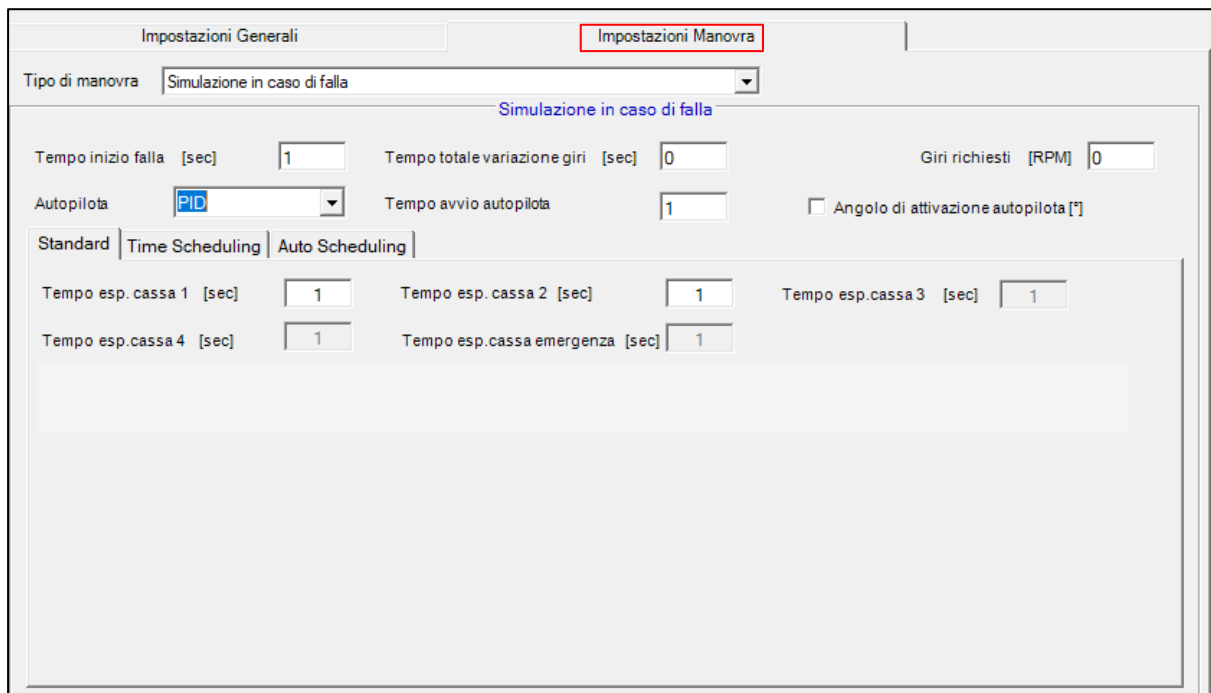


Figure 47 Specific maneuver settings

## 5 Genetic Algorithm

### *5.1 Introduction to genetic algorithms*

Genetic algorithms are artificial intelligence tools inspired by Darwin's theory of evolution: natural selection, adaptation and survival theory are used by these tools to solve computationally difficult optimization problems.

In the late fifties and early sixties of the last century, we began to take inspiration from natural systems in the belief that they could be a model for new optimization algorithms. In fact, the mechanisms of natural evolution may be suitable for addressing some of the most pressing computational problems, such as those concerning the search for solutions among a huge number of alternatives. In fact, biological evolution is like a research method within a very large number of solutions, consisting of the set of all genetic sequences, the results of which, that is, the desired solutions, are highly adapted organisms, endowed with a strong capacity for survival and reproduction in a changing environment, which will then transmit their genetic material to future generations.

In this context, organisms can therefore be considered as excellent problem solvers since they are able to survive in their environment by developing behaviors and skills that are the result of evolution itself.

Natural evolution is the basic theory on which Darwin's thought is based; he argues that the evolution of the species can take place through the following modes of action.

Natural evolution acts on the genetic material, that is, on the genotype, of an individual and not on his physical characteristics, the phenotype: every variation that favors the adaptation of an individual emerges from the genetic heritage, not from what the parents will have possibly learned during their life.

Natural selection favors the reproduction of individuals that improve adaptability to the changing environment and eliminates individuals with lower reproductive potential. From the genetic point of view, natural selection promotes those genetic combinations that give life to a more efficient organism.

Reproduction is the central nucleus of the evolutionary process: the generational variability of a Species is determined by gene recombination and small random mutations of the genetic

code. Reproduction results in the recombination of the parents' genetic material, generating a much faster evolution than would be achieved if all the descendants simply contained a copy of a parent's genes, randomly modified by a mutation. It is a process with a high degree of parallelism: it does not operate on one species at a time, but tests and modifies millions of species in parallel.

Natural evolution operates on entire populations through cyclic and generational processes determined exclusively by environmental contingencies and interactions between various organisms.

The combination of Darwinian hypotheses with genetics has given rise to principles that form the basis of population genetics, that is, the explanation of the evolution at the genetic level of populations.

A population is defined as a group of individuals of the same species, operating and interbreeding in the same place.

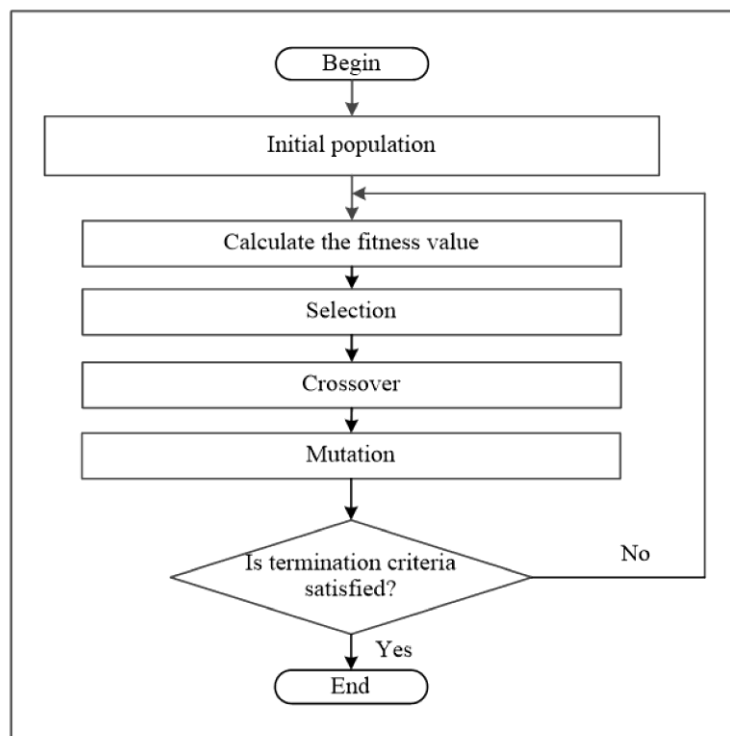


Figure 48 Genetic algorithm flow chart

In biology, chromosomes are the strands of DNA that serve as a model for the organism: each of them is composed of genes, which, through the coding of a particular protein, determine the specific characteristics of the organism, such as eye color. The locations of genes within the

chromosome are called locuses, and the different configurations of proteins are called alleles. Most organisms have more than one chromosome, the whole of which is called a genome. A genotype is the set of genes in the genome. The end result of fetal evolution, that is, the individual, is called the phenotype.

Sexual reproduction consists in the recombination of the genetic material of the parents, which gives rise to a new complete patrimony for the descendants; however, mutations can occur on individual parts of DNA.

Physical fitness is the suitability of the individual, that is, the probability that he lives long enough to reproduce. Natural selection promotes as parents for next-generation individuals who have the most suitable phenotypes, encoded by particular genotypes.

The evolution is therefore based on the following mechanisms:

1. Mutation of alleles: primary source of genetic variability.
2. Gene flow: variation in the frequencies of alleles, due to the migratory movements of some individuals, resulting in the introduction or removal of certain genotypes.
3. Genetic drift: unpredictable changes in the frequency of alleles in the event that a population has a small number of components.

### ***5.1.1 Selection***

Due to complex phenomena of nonlinear interaction, it is not obvious either that two promising solutions will give rise to a more promising third or that two solutions with low fitness values will generate a third with a lower fitness value. To overcome these problems, when choosing the candidate solutions for evolution, in addition to the parameter obtained from the fitness function, we also rely on particular "selection" techniques. The most common are:

- Roulette selection: the probability that a solution will be chosen to make it evolve is directly proportional to the value returned by the fitness function. This technique presents problems in case there are large differences in values because the worst solutions would be selected too rarely.

- Selection by category: similar to the selection for roulette but the evaluation is carried out in proportion to the sum of the value of the fitness function for each possible pair of solutions. The problem presented by this technique of choice is represented by the slowness of convergence if there are too small differences between pairs of candidate solutions.
- Tournament selection: the solutions are grouped together and evaluated with an algorithm like the one presented in the following lines.
  - A. Randomly choose the individuals belonging to the population.
  - B. Choose the best individual and set his probability of choice to  $\rho$
  - C. Choose the second best individual and set the probability of choice to  $\rho * (1 - p)$
  - D. Choose the third best individual and set his probability of choice to  $\rho * (1 - p)^2$
- Boltzmann selection: the solutions are chosen with a degree of probability that, at the beginning of the algorithm, favors exploration and then tends to stabilize

### 5.1.2 Crossover

According to an initially established operator, some parts of the genes of the candidate solutions for evolution are mixed to obtain new solutions.

The most used operators are:

- **One-point crossover**

Crossover at one point: it consists of considering two solutions suitable for evolution and cutting their coding vectors at a random or predefined point to obtain two heads and two tails. The first new solution obtained will be given by the combination of the head of the first solution with the tail of the second, while the second new solution will be given by the tail of the first solution with the head of the second (figure 49).

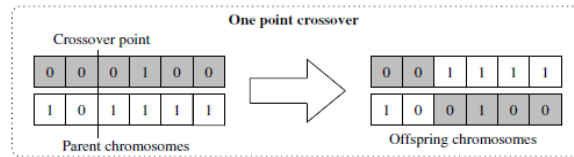


Figure 49 One point crossover working principle

### Two-point crossover

Two-point crossover: it consists in considering two solutions suitable for evolution and in cutting their coding vectors into two predefined or random points to obtain a head, a central part and a tail from the first and second solution. The first new solution will be given by the head and tail of the first solution and the central part of the second solution. The second new solution will be given by the central part of the first solution and the head and tail of the second solution figure (50).

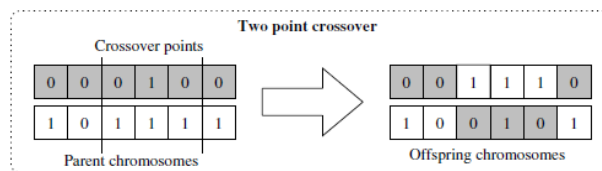


Figure 50 Two point crossover

- **Uniform crossover**

Uniform crossover: consists of the random exchange of bits between the candidate solutions for evolution. It should also be noted the existence of partial uniform crossovers, that is, uniform crossovers in which the exchange of bits is limited to a fixed or dynamic percentage of the candidate chromosomes for evolution (figure 51).

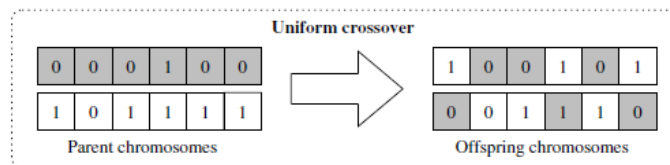


Figure 51 Uniform crossover

- **Arithmetic crossover: consists of using an arithmetic operation to create the new solution**

### 5.1.3 Mutation

The mutation consists of the pseudorandom modification of certain parts of the genes according to previously defined coefficients. These modifications are used both to improve fitness function but also to improve the overall variability of the data, thus preventing the genes from becoming all the same or all excellent. The frequency with which a mutation must occur is generally done according to a parameter defined as  $p_m$ .

The purpose of the mutation in GA is to introduce diversity into the sampled population. Mutation operators are used to avoid local minimums by preventing the chromosome population from becoming too like each other, slowing down or even stopping convergence towards the overall best value. This reasoning applies in a preventive manner on the GA avoiding taking only the most suitable of the population to generate the next generation. In fact, is selected a random (or semi-random) set with a tendency towards those that are more in shape (figure 52).

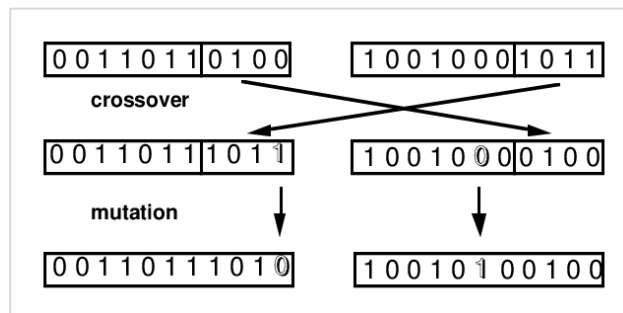


Figure 52 Mutation

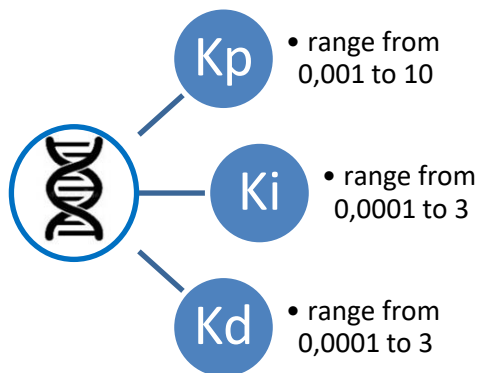
## 5.2 Setting the algorithm for the problem

The developed algorithm utilized for the optimization initially randomizes a population of 30 candidates by modifying values of the three constants of a PID in different ranges. Then a test is prepared from the dedicated interface where it is chosen:

1. starting depth of the drone
2. speed in rpm (kept constant throughout the test)
3. activation time of the emergency system (standardized to 20 seconds)

Each individual in the population has 3 genes:

- **Kp** gene, containing the proportionality parameter of the PID
- **Ki**, gene containing the PID integration parameter
- **Kd** gene containing the PID derivation parameter



The ranges were chosen based on a criterion of response of the rudders, which having as a maximum angle 35 ° cannot handle high parameters of **Ki** and **Kp** (figure 53).

Figure 53 Constant of PID and their ranges

To have uniform performance it was decided to relate the PID optimized for the stern rudders also for the bow rudders managing the three variables trying to get the angle of the bow rudders in saturation together with those of the stern.

Accordingly:

$$PID\ Genes\ 2\ (bow) = \frac{20}{35} PID\ Optimized\ Genes\ 1(stern)$$

After that the first population has been created, a test is made for each individual and a score is applied based on the result obtained, consequently is applied a criterion like that of the tournament, where the best candidates remain in the race and the rest are modified.

The criterion of the fitness curve is as follows; the score is given according to:

- Surface reached
- Time needed to reach the surface
- Maximum angle of emergence obtained during the test

Subsequently, when all 30 candidates have received the score, we move on to the selection:

- The top 10 candidates with the best score are kept and saved for the next test
- The worst 10 are discarded and in their place another 10 random values are created based on the average of the top 10 best
- The remaining 10 are undergoing a mutation with the parameters of the first

In this way an improvement is obtained based on the first 10 individuals who affect the 10 medians (figure 54).

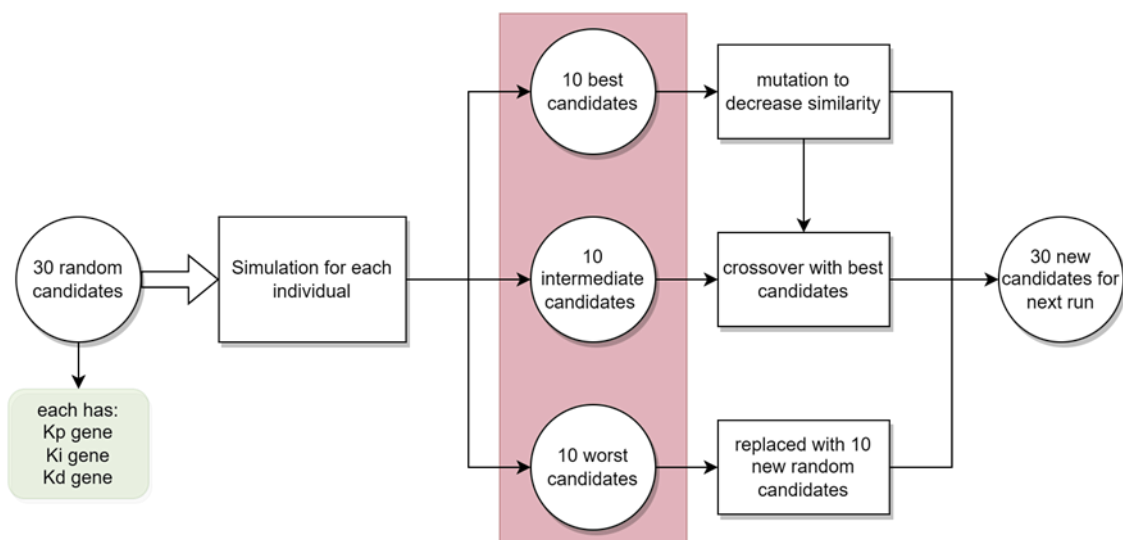
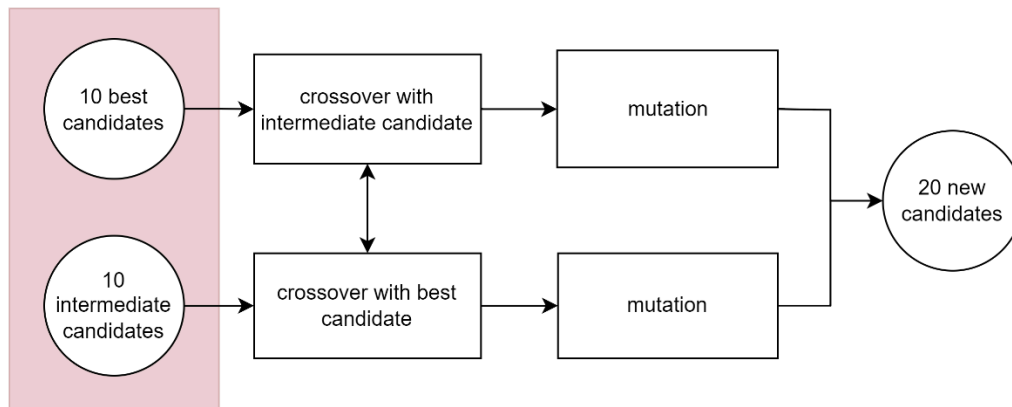


Figure 54 Scheme of used genetic algorithm

When the first 10 solutions tend to be similar to the 10 intermediates, then is executed a crossover with both. After this step the new candidates obtained undergoes a random mutation (figure 55).



*Figure 55 Progressive crossover and mutation for diversification*

During the tests random mutations are performed, always for the aim of obtaining different values.

All evidence is saved and stored in a file that communicates with the system, which allows to update the variables according to the conditions of use.

The use of the genetic algorithm was very useful to create a depth/speed graph able to allow the analysis of the test in case of a leak.

In addition, the algorithm was also used for tuning situations in linear conditions of the system, in fact it was always possible to obtain the best tuning of the PID for different manoeuvres such as changing depth or immersion from the surface.

## 6 Analysis and results

### *6.1 Simulation in case of a leak*

One of the most important tests that has been introduced in the simulator is the emergence in case of leak, in fact in this condition the drone embarks in a short time a lot of water increasing its inertia and making the action of the rudders much more difficult. Without the support of the additional emergency thrust it would be impossible to bring it back on surface especially based on bigger depths.

The extent of the damage can be varied, generally one of the main reasons is precisely the breakage of a seacock, due to a shock wave or an impact. Considering that the transmission of data in the sea is difficult and the drone would proceed in autonomous driving once immersed, it is expected that in such a situation, after a certain period, the emergence maneuver will begin. The objective of this test is to be able to bring the drone to the surface to allow the transmission of data and indicate its position, to allow the recovery or return to a safe point in case of limited damage, in fact, depending on the damage, the drone even if hit can still move on the surface, this is due to the fact that the air introduced into the crates on the surface increases its effectiveness thanks to a lower external pressure.

In this simulation is considered the leak is caused by a shockwave that breaks the inlet of the diesel engine that uses external water for cooling.

A fixed datum is the activation time of the emergency system that has been finalized to 20 seconds, which is a very high safety value, considering that the sensors inside the drone can immediately become aware of the possible ingress of water into the floodable rooms. However, extending the boot time to 20 seconds is a precaution to consider even the worst case where the support system does not act immediately.

More complicated situation is that of the emergence without engine support, this can happen when embarking water also fails the engine, or when the propeller has been damaged. The simulation in this case only exploits the crates to get thrust and use the rudders to maintain a controlled angle.

The worst condition is the damage to the central system, but this would not allow the use of crates or rudders, consequently it is excluded as a situation to simulate since the drone cannot emerge.

During the simulation the main requests of the project are the time and angle of emergence to emphasize the necessary ascent time and the angle of ascent, this data is important to keep it below  $45^\circ$  to allow a correct functionality of the internal systems and joints of the engine, the optimal angle required however would be  $30^\circ$  with the peak of overshoot of  $35^\circ$ .

The values obtained from these two parameters are the basis of the Fitness function of the genetic algorithm to evaluate the parameters of the PIDs

### **Methodology for the analysis of the maneuver**

The final goal for which the maneuvers were performed in case of a flaw was to create a depth-speed graph to visualize where the drone can emerge and at what angle. The procedure by which they were carried out is therefore as follows:

- Initially, open loop tests were carried out, using only the filling of the crates as a method of ascent, the behavior of the drone at different depths was observed considering the thrust generated by the filling of the crates and the angles obtained from the Pitch and the Roll. From this analysis the areas where the drone was able to manage the negative thrust obtained from the water embarkation were considered.
- Subsequently, closed loop tests were carried out both for the pitch and for the roll, from these tests it was possible to draw the graph of the depths and the maximum angle reached during the test thus understanding the range of operability of this maneuver.

- Using the genetic algorithm every single test carried out in closed loop was re-performed and each value of the optimized parameters was saved in a table.
- After having obtained all the optimized parameters for each ascent point, the actual improvement compared to the static optimized by the genetic algorithm occurred through the dynamic PID function.

### General parameters emersion tests

Although many tests have been done, the variables changed in the general settings have always been the starting altitude and the initial speed. The remaining variables were chosen to keep them equal (figure 56).

Figure 56 General settings for leak simulation

The initial speed also establishes the rpm of the propeller with which the system starts, however it was chosen to keep the rpm constant during the test, this means that, once the drone becomes heavier, at the same rpm value, a lower speed is obtained.

## Maneuver settings parameters

In the simulations it was chosen to keep the rpm constant, so on this page the change in rpm during execution must be set to 0 (figure 57).

Impostazioni Generali		Impostazioni Manovra			
Tipo di manovra: Simulazione in caso di falla					
Simulazione in caso di falla					
Tempo inizio falla [sec]	1	Tempo totale variazione giri [sec]	0		
		Giri richiesti [RPM]		0	
Autopilota	PID	Tempo avvio autopilota	1	<input type="checkbox"/> Angolo di attivazione autopilota [°]	
Standard   Time Scheduling   Auto Scheduling					
Tempo esp. cassa 1 [sec]	20	Tempo esp. cassa 2 [sec]	20	Tempo esp. cassa 3 [sec]	1
Tempo esp. cassa 4 [sec]	1	Tempo esp. cassa emergenza [sec]	1		

Figure 57 Interface with standard data for manoeuvres: In red data that is never changed during simulation

The ballast tanks are only two, one in the stern and one in the bow, which has been chosen to activate at 20 seconds together with all the nine-air system for the ascent of the drone. The software however considers the possible insertion of 3 more tanks, their position can be changed from the configuration section (figure 58).

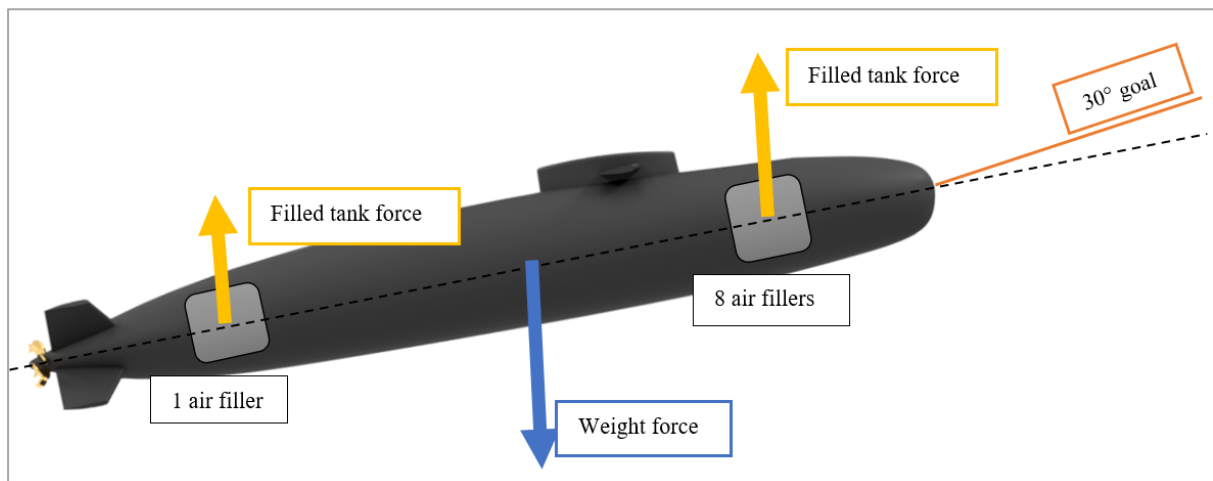


Figure 58 Example of Forces During the Leak Situation

## 6.2 Behavior in case of leak

Initially we wanted to verify the behavior of the drone in the case of a flaw, as shown in figure 59, the drone begins to sink finding an angle of balance around  $10^\circ$  degrees and retreating, this is since the center of thrust moves to the left of the center of mass due to the increase in weight of the vessel.

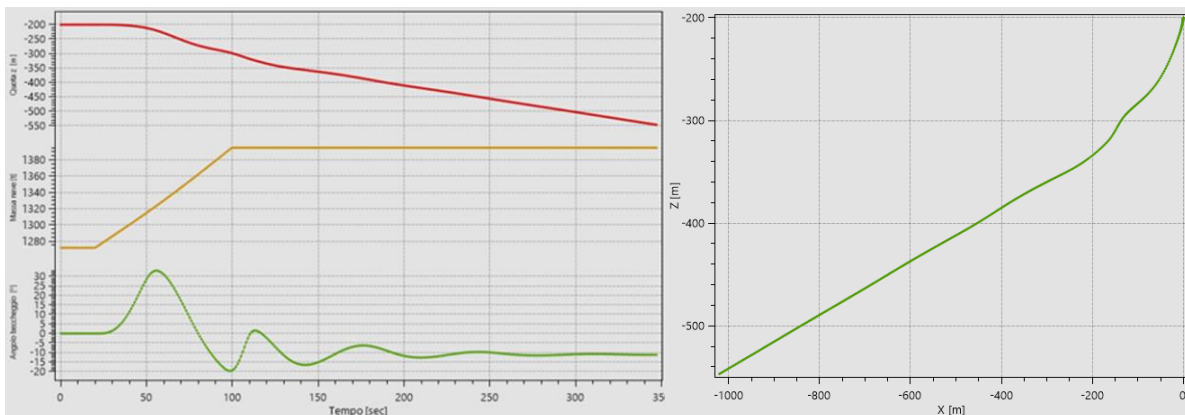


Figure 59 Behavior in case of leak with 0 speed, on left from the top are shown quote mass and pitch angle, on the right the movement on the plane Z-X

Simulating the same behavior with a positive initial speed instead shows how the excessive weight still wins on the thrust of the engines making the drone sink with a pitch angle of about  $-10^\circ$  degrees (figure 60), however the thrust of the engines generates an oscillatory behavior of the bow that sways in a range between  $40^\circ$  and  $-30^\circ$  degrees until it stabilizes.

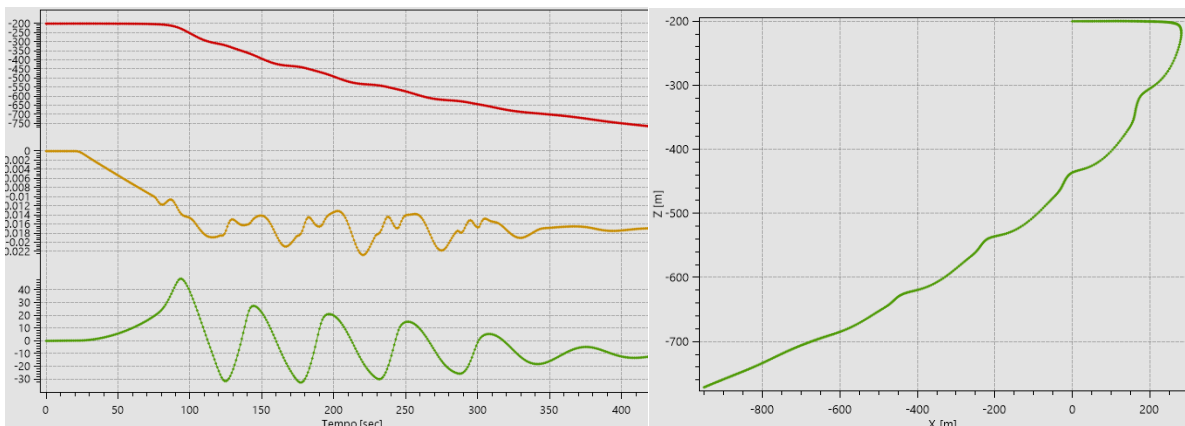


Figure 60 Behavior in case of leak with 40 rpm, on the left are shown quote, roll angle and pitch angle, on the right the movement on plane Z-X

### 6.3 Simulation at 120 depth and 0 rpm

#### 6.3.1 Open-loop analysis

In the open-loop test the submarine emerges with a time of 50.55 seconds with an angle of 82.48° and a roll peak at 23.29°, due to non-aligned tanks and no roll control.

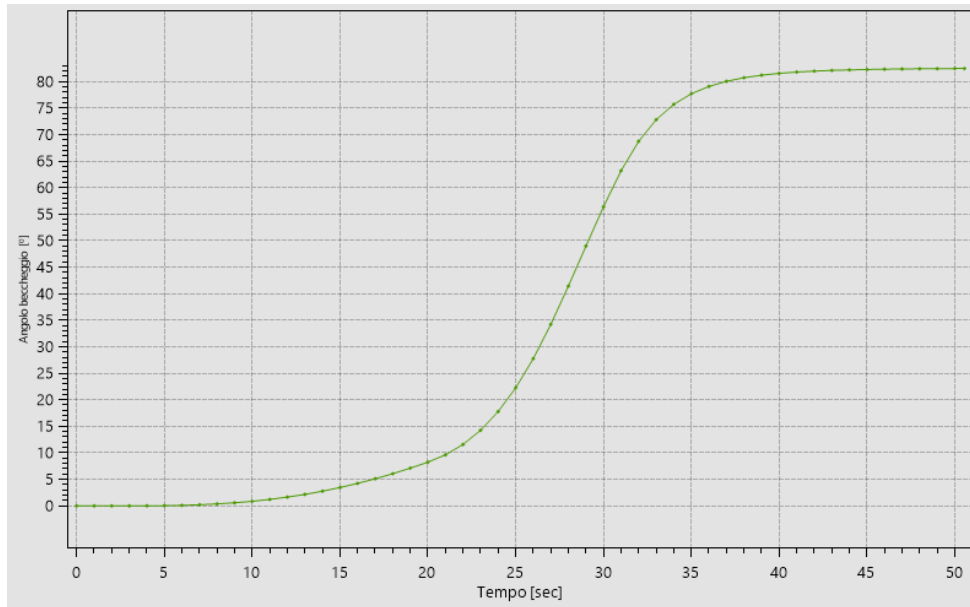


Figure 61 Pitch angle

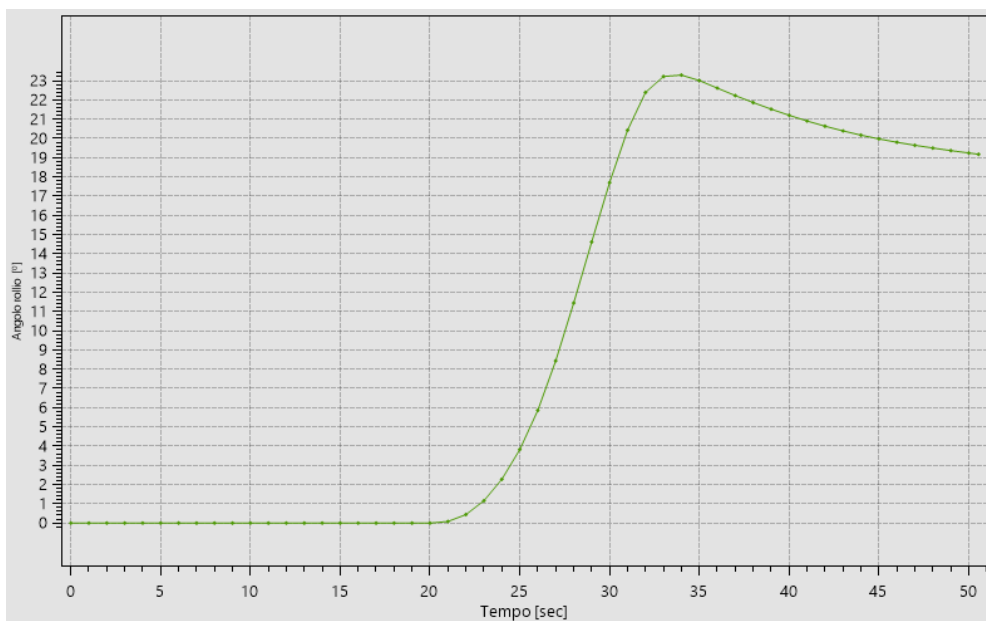


Figure 62 Roll angle

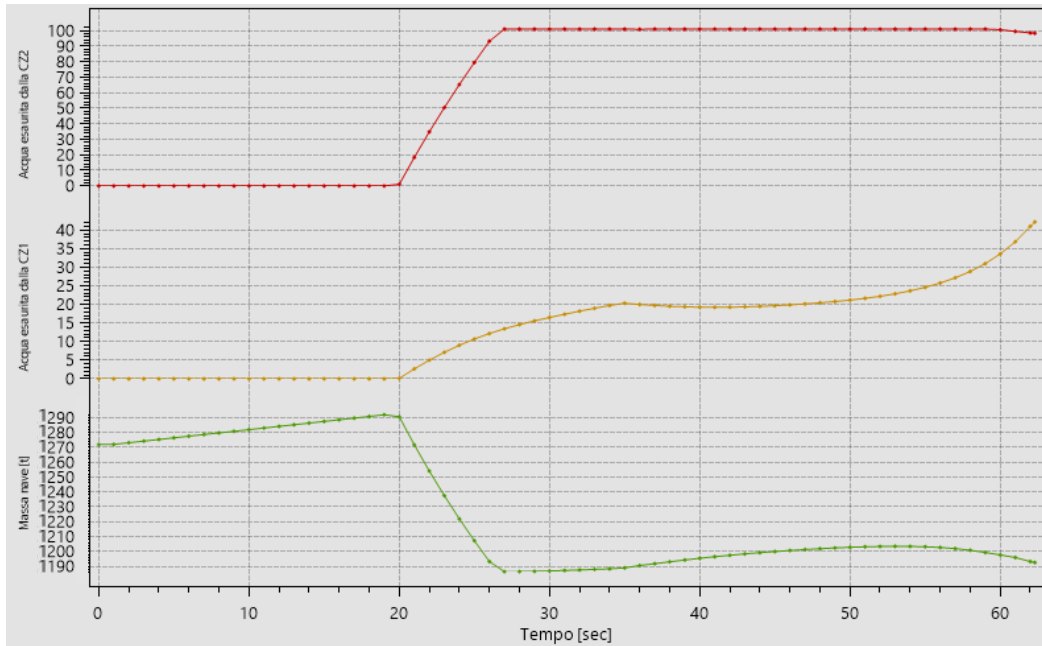


Figure 63 mass of the vessel with respect to the leak and filling of the crates

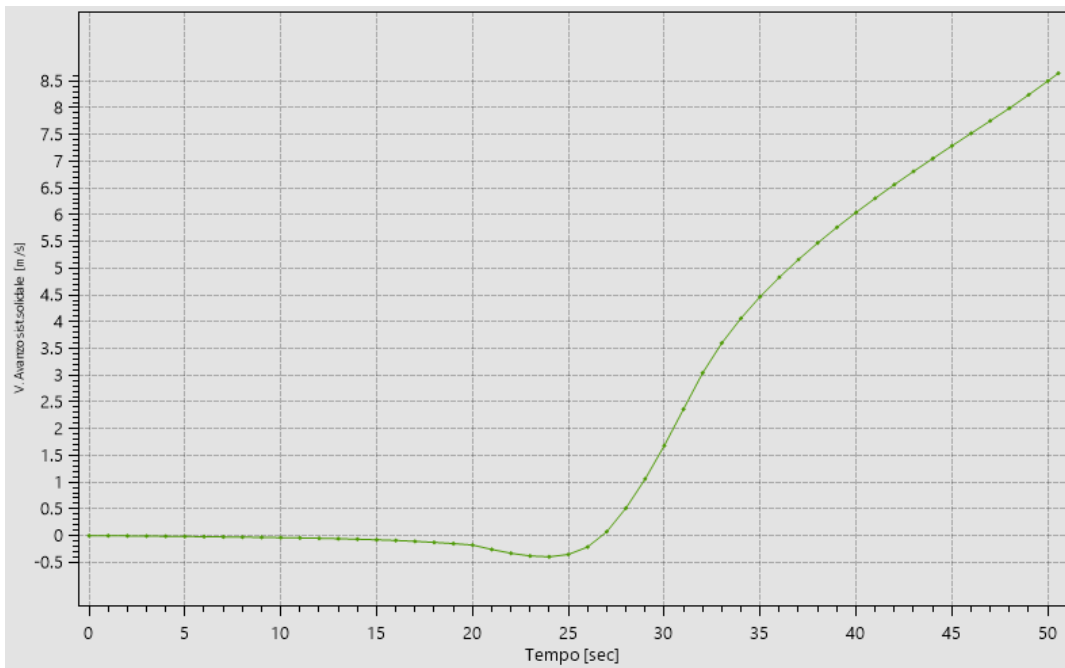


Figure 64 System speed

The filling of the crates generates a thrust of ascent that translates into speed of the system, considering that in the bow there are more crates is justified the increase of the pitch angle to  $82^\circ$ , also in the first 20 seconds the speed tends to negative, this is because the flaw that cause an increase in mass, so the the drone begins to retreat.

The effect of the compressed air is evident at this depth, in fact we have a loss of 120 tons of water.

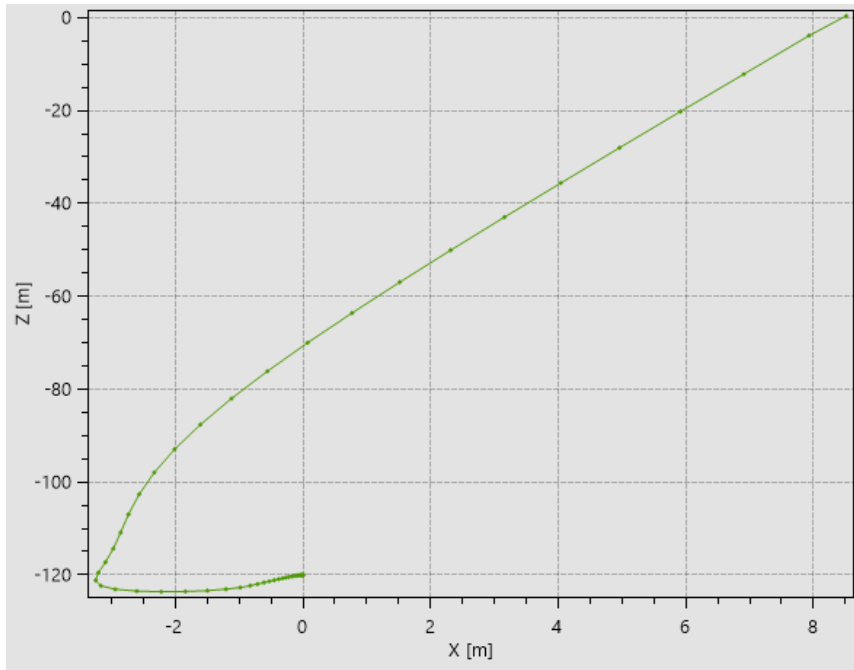


Figure 65 X-Z plane

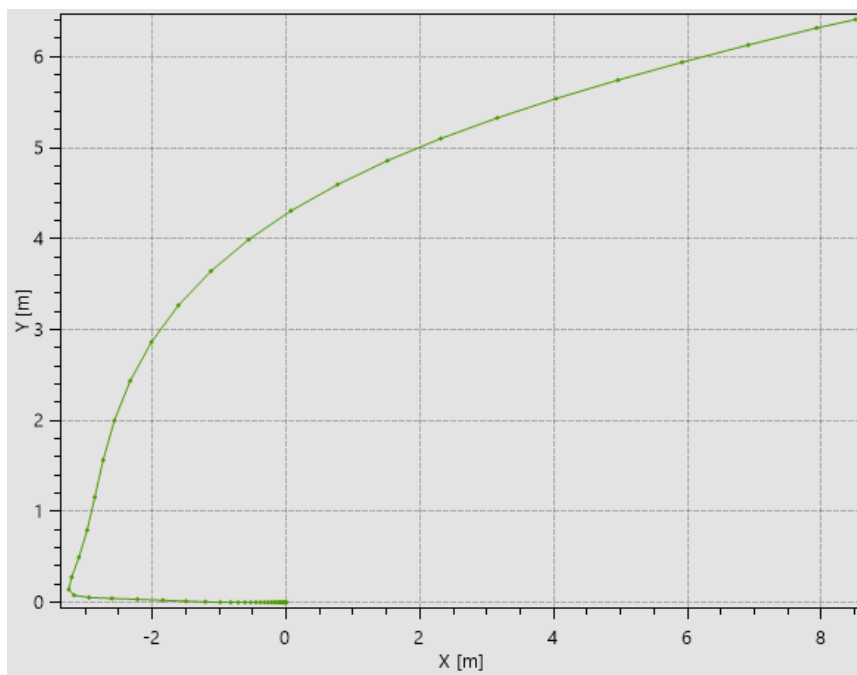


Figure 66 X-Y plane

Due to the flaw the drone initially retreats and moves positively on the Y axis of almost 7 meters, after the activation of the filling system the emergence takes place, which in just 8 meters of leftover brings the drone to the surface, this is due to a very high angle of pitch that would certainly lead to internal damage to the vessel.

### 6.3.2 Closed Loop analysis

In the closed-loop test the submarine emerges with a time of 62.3 seconds with an angle of  $83.52^\circ$  and a roll peak at  $23.19^\circ$

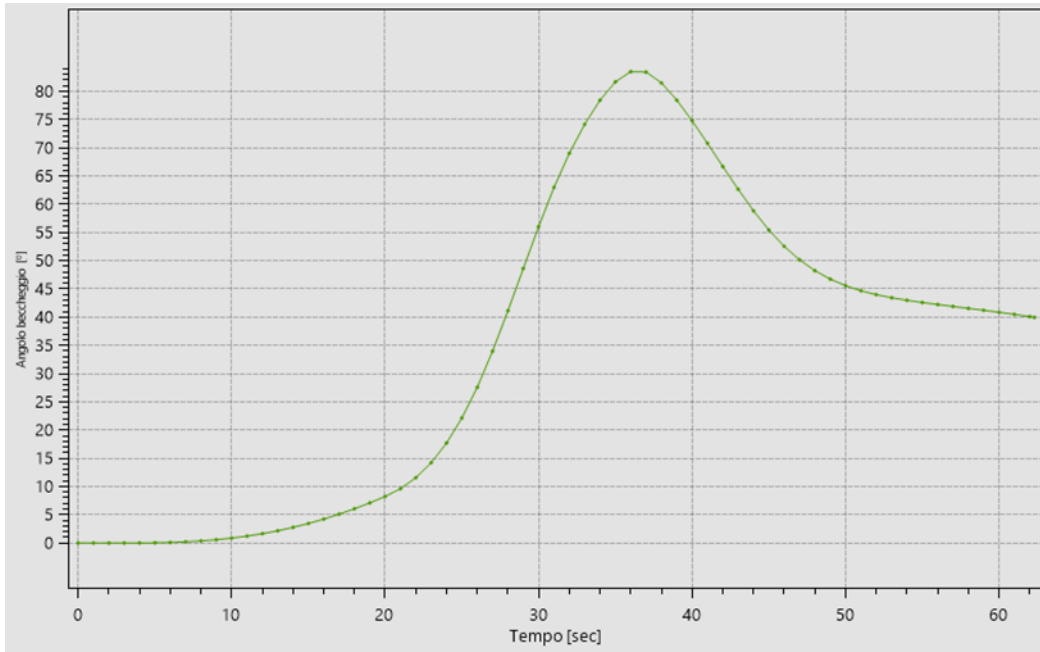


Figure 67 Pitch with PID

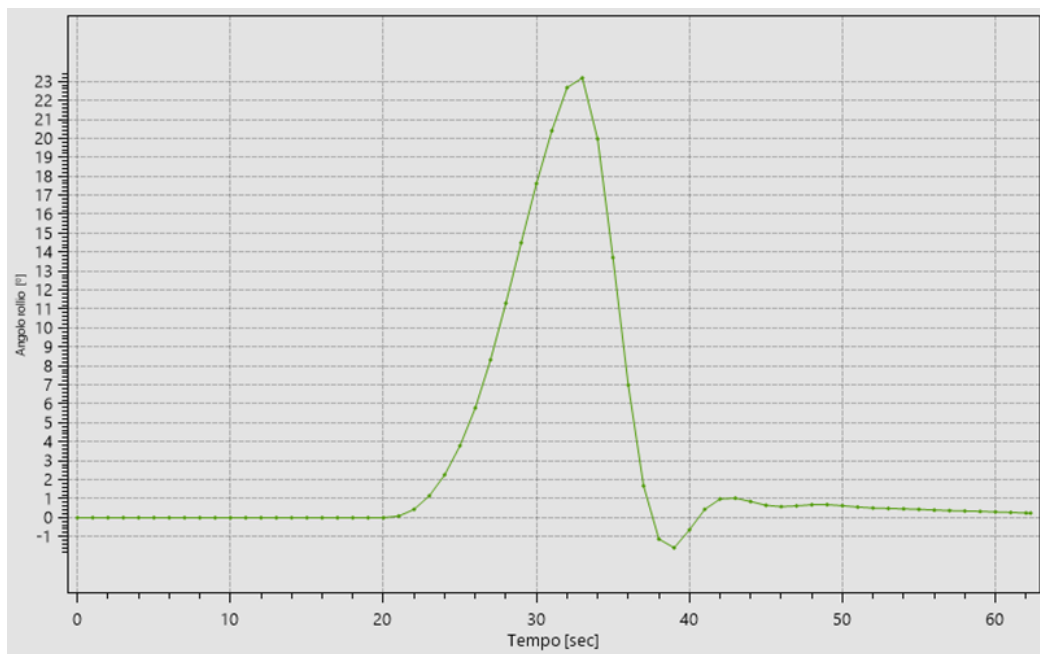


Figure 68 Roll with PID

The roll, thanks to the control of the rudders, is reduced to a maximum of  $23^\circ$ , is not a functional angle but at low speeds the roll control is not very effective, however it is important to see the effect of the control that manages to bring it towards 0.

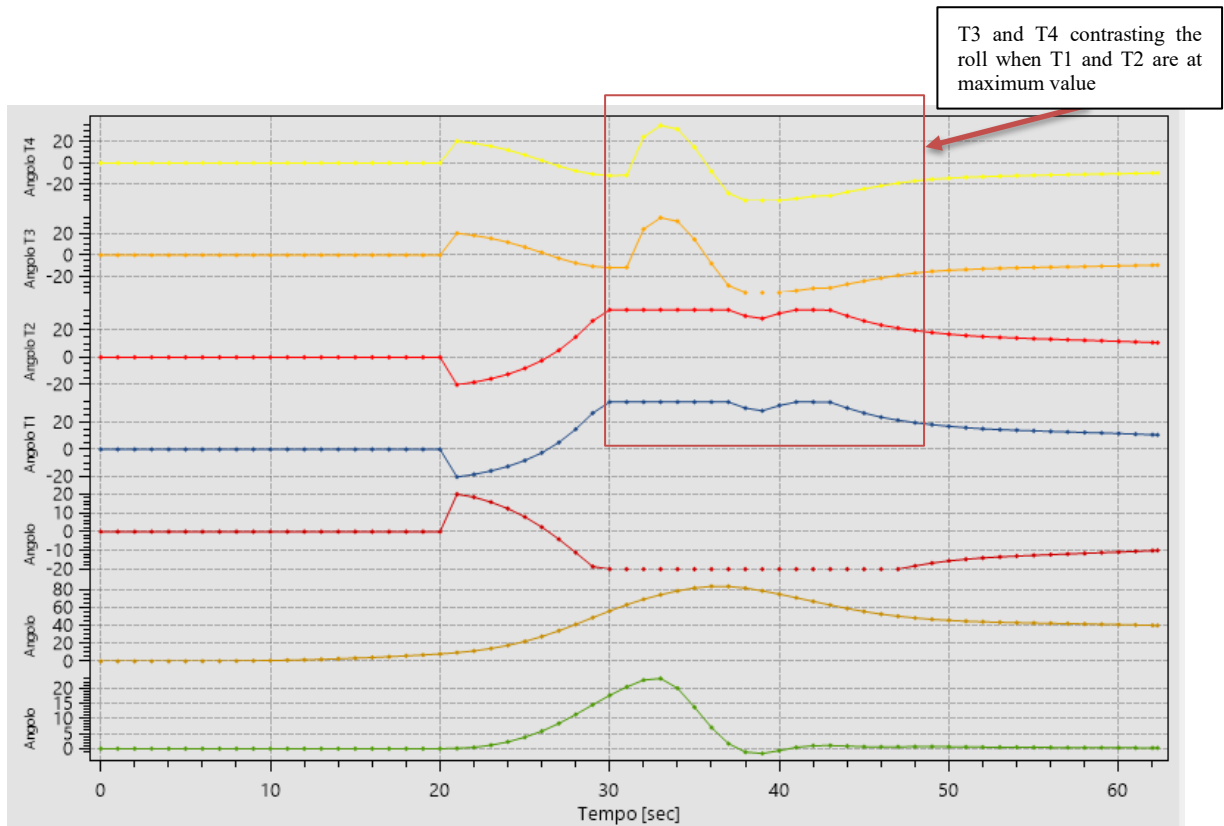


Figure 69 Rudder angles respect pitch and roll

In this test it is possible to notice the effect of the rudders with respect to the pitch angle and roll. It is clear how the effect of the roll is distributed on the T4 and T3 rudders to be able to compensate for it (figure 69).

From the graph below is evident how the speed of the drone increase but does not reach 8 m/s as in the open-loop test due to the use of rudders that contrast the water flow.

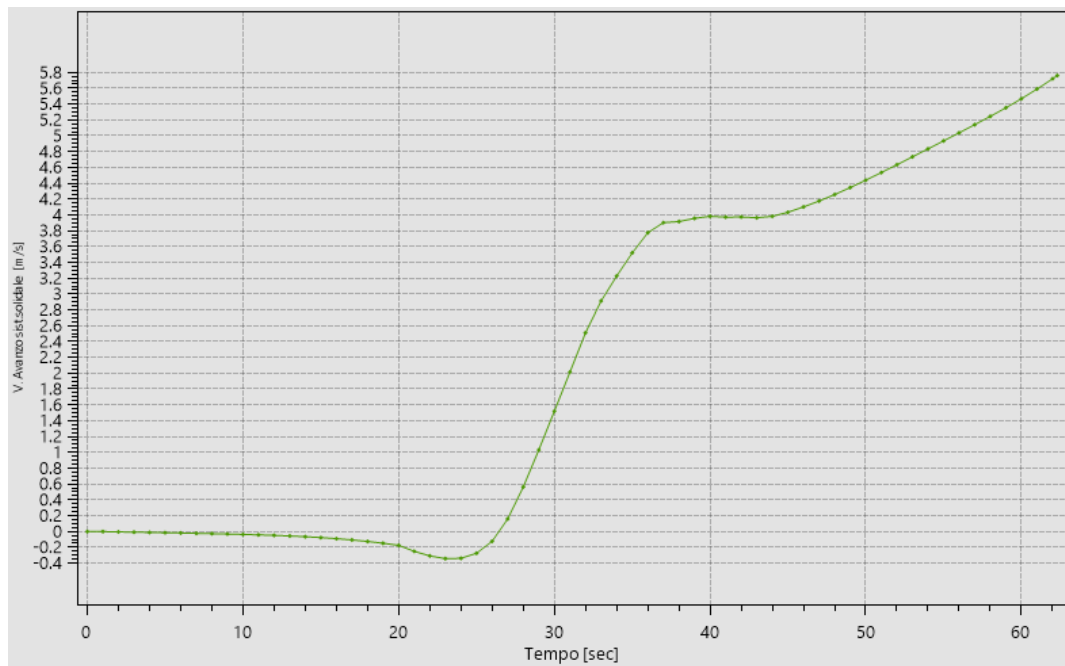


Figure 70 Speed of the drone

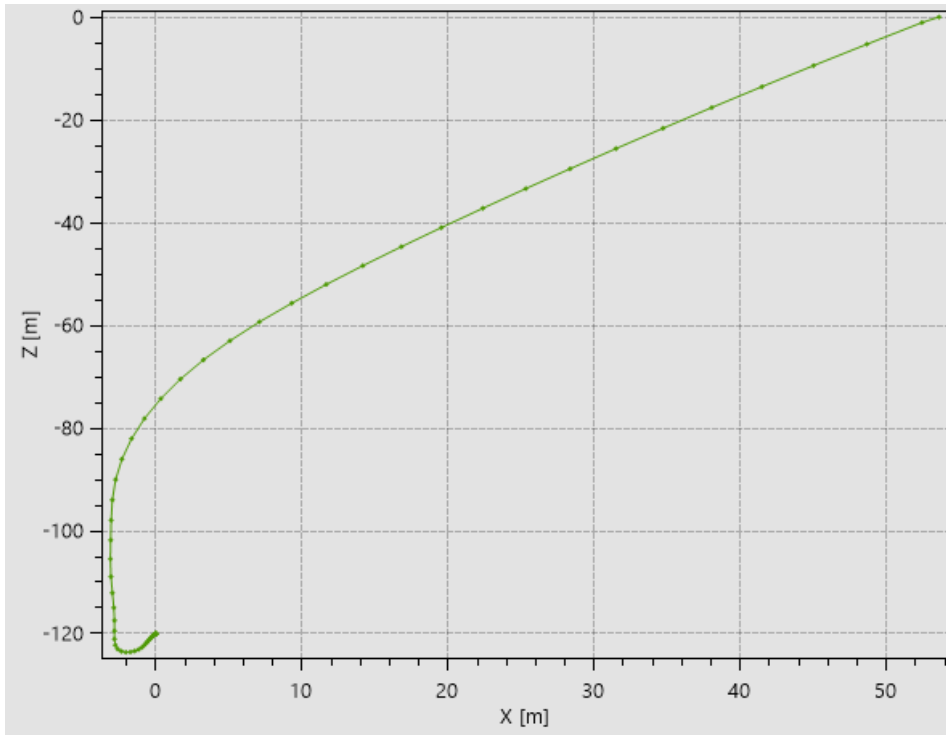


Figure 71 X-Z plane

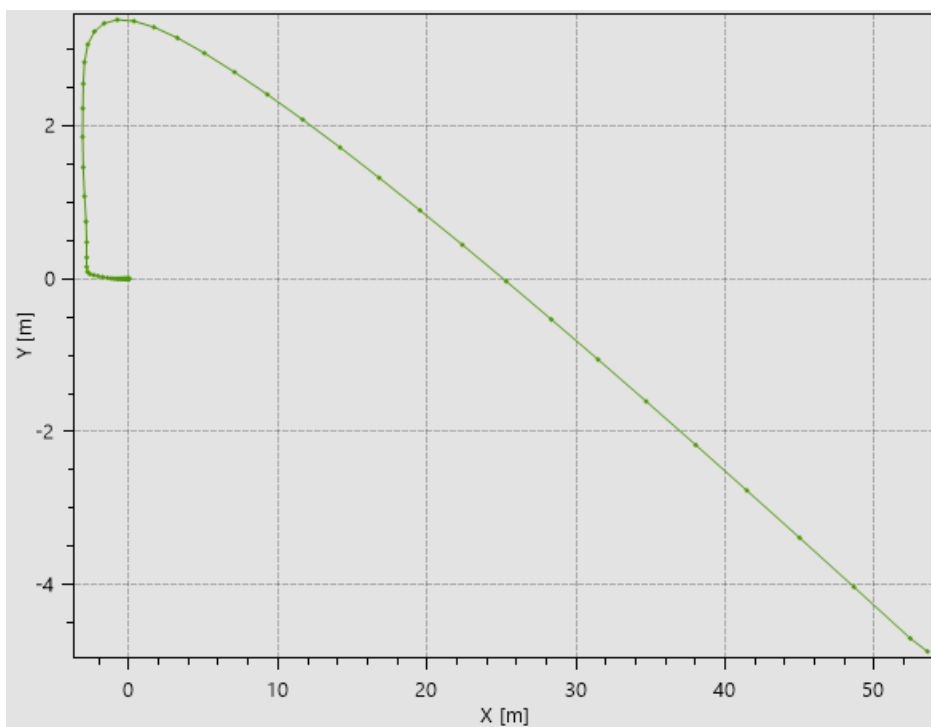


Figure 72 X-Y plane

The trajectory obtained in closed-loop increases drastically at the level of meters traveled and consequently also as a lift time, while the effect of roll control brings the drone back from 3 meters to -5 on the Y axis.

### 6.3.3 Optimization with Genetic Algorithm

The genetic algorithm software produces 4 graphs containing information regarding the optimization: On the top left is shown the fitness score of the various generations and in red the curve of the candidates. At the top right the emergence time and the angle value of the best tests performed by the individuals of the population.

In bottom left the graph containing the best test obtained, showing pitch angle and rudders action respect to the time, instead at the bottom right the depth with respect to the time

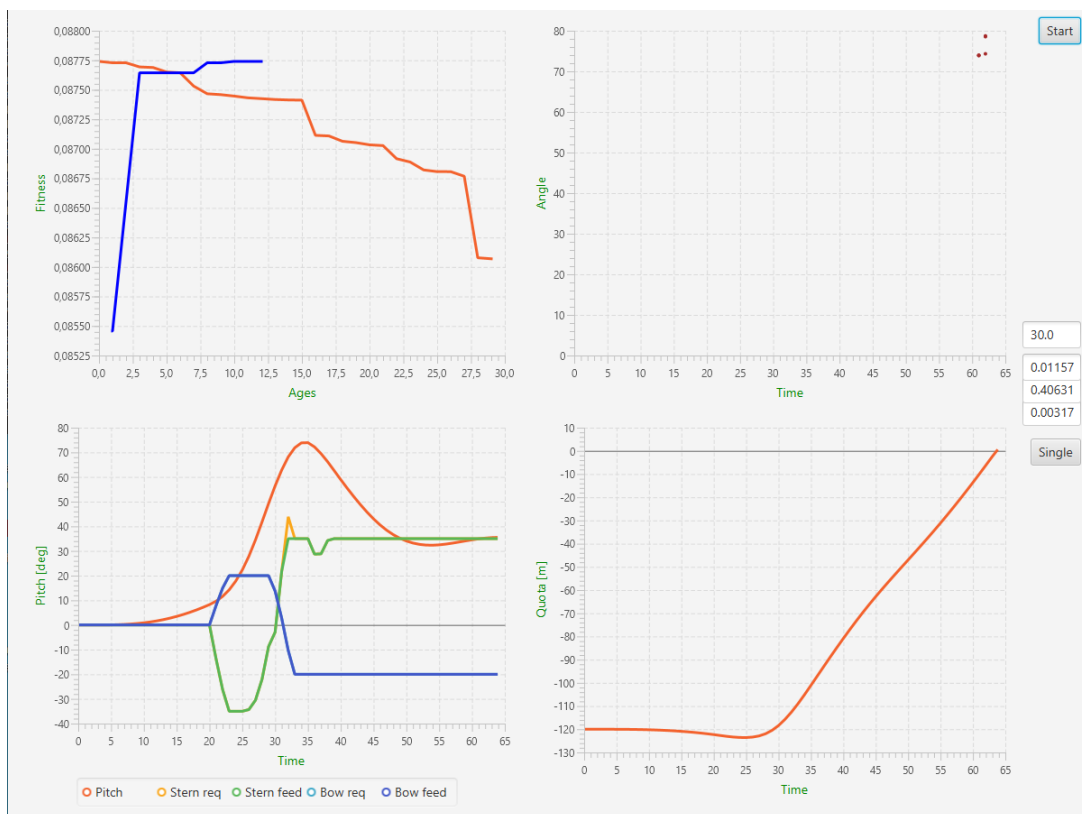


Figure 73 Genetic Algorithm results

The best results are saved in a file where all the best evidence is saved, the text strips of the file contain all the information, including the ascent time, the fitness score and the PID constants:

0.0854571	0.0000000	0.0854571	30.0000000	0.3345918	0.9906724
0.0033218	0.1911953	0.5660985	0.0018982	62.0000000	74.3202700
0.0876441	0.0000000	0.0876441	30.0000000	0.0115728	0.6426647
0.0979283	0.0066130	0.3672370	0.0559591	61.0000000	73.9304800
0.0877286	0.0000000	0.0877286	30.0000000	0.0115728	0.6426647
0.0367545	0.0066130	0.3672370	0.0210026	61.0000000	73.9214900
<b>0.0877406</b>	<b>0.0000000</b>	<b>0.0877406</b>	<b>30.0000000</b>	<b>0.0115728</b>	<b>0.6426647</b>
<b>0.0271493</b>	<b>0.0066130</b>	<b>0.3672370</b>	<b>0.0155139</b>	<b>61.0000000</b>	<b>73.9203300</b>

From the last test executed by the software the values of the three constants are:

$$Kp=0.0115728 \quad Ki=0.6426647 \quad Kd=0.0271493$$

And an angle of emergence of **73.92°**.

Re-running the Open-Loop test with the new values gives the best possible ascent maneuver for that depth and speed:

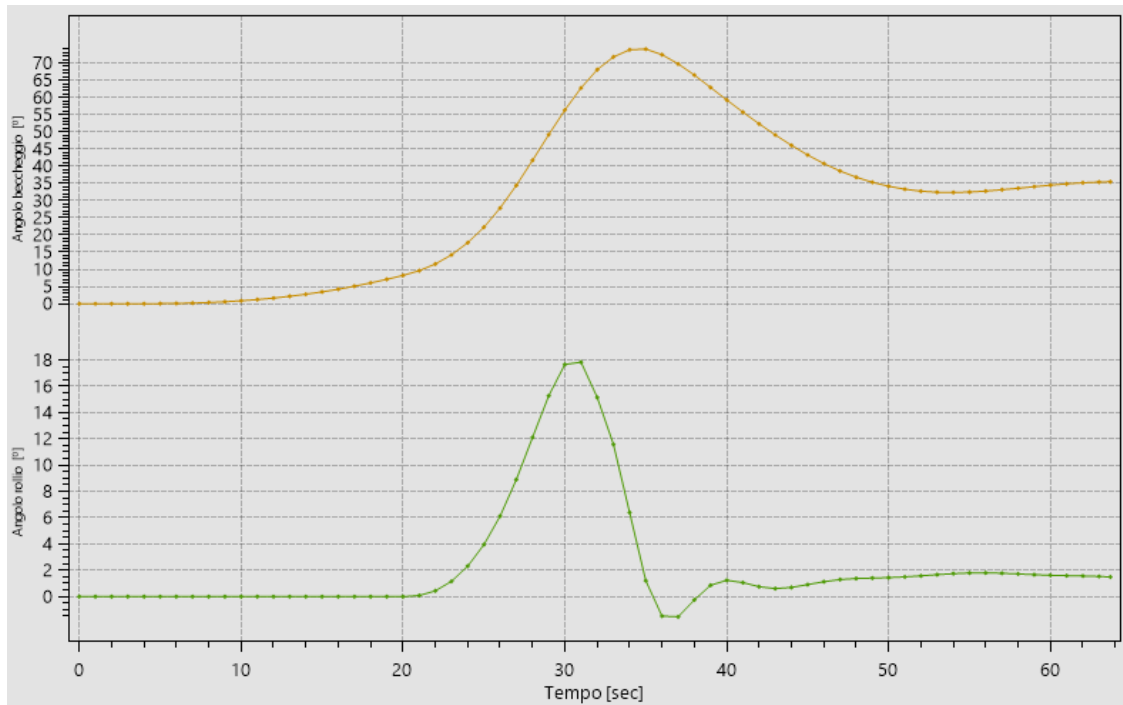


Figure 74 Results with tuned PID on pitch

We can therefore notice an improvement of the angle of ascent at the expense of time, even if the request of 45° is not respected it is still a good result that the system then goes to 35° after the peak, consequently it can still be considered an acceptable condition of emergence, even if the abrupt change of angle could cause problems to the drone.

The final results show an improvement in all angles thanks to the tuning:

Table 3 Simulation results of 120 depth and 0 rpm

	Open loop	Closed Loop	PID
Maximum angle	82°	83	73°
Maximum roll	23°	23°	18°
Time	50 s	62 s	65 s

## 6.4 Simulation at 250 depth and 60 rpm

### 6.4.1 Open-loop analysis

In the open loop test the submarine emerges with a time of 60 seconds with an angle of  $75^\circ$  and a roll peak at  $7.76^\circ$  since the ballast crates are not perfectly aligned.

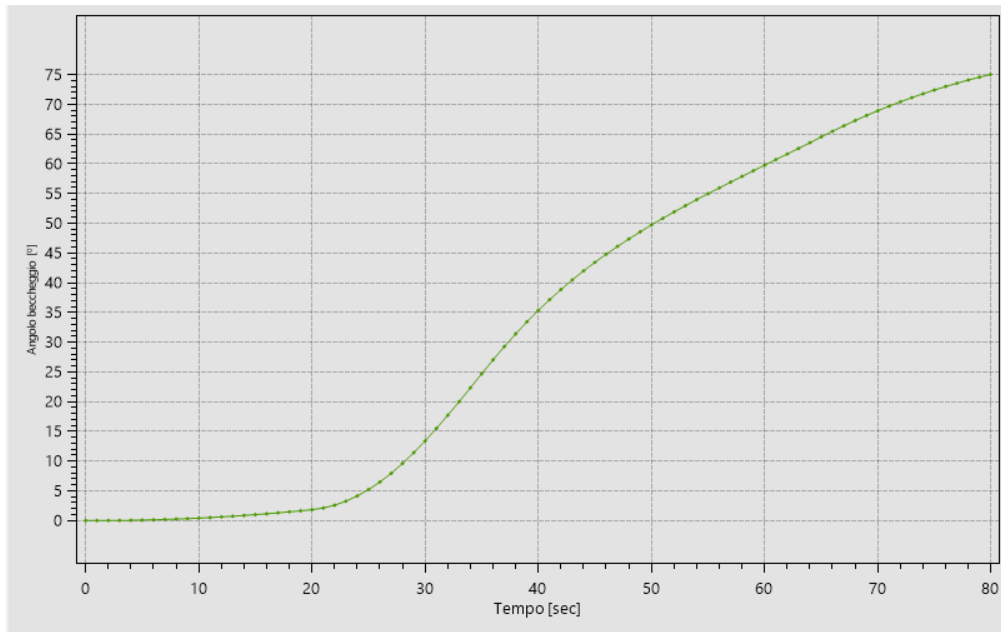


Figure 75 Pitch angle

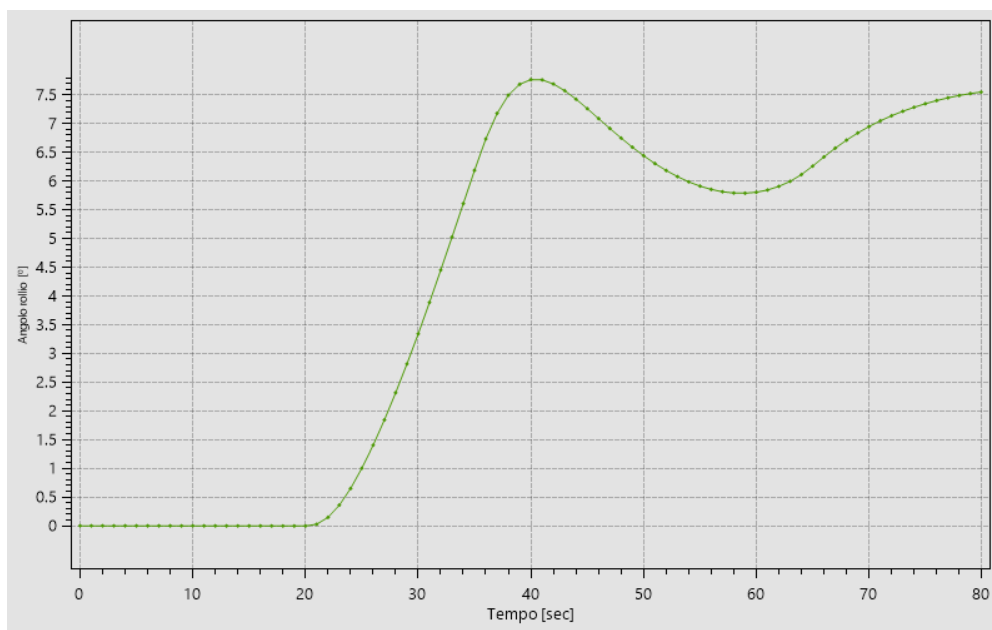


Figure 76 Roll angle

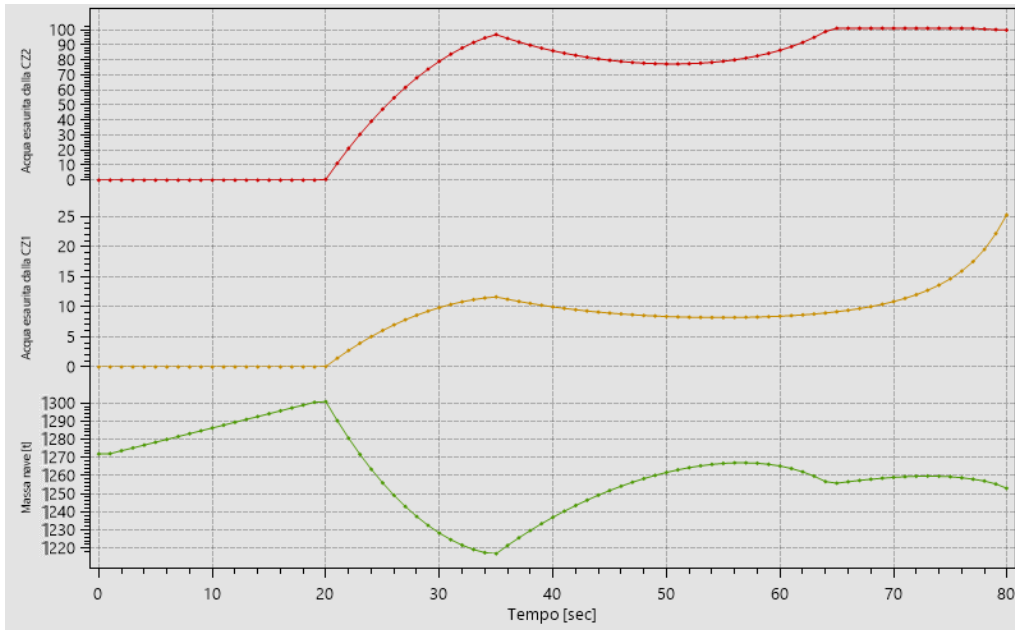


Figure 77 Mass of the drone respect the filling by compressed air

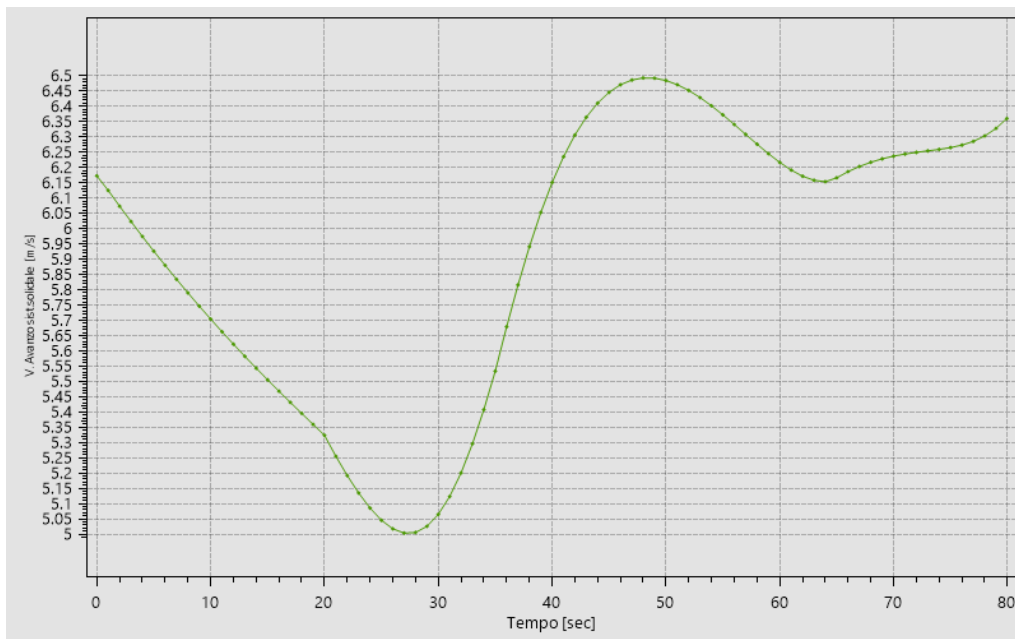


Figure 78 Drone speed

The ratio between system speed and mass is highlighted by these two graphs (figure 77 and 78), it is evident that the speed gain is caused by the filling of the drone crates, while in the first 20 seconds of water boarding happens a progressive loss of speed. It can be noted that compared to the previous test the system of filling the crates with air is much less effective, in fact in the first 20 seconds more water enters the floodable room and due to the higher pressure of it the air has less effect.

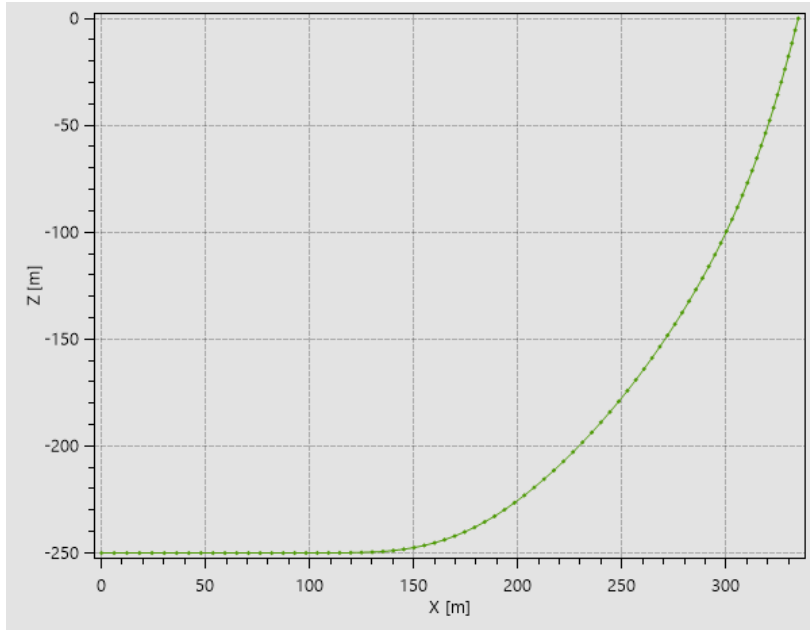


Figure 79 X-Z plane

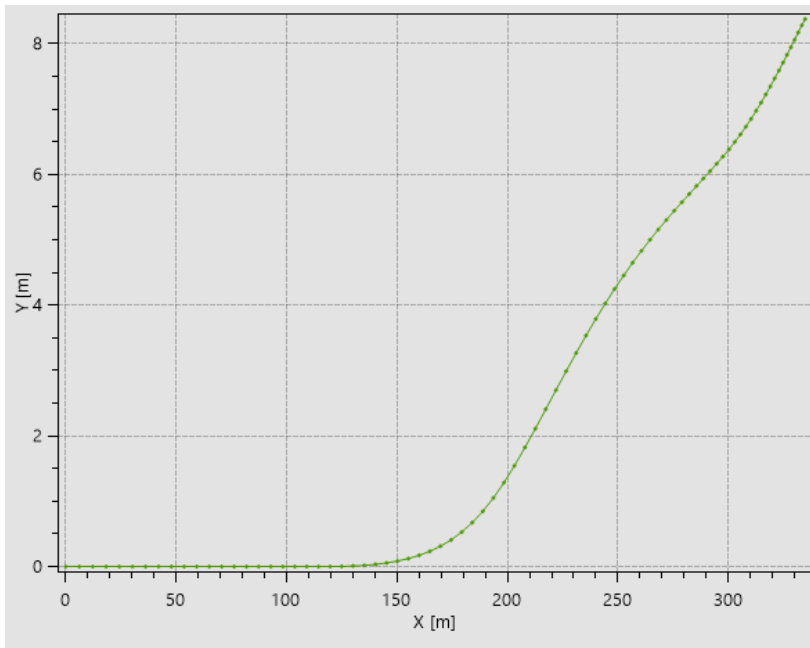


Figure 80 X-Y plane

The final trajectory is shown in the following graphs where it is highlighted how the roll causes a shift on Z of 8 meters in 150 meters of travel, this is since the rudders, even if not operating, divert the movement to the left due to the moment of roll

### 6.4.2 Closed Loop analysis

For the following test, together with the filling of the crates, the feedback of the system was also activated by using the stern and bow rudders in discordant configuration.

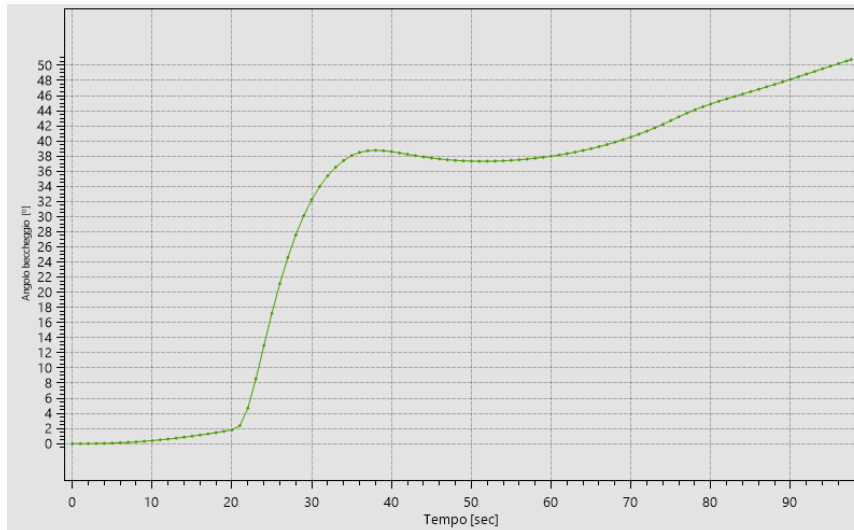


Figure 81 Pitch with PID

Compared to the open loop test the control of the angle of emergence has increased the ascent time, however the maximum angle is  $50.72^\circ$ , better than the previous one.

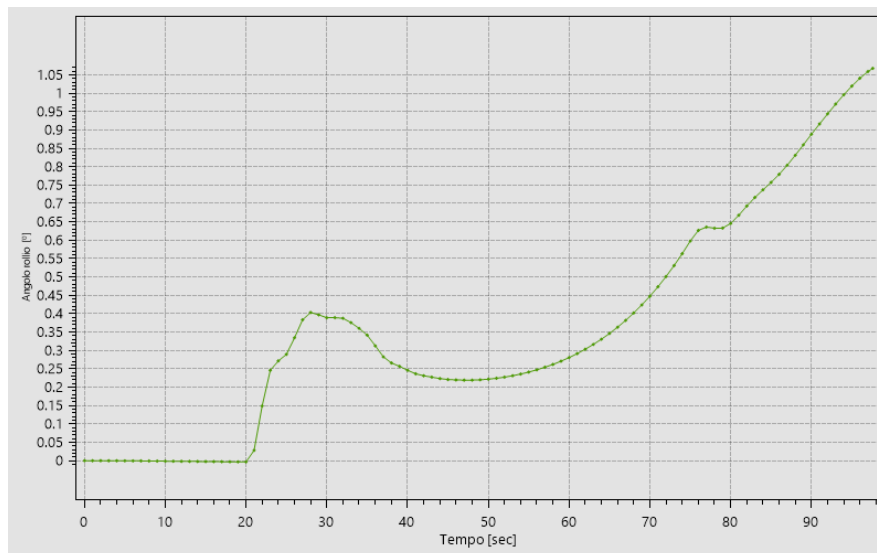


Figure 82 Roll with PID

The roll, thanks to the control of the rudders, is reduced to a maximum of  $1^\circ$  which is considered acceptable

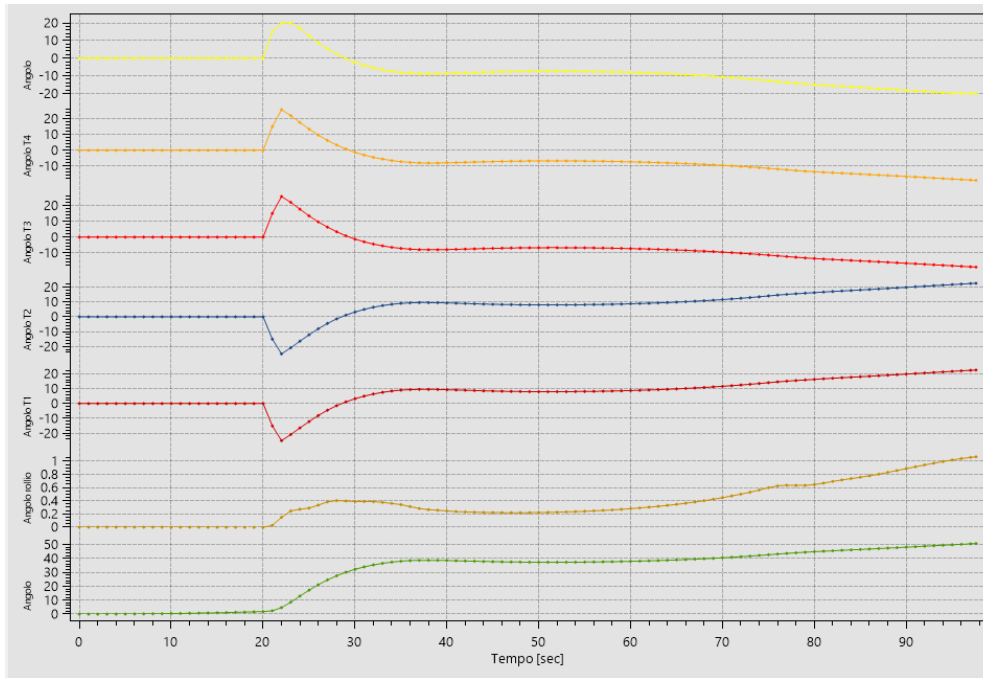


Figure 83 Rudders angles

In this test it is possible to notice the effect of the rudders with respect to the pitch angle, the roll is managed effectively thanks to the configuration, in fact in the second 30 to counteract  $0.34^\circ$  degrees of roll the rudders 3 and 4 are at  $-1.25^\circ$  while 1 and 2 at  $3.24^\circ$ .

From the graph below the speed of the drone decrease, in fact by contrasting the flow of water to compensate for the angle control the speed is reduced, this causes a loss of performance during the ascent.

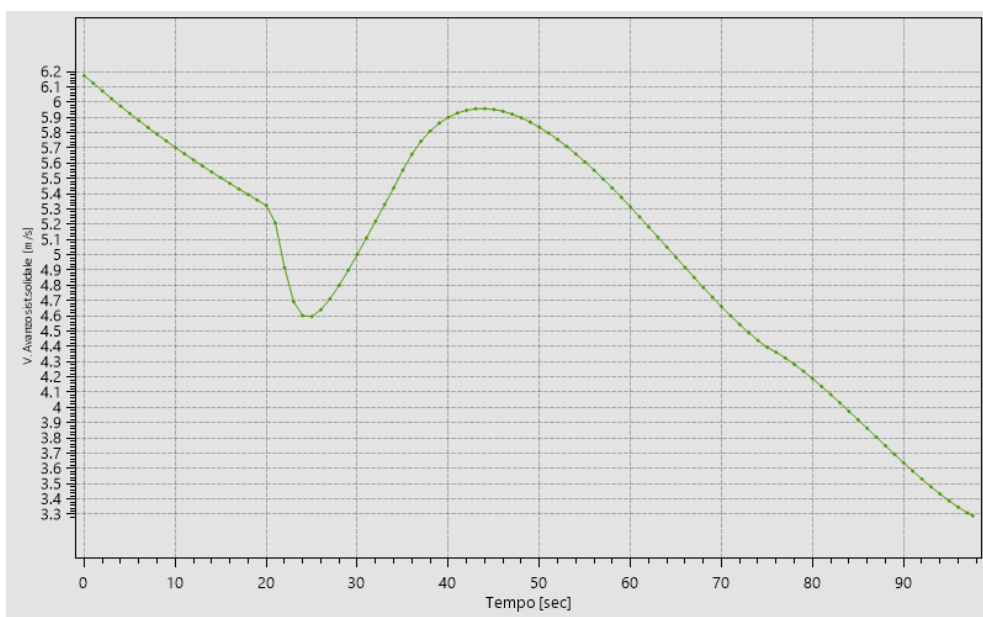


Figure 84 speed of the drone

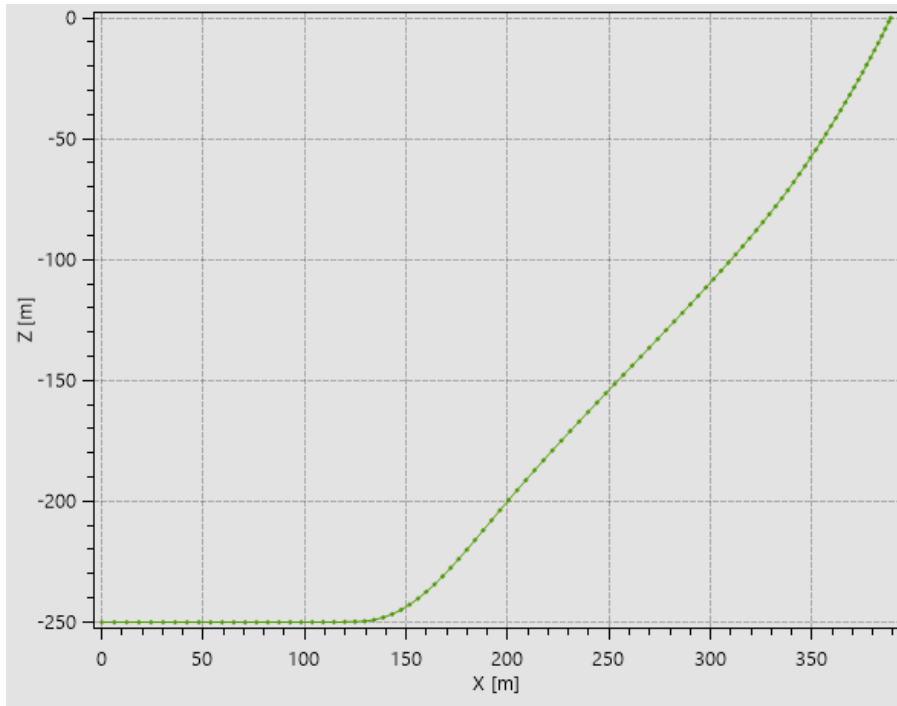


Figure 85 X-Z plane

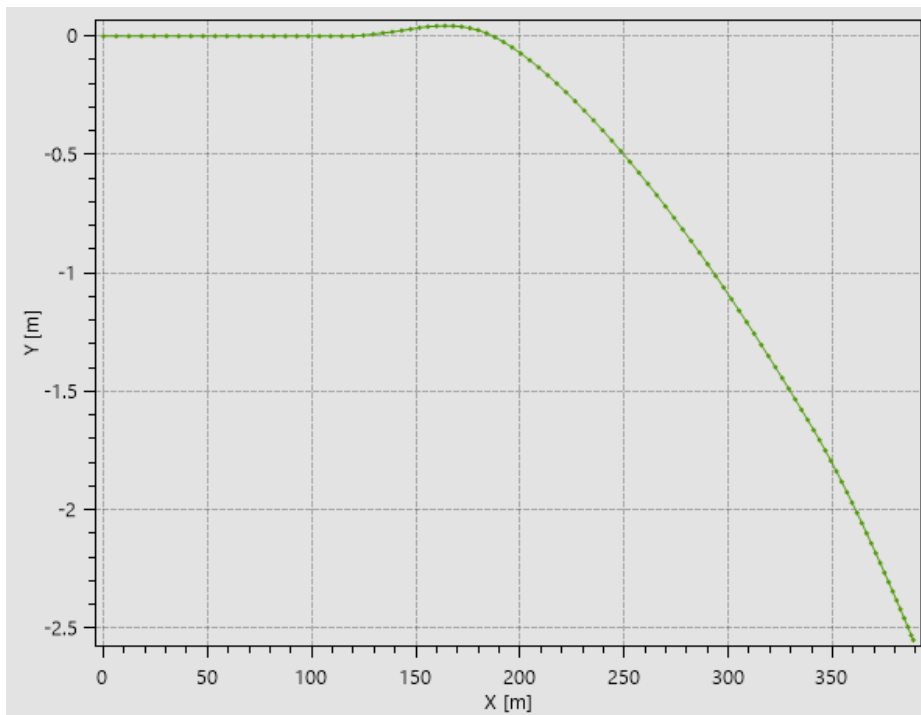


Figure 86 X-Y plane

The final trajectory with respect to the open loop is improved as the pitch during emersion maintains a smaller angle and the reduced roll cause just 2.5 meter on the Y axis, however due to the increased time for the conclusion of the test the drone emerges after 388 meters compared to the 346 of the open loop tests.

### 6.4.3 Optimization with Genetic Algorithm

For the optimization the genetic algorithm is again performed, from the graphs is shown how with the continuation of the simulations the results become better, in fact in the “ages” the blue fitness score improves.

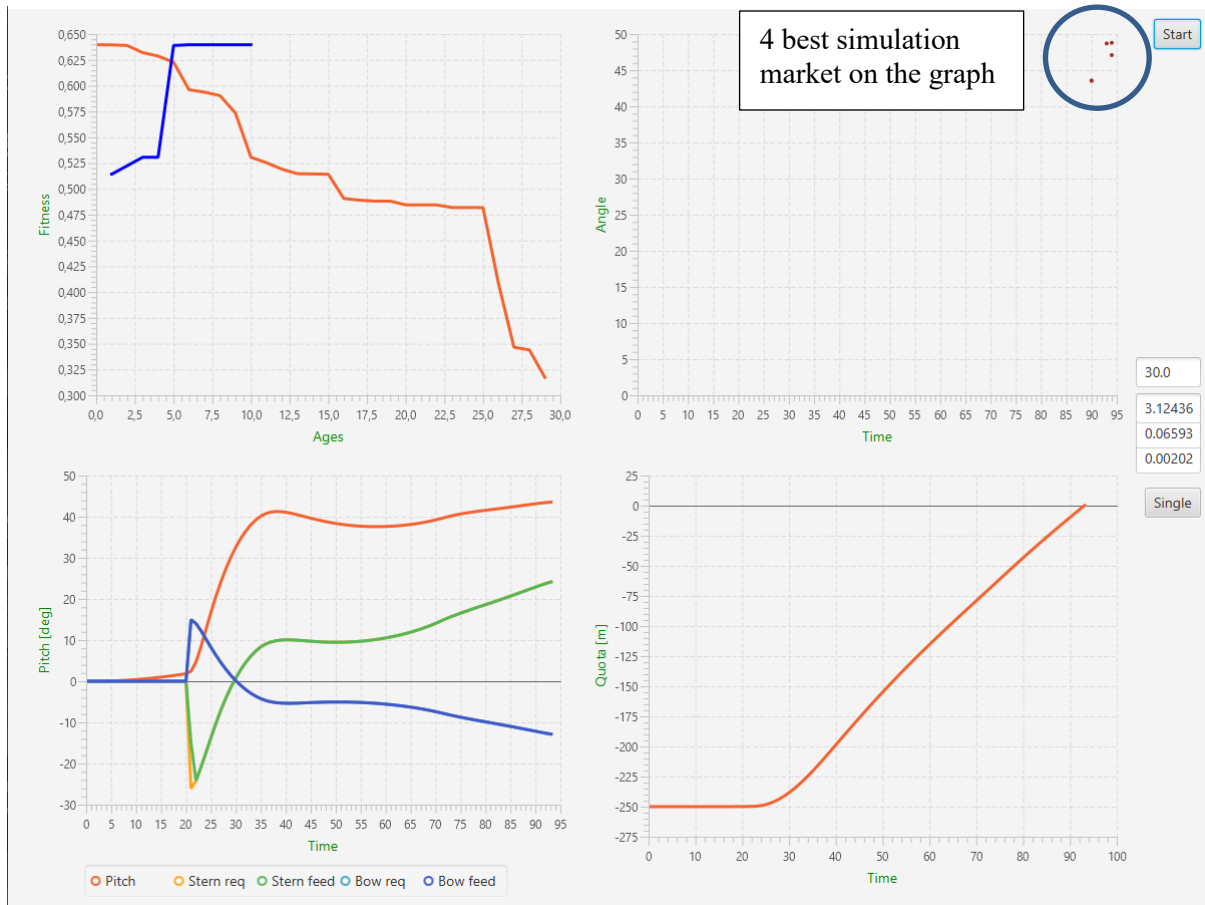


Figure 87 Genetic Algritm results

From the saved best results is taken the last one:

0.5306053	0.0000000	0.5306053	30.0000000	0.5434597	0.0659372
0.0791975	0.3105484	0.0376784	0.0452557	93.0000000	48.7037600
0.5937594	0.0000000	0.5937594	30.0000000	1.1361901	0.0188580
0.0020493	0.6492515	0.0107760	0.0011710	94.0000000	47.0878500
0.6389485	0.0000000	0.6389485	30.0000000	0.9300305	0.0204928
0.0093644	0.5314460	0.0117102	0.0053511	90.0000000	43.5485800
<b>0.6396915</b>	<b>0.0000000</b>	<b>0.6396915</b>	<b>30.0000000</b>	<b>0.9300305</b>	<b>0.0204928</b>
<b>0.0539560</b>	<b>0.5314460</b>	<b>0.0117102</b>	<b>0.0308320</b>	<b>90.0000000</b>	<b>43.5535300</b>

From the last test executed by the software the values of the three constants are:

$$Kp=0.9300305 \quad Ki=0.0204928 \quad Kd=0.0539560$$

And an angle of emergence of **43.553°**

Re-running the Open-Loop test with the :new values gives the best possible ascent maneuver for that depth and speed:

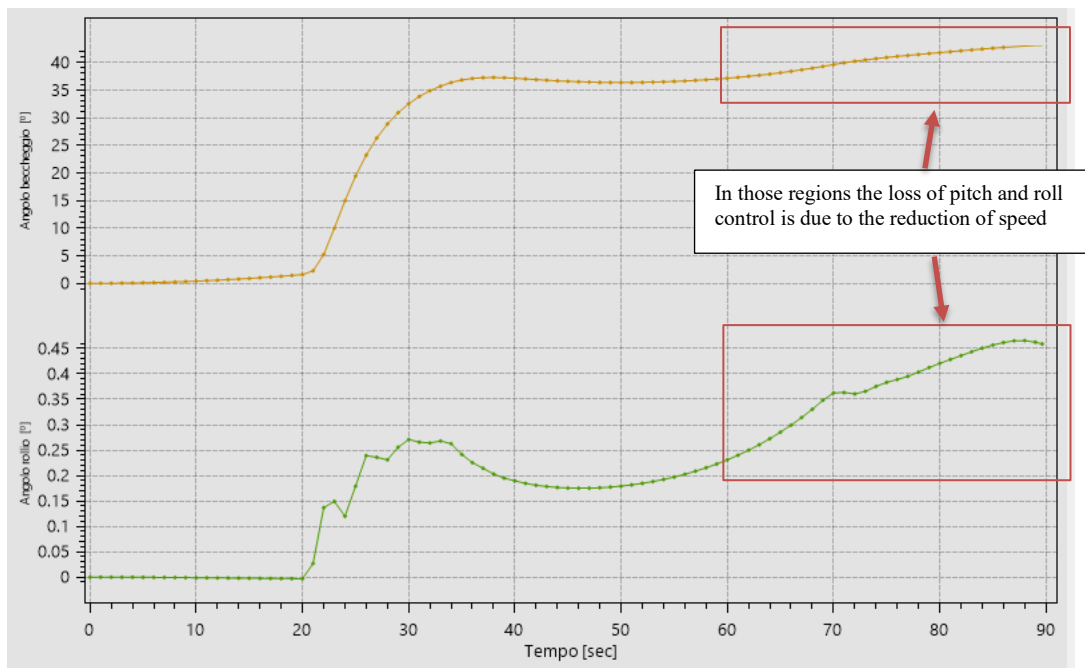


Figure 88 Results with tuned PID on pitch

The final part of the ascent suffers a loss of performance, this is because the speed decreases and the effect of the rudders is less effective, so even if the PID tries to stem the angle, its effect is not enough. Increasing its effect in this area would cause an excessive reduction in speed that would lead to sinking.

As shown in the table, the last simulation has a smaller pitch and roll value and respect to the closed-loop one, is obtained a smaller time of ascent.

Table 4 Simulation results 250 depth and 60 rpm

	Open loop	Closed Loop	PID
Maximum angle	75°	50°	43°
Maximum roll	7.5°	1.1°	0.45°
Time	80 s	98 s	91 s

## 6.5 Simulation at 350 depth and 148 rpm

### 6.5.1 Open-loop analysis

The open-loop test at maximum speed shows how once the air tanks are activated the drone maintains the angle caused by the 8 ones in the bow, it takes a time of 103 seconds from the beginning of the flaw to reach the surface. The angle in other simulation at greater depths is lower as the air filler are less effective.

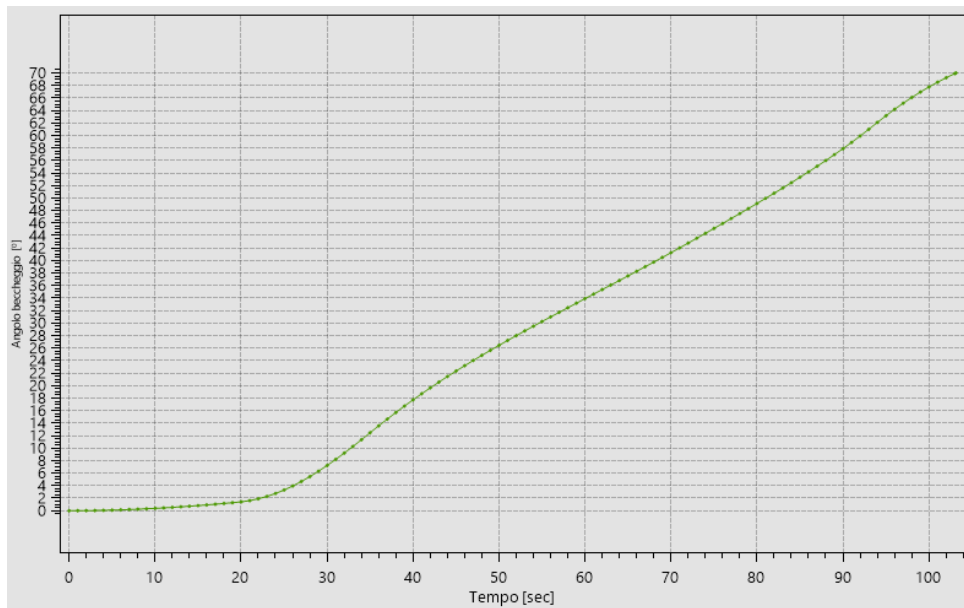


Figure 89 Pitch angle during the test

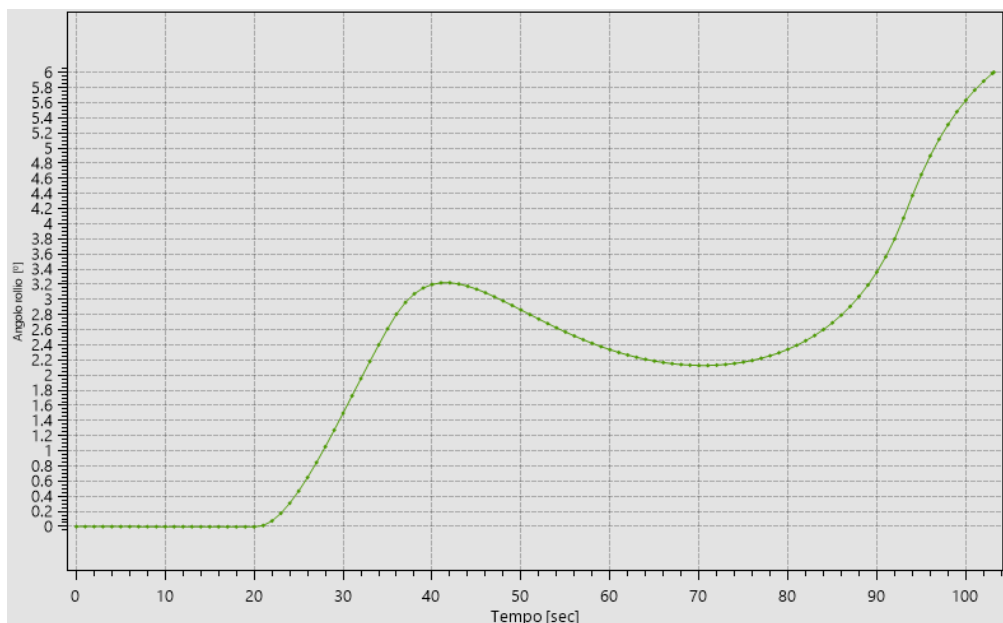


Figure 90 Roll angle during the test

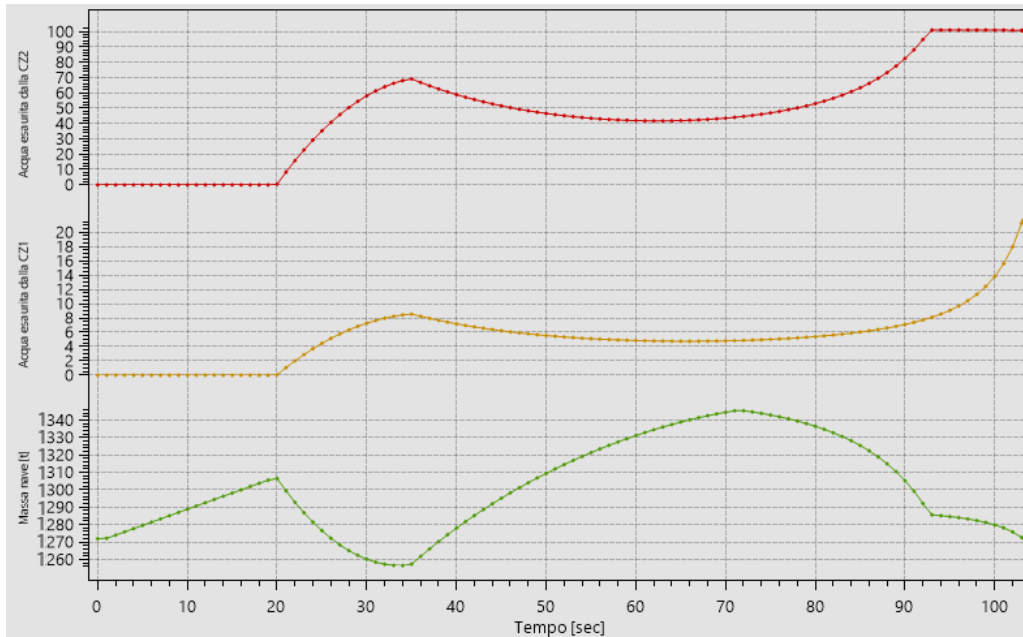


Figure 91 mass of the vessel with respect to the leak and filling of the crates

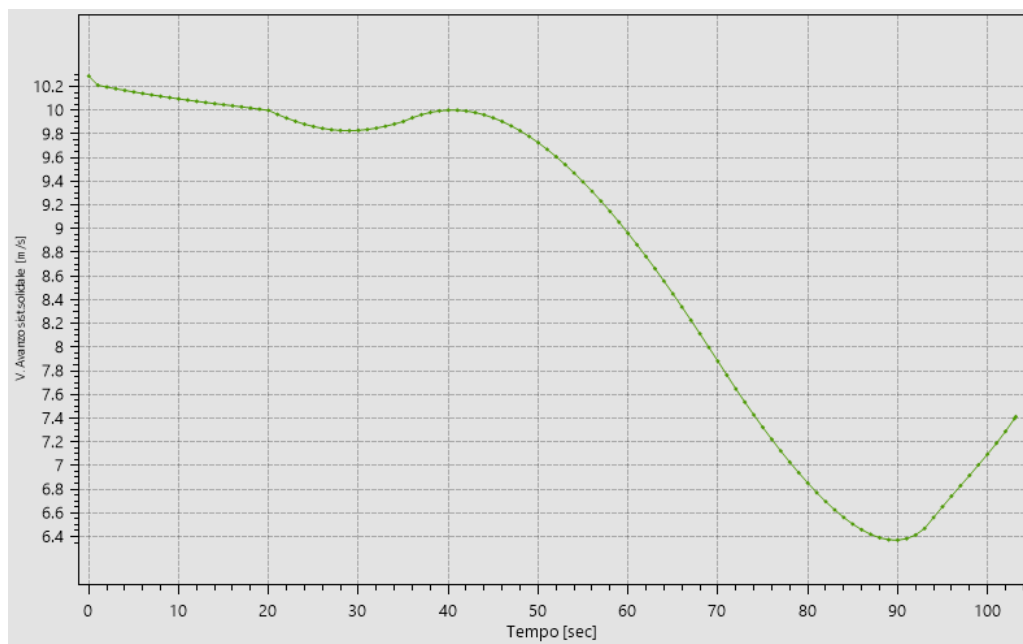


Figure 92 Drone speed

Even if the system proceeds quickly from the beginning and undergoes the help of the maximum revolutions of the propeller, the speed still decreases for the entire duration due to the continuous increase in mass and the effect of the rudders that counteract the flow of the water (figure 91).

In the last part there is a gain in speed since the air in the crates expands further thanks to the lower external pressure (figure 92).

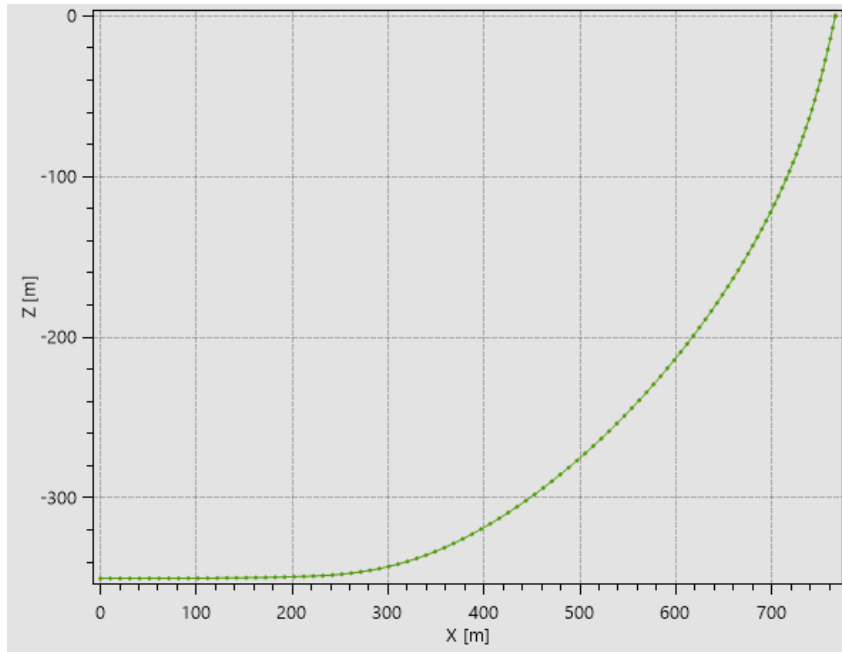


Figure 93 X-Z plane

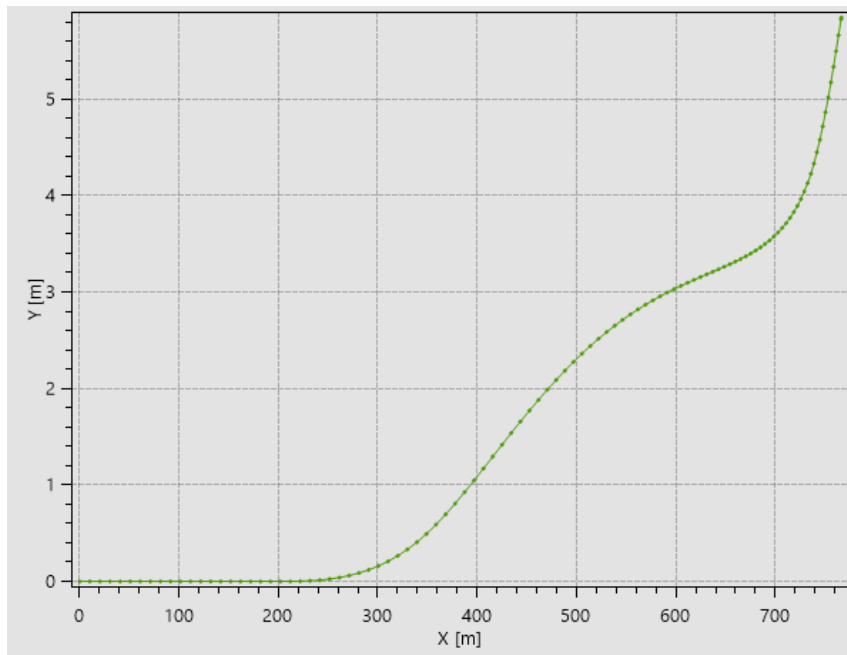


Figure 94 X-Y plane

The final trajectory is shown in the following graphs where it is highlighted how the roll causes a shift on  $Z$  of 8 meters in 150 meters of travel, this is since the rudders, even if not operating, divert the movement to the left due to the moment of roll.

### 6.5.2 Closed Loop analysis

For the following test, together with the filling of the crates, the feedback of the system was also activated using the stern and bow rudders in discordant configuration.

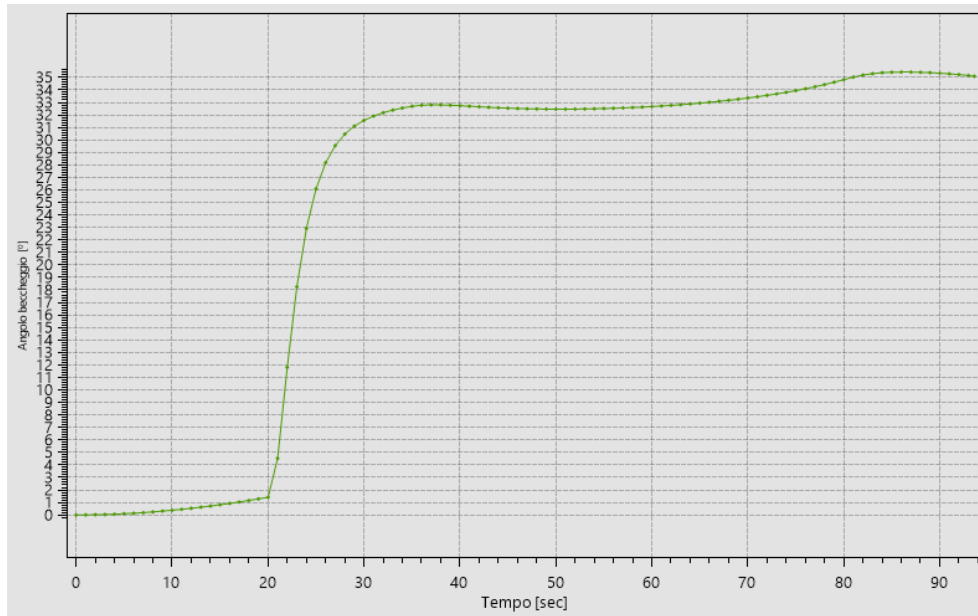


Figure 95 Pitch with PID

Compared to the open loop test the control of the angle of emergence has increased the ascent time, however the maximum angle is  $50.72^\circ$ , better than the previous one.

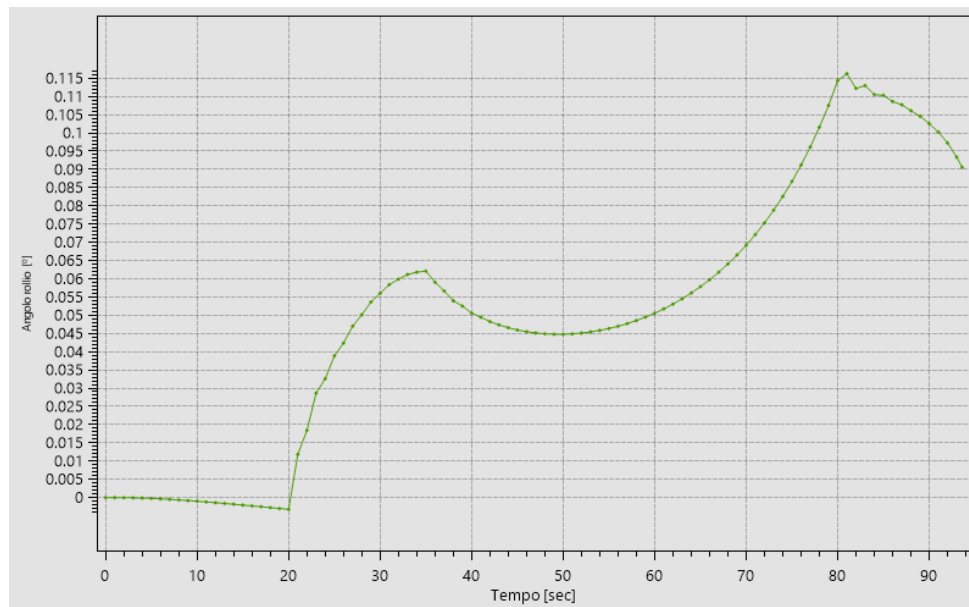


Figure 96 Roll with PID

The roll, thanks to the control of the rudders, is reduced to a maximum of  $1^\circ$ , which is considered acceptable.

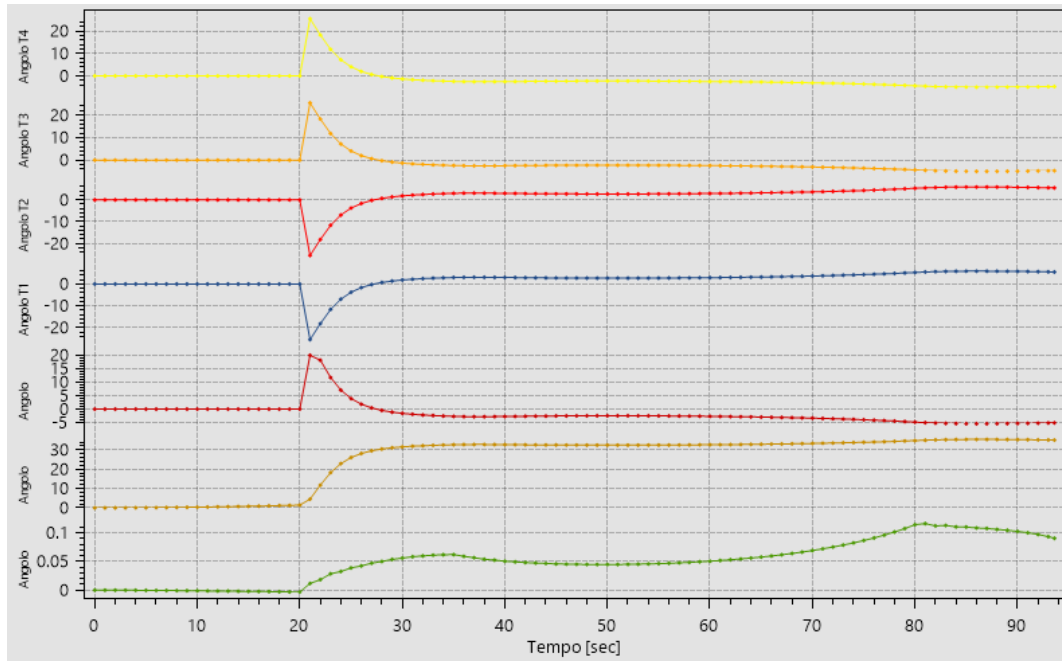


Figure 97 Rudders angles

In figure 97 is possible to notice the effect of the rudders with respect to the pitch angle, the roll is managed effectively, in fact in the second 30 to compensate 0.34 degrees of roll the rudders 3 and 4 are at  $-1.25^\circ$  degrees while 1 and 2 at  $3.24^\circ$ .

In picture 98 is reported the speed of the drone, it decreases due the rudders that contrast the flow of water to control pitch and roll angles, this causes a loss of performance during the ascent.

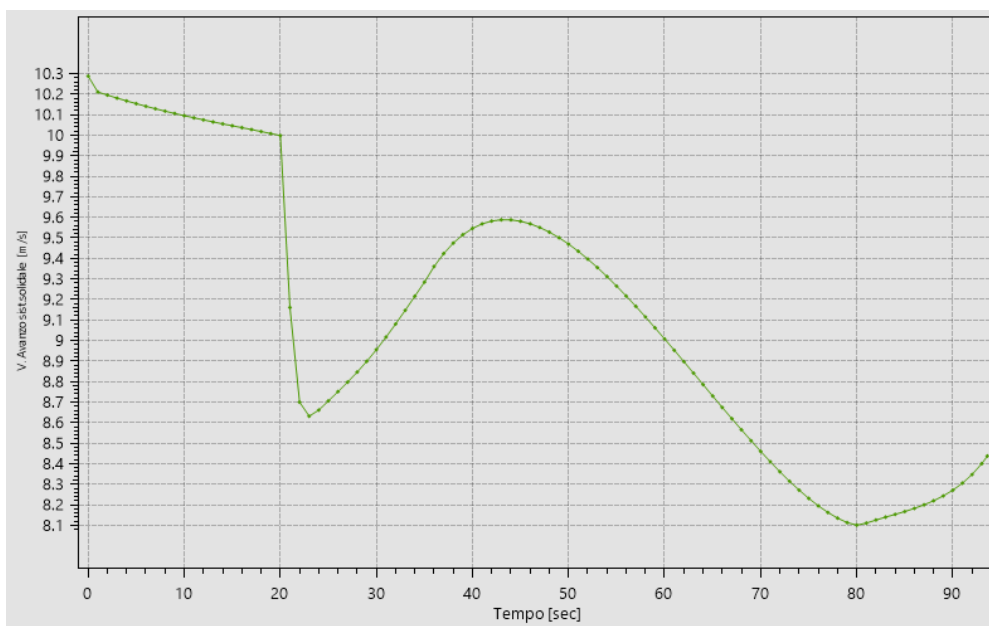


Figure 98 speed of the drone

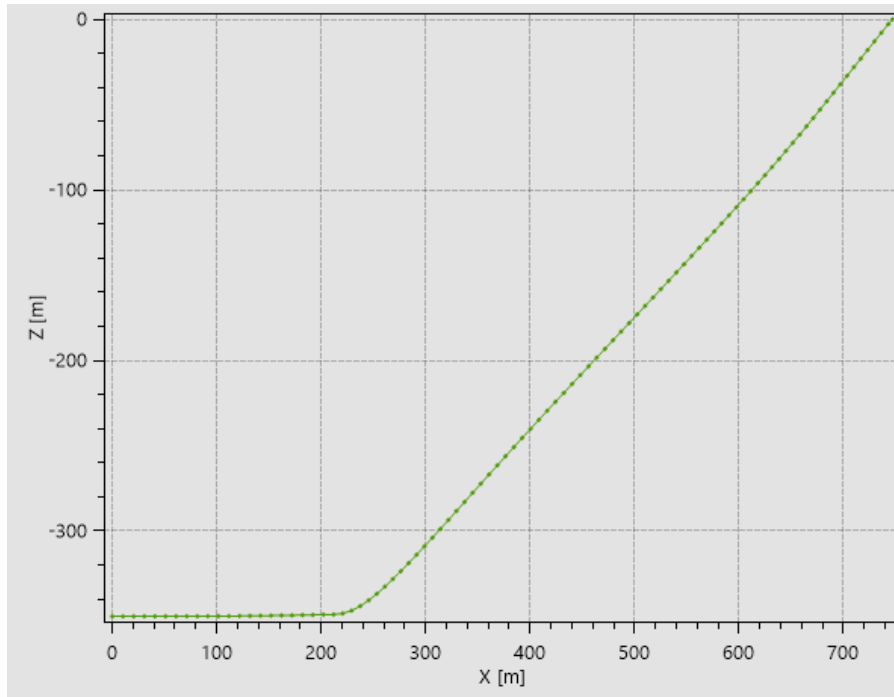


Figure 99 X-Z plane

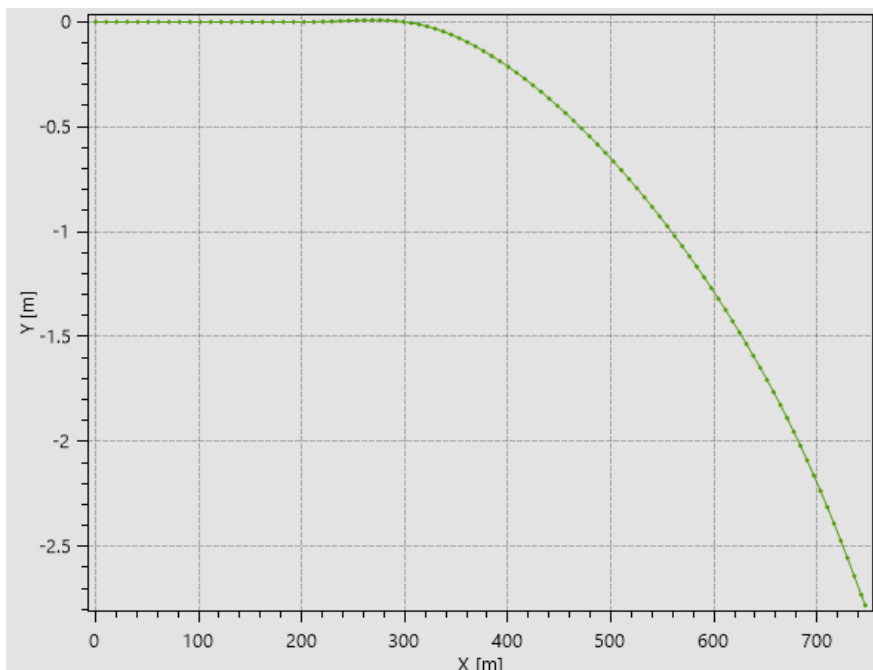


Figure 100 X-Y plane

The final trajectory with respect to the open loop is improved as the pitch, during emersion, maintains a smaller angle and the reduced roll cause just 2.5 meter of movement on the Y axis, however due to the increased time for the conclusion of the test the drone emerges after 388 meters compared to the 346 of the open loop tests.

### 6.5.3 Optimization with Genetic Algorithm

With the genetic algorithm we obtain the values of the best PID constants for this test, as shown in figure 101, is possible to see how the results obtained are progressively improved, until the best condition is reached.

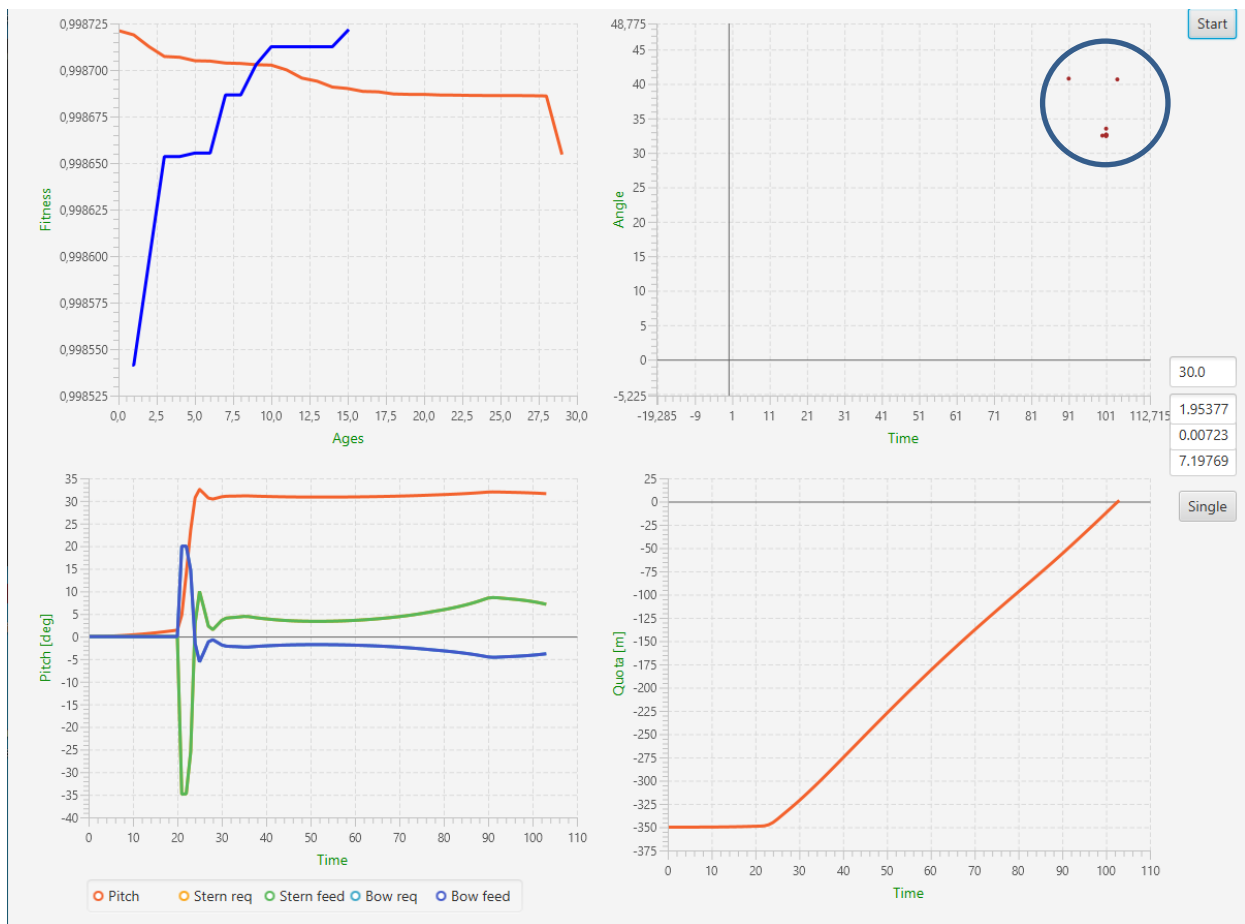


Figure 101 Genetic Algorithm results

The five best proofs are saved in a line of text where is get the improved PID values of the best one:

0.9986866	0.0000000	0.9986866	30.0000000	3.9366305	0.0071977
0.0030569	2.2495032	0.0041130	0.0017468	101.0000000	32.6234000
0.9987028	0.0000000	0.9987028	30.0000000	3.9366305	0.0071977
0.0922148	2.2495032	0.0041130	0.0526941	101.0000000	32.4739800
0.9987125	0.0000000	0.9987125	30.0000000	3.9366305	0.0052020
0.0922148	2.2495032	0.0029726	0.0526941	101.0000000	32.4424400
0.9987189	0.0000000	0.9987189	30.0000000	3.9593441	0.0039461
0.0074358	2.2624823	0.0022549	0.0042491	101.0000000	32.5716700
<b>0.9987212</b>	<b>0.0000000</b>	<b>0.9987212</b>	<b>30.0000000</b>	<b>3.9934255</b>	<b>0.0071977</b>
<b>0.0516516</b>	<b>2.2819575</b>	<b>0.0041130</b>	<b>0.0295152</b>	<b>101.0000000</b>	<b>32.5593800</b>

From the last test executed by the software the values of the three constants are:

$$Kp=3.9934255 \quad Ki=0.0071977 \quad Kd=0.0516516$$

And an angle of emergence of **32.55°**

Re-running the Open-Loop test with the new values gives the best possible ascent maneuver for that depth and speed

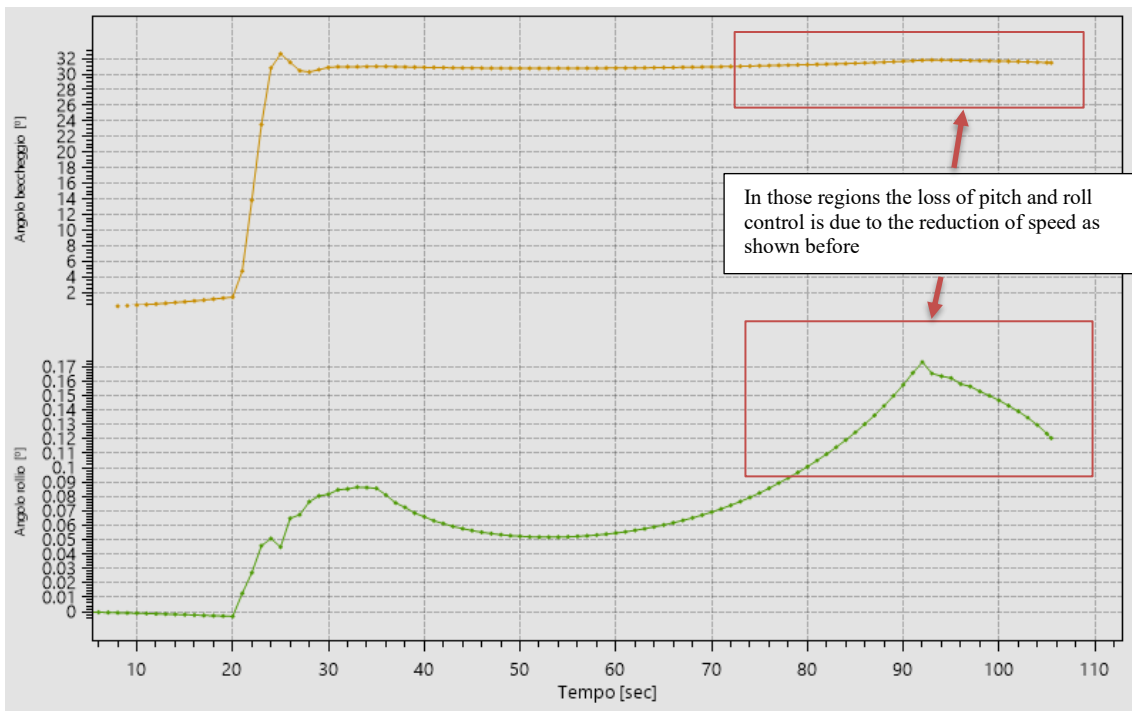


Figure 102 Results with tuned PID on pitch

Looking at the data of the three tests made, through the optimization a better angle is obtained both at the pitch and roll level, however a general is got an increase in the time of the emergence test.

Table 5 Results of simulation at 350 depth at 148 rpm

h	Open loop	Closed Loop	PID
Maximum angle	75°	36°	32°
Maximum roll	7.5°	1.1°	0.45°
Time	80 s	92 s	105 s

## 6.6 Speed depth graph

After have performed many tests, it was possible to create a depth/speed(Rpm) graph containing all the angles of ascent for both closed-loop without PID and closed-loop with tuned PID.

From the graph is immediately noted how the speed affects the system by lowering the maximum angle reached during the various emergences and making it possible to emerge even at higher depths. However, for the lowest speeds the ascent is very limited and the achievement of the angle of 35 ° was never reached.

Table 6 Table containing pitch angle of emersion in different depth with different speed, "0" means that the drone couldn't emerge

	0	20	40	60	80	100	120	148
-50	69.64	40.21	37.80	36.12	34.20	33.43	33.04	32.66
-100	79.00	42.50	39.30	36.75	35.04	33.90	33.39	32.95
-120	83.00	43.45	39.34	36.78	35.88	34.13	33.45	33.01
-140	87.00	44.34	39.90	36.84	36.01	34.26	33.52	33.08
-150	0.00	45.50	40.56	37.00	36.56	34.39	33.74	33.21
-200	0.00	54.50	41.72	38.28	36.80	34.62	33.96	33.33
-215	0.00	84.33	45.39	42.89	37.25	34.72	33.74	33.43
-220	0.00	0.00	60.54	43.21	37.64	34.82	34.09	33.54
-240	0.00	0.00	83.31	44.70	38.04	34.92	33.45	33.65
-250	0.00	0.00	0.00	51.00	38.10	35.05	34.18	33.76
-265	0.00	0.00	0.00	85.00	40.88	37.32	35.40	33.87
-290	0.00	0.00	0.00	0.00	76.00	39.04	37.62	33.98
-300	0.00	0.00	0.00	0.00	0.00	42.39	38.44	34.85
-330	0.00	0.00	0.00	0.00	0.00	84.00	40.54	35.35
-350	0.00	0.00	0.00	0.00	0.00	0.00	46.77	36.80
-370	0.00	0.00	0.00	0.00	0.00	0.00	74.00	38.47
-400	0.00	0.00	0.00	0.00	0.00	0.00	0.00	41.69
-455	0.00	0.00	0.00	0.00	0.00	0.00	0.00	72.00

From the results is highlighted a limit curve beyond which the drone sinks, from which is understood how much to increase the speed to re-enter an area of the graph where the emergence is considered possible.

After optimizing all the previous tests made, the table was updated thus demonstrating a general improvement of the emersions, the best results are noticeable at higher speeds, where the drone manages to reach the goal of 30°. On the limit curve the angles undergo a considerable improvement, as for example the case at depth -290 and speed 80 the angle of pitch was 78°, with tuned PID it is possible to maintain a maximum angle of 48°.

Table 7 Table containing pitch angle of emersion in different depth with different speed with PID

	0	20	40	60	80	100	120	148
-50	63.37	42.12	37.28	35.37	34.09	33.87	31.03	30.02
-100	71.30	43.55	38.00	35.65	34.87	33.50	32.43	31.10
-120	75.78	44.01	38.52	35.78	34.93	33.70	32.50	31.21
-140	80.00	44.54	38.92	35.89	35.02	33.52	32.62	31.35
-150	0.00	47.10	39.82	36.02	35.13	33.44	32.84	31.45
-200	0.00	49.88	41.89	36.21	35.80	33.35	32.94	31.87
-215	0.00	52.68	43.74	37.65	35.92	34.13	33.48	31.98
-220	0.00	57.71	44.45	38.18	36.01	34.56	33.79	32.01
-240	0.00	0.00	50.67	40.35	36.12	34.70	34.11	32.05
-250	0.00	0.00	62.20	44.03	36.36	34.98	34.42	32.08
-265	0.00	0.00	0.00	48.00	39.08	36.28	34.73	32.18
-290	0.00	0.00	0.00	0.00	48.00	37.03	34.92	32.22
-300	0.00	0.00	0.00	0.00	59.02	37.17	35.35	32.30
-330	0.00	0.00	0.00	0.00	0.00	53.00	35.85	32.47
-350	0.00	0.00	0.00	0.00	0.00	0.00	39.54	32.65
-370	0.00	0.00	0.00	0.00	0.00	0.00	48.00	34.79
-400	0.00	0.00	0.00	0.00	0.00	0.00	0.00	35.00
-455	0.00	0.00	0.00	0.00	0.00	0.00	0.00	48.00

From the results is obtained a final graph containing the 3 regions of the angles of emergence:

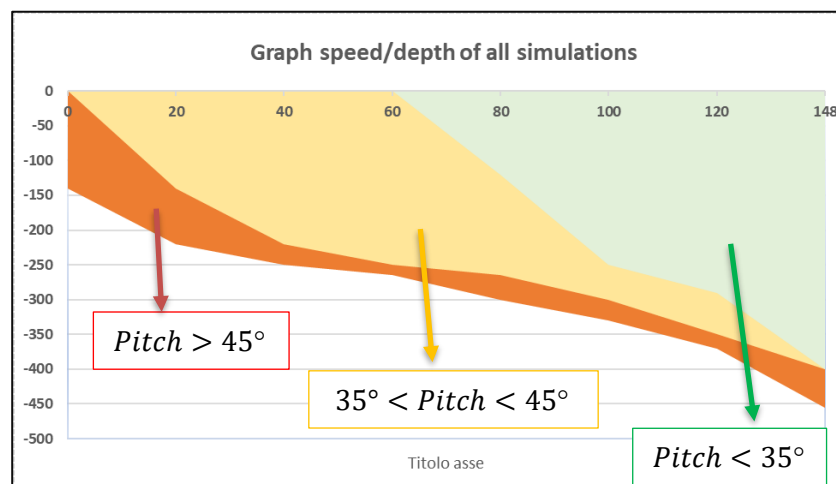


Figure 103 Region of emergence

Analyzing the values of the prove you can see how the optimized PID makes you gain degrees especially close to the values of non-emergence, even allows in some cases to emerge for higher depths depending on the speed considered.

For higher speeds the improvement effect is almost non-existent, is always gained a few degrees compared to the closed-loop test, this shows how the drone is faster and the more the rudders working perfectly even without the optimization of the PID.

Table 8 Difference between closed loop and closed loop with tuned PID

	0	20	40	60	80	100	120	148
-50	6,2700	-1,9100	0,5200	0,7500	0,1100	-0,4400	2,0100	2,6400
-100	7,7000	-1,0500	1,3000	1,1000	0,1700	0,4000	0,9600	0,5600
-120	7,2200	-0,5600	0,8200	1,0000	0,9500	0,4300	0,9500	0,4400
-140	7,0000	-0,2000	0,9800	0,9500	0,9900	0,7400	0,9000	0,3400
-150		-1,6000	0,7400	0,9800	1,4300	0,9500	0,9000	0,3000
-200		4,6200	-0,1700	2,0700	1,0000	1,2700	1,0200	0,2500
-215		31,6500	1,6500	5,2400	1,3300	0,5900	0,2600	0,1700
-220		-57,7100	16,0900	5,0300	1,6300	0,2600	0,3000	0,1100
-240			32,6400	4,3500	1,9200	0,2200	-0,6600	0,0500
-250			-62,2000	6,9700	1,7400	0,0700	-0,2400	-0,0200
-265				37,0000	1,8000	1,0400	0,6700	-0,0800
-290					28,0000	2,0100	2,7000	-0,1400
-300					-59,0200	5,2200	3,0900	0,5500
-330						31,0000	4,6900	0,8800
-350							7,2300	2,1500
-370							26,0000	3,6800
-400								6,6900
-455								24,0000

## 6.7 Considerations

It was decided to evaluate the event of emergence in case of leak as it is a complete critical situation where the capacity of the simulator is tested, the results obtained are clearly modified with respect to the correct values, but their tendency has been maintained to demonstrate how the simulator has managed to provide credible data and allow the study of a control system for this type of maneuver.

These results are to be considered indicative, as the water conditions vary depending on the area of the world where the drone navigates, however, the time limit of 20 seconds before activating the emersion system, as previously mentioned, guarantees a general improvement in results since thanks to the sensors the drone can immediately activate the ascent maneuver.

The genetic algorithm works better for long periods of time, consequently the tests already performed could be further improved by making the algorithm perform as many interactions as possible also the tuning of the PID should be re-performed every time the conditions of the system are changed, any change that leads to a change of mass or a change of speed produces a different response that should need to be optimized to find the optimal value of the three parameters.

From all the tests carried out it is evident how the controller, increasing speed, works better and consequently the **K<sub>p</sub>** values increase, passing from about 0.30 for the limit values of emergence up to 3.99 in the conditions of greater speed. In condition of lower **K<sub>p</sub>** is favored the ascent from the thrust of the crates trying not to lose speed by using too much the rudders, while in conditions of higher speed the proportional value is higher and manages to make better use of them. The constants **K<sub>i</sub>** and **K<sub>d</sub>** instead follow a trend where **K<sub>i</sub>** is higher around the limit values and goes down towards the speed conditions while **K<sub>d</sub>** follows the trend of **K<sub>p</sub>**.

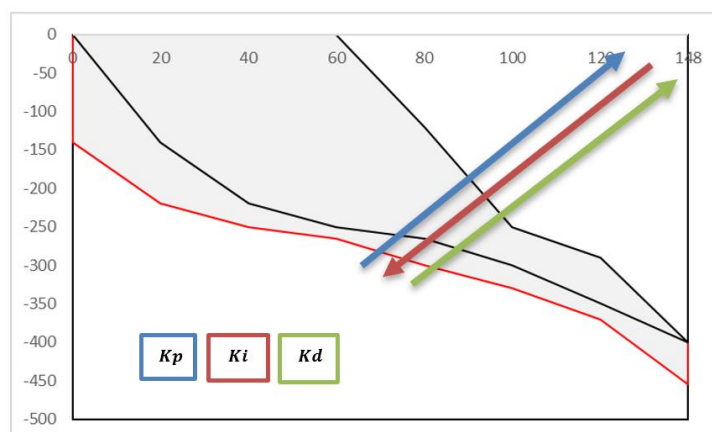


Figure 104 Constant behaviour

## 7 Conclusions

This project aims to demonstrate the effectiveness of simulators for the study of the dynamics of a drone, in the case of the thesis, a large underwater drone.

Thanks to the flexibility of coding, many plausible situations can be created, and the use of a very precise dynamic model allows to obtain results very close to the real ones.

Starting from the simulator developed by Cetena and after analysing the dynamics of the drone it was possible to readapt the software to the new model and verify the manoeuvrability, it was necessary to introduce the X-shaped rudders and all the control systems. Through the various tests it was possible to evaluate the correct behavior, in particular thanks to the emergence test with flaw, which considers a very particular critical situation where the drone loses controllability depending on mass and speed.

With the development of the simulator, it was possible to create a tool able to evaluate any possible modification to optimize the design of the underwater drone, this tool will in fact be used by Cetena to move forward in the project of remotely piloted underwater drones.

The next steps for project optimization will be:

- Changing the interface to make it more compact
- Introduction of a three-dimensional view and graphic reconstruction of the movement of any manoeuvres in the marine environment
- Inserting a new, more advanced control system

As for the drone, thanks to the tests carried out it is expected to:

- Increase rudder area to improve control
- Increase the number of compressed air cylinders to increase the uphill thrust
- Improves propeller thrust by improving blade sizing and the number of possible revolutions

The next step instead for the development of the drone will be the creation of the automatic guidance system for the immersed drone.

## Bibliography

- Bystrom L., “SUBCOF – Program for Calculation of Hydrodynamic Maneuvering Coefficients for Submarine”, Report 5030, SSPA Maritime Consulting, 1988
- “SIMOS – Manuale sviluppatore”, 2021
- Mazzarello, G. “Appunti formule calcolo coefficienti idrodinamici - SUBCOF”
- Feltman, J. “Revised standard submarine equations of motions”, David W: Taylor Naval Ship Research and Development Center, 1979
- Gertler, M. “Standard Equations of Motion for Submarine Simulation”, 1967
- Van Lammeren W.P.A., Van Manen J.D., Oosterveld M.W.C., “The Wageningen B-Screw Series”, SNAME Annual Meeting – New York, 1969
- Dallinger, “Submarine – High – Pressure – Air System”
- “RISALITA DEL SOMMERSIBILE” in caso di falla non intercettabile, rapporto interno del CNI
- Saphiro A.H., “The dynamics and Thermodynamics of compressible fluid flow”
- Mitchell, Melanie (1996). An Introduction to Genetic Algorithms. Cambridge, MA: MIT Press.
- Eiben, A. E. et al (1994). "Genetic algorithms with multi-parent recombination". PPSN III: Proceedings of the International Conference on Evolutionary Computation
- Christopher J. Bett, in The Electrical Engineering Handbook, 2005
- Thor I. Fossen(auth.) - Handbook of Marine Craft Hydrodynamics and Motion Control (2011)
- Ridley P., Fontan J., Corke P. (2003), Submarine dynamic modelling
- Australian Conference on Robotics and Automation, 2nd -4th December, 2003,

